LAPPEENRANTA-LAHTI UNIVERSITY OF TECHONOLOGY LUT

LUT School of Energy Systems

LUT Mechanical Engineering

Juhani Veijalainen

**MECHANICAL PROPERTIES OF STEEL SANDWICH PANEL WITH CORRUGA-
TED CORE**

18.11.2020

Supervisors: Dr (Sc.) Timo Björk

                  Dr (Sc.) Anna Fellman

TIIVISTELMÄ

Lappeenrannan-Lahden teknillinen yliopisto LUT
LUT School of Energy Systems
LUT Kone

Aaltoprofiiliytimellisen teräskennolevyn mekaaniset ominaisuudet
Diplomityö
2020
60 sivua, 32 kuvaa, 7 taulukkoa and 10 liitettä
Tarkastajat: TkT Timo Björk
               TkT Anna Fellman
Hakusanat: aaltoprofiiliydin, teräskennolevy, kestävyys, tasakuorma

Työn tarkoituksena oli tutkia HT-Laserin valmistaman aaltoytimellisen teräskennolevyn kestävyyttä. Tutkimus toteutettiin analyyttisin laskennoin, FEM:llä ja laboratoriokokeilla. Tutkimuskysymyksiä oli kuusi: 1) Mikä on aaltoytimellisen teräskennolevyn staattinen kestävyys? 2) Miten kuormitussuunta ja -tyyppi vaikuttavat kestävyyteen? 3) Miten valmistusvirheet vaikuttavat kestävyyteen? 4) Mikä on paikallisen lommahduksen riski? 5) Millaiset parannukset nostavat kestävyyttä? 6) Kuinka hyvin analyyttiset laskennat ja FEM-tulokset vastaavat laboratorituloksia? FEM- ja analyyttiset laskennat voivat ennustaa laboratoritesteissä mitattua kennolevyn globaalia käyttäytymistä. Maksimimaalinen sallittu poikittainen kuormitus kennolevylle oli 21.2 kN/m^2 päistään tuettuna, ja 22.9 kN/m^2 jokaiselta sivulta tuettuna. Muita kuormitussuuntia ei testattu, mutta tuentatyypillä oli vaikutus kestävyyteen. Paikallinen lommahdus tapahtuu pintalevyssä. Epälineaarinen FEM-laskenta ei ennustanut pintalevyn lommahdusta. Katastrofaalista hajoamista, kuten useiden kiinnityshitsien yhtäaikaista pettämistä tai kuormankantokyvyn yllättävää menetystä, ei tapahtunut, ja kennolevyllä oli paljon plastista kapasiteettia. Valmistusvirheiden ei havaittu vaikuttavan kestävyyteen. Neljää vaihtoehtoista FEM-mallia kestävyyden parantamiseksi testattiin. Jokainen malli paransi kennolevyn kestävyyttä ja vaatii eritasoisia muutoksia valmistusprosessiin. 1 mm pintalevy vaatii ainoastaan laserhitsausparametrien muutoksen. Lisätutkimuksia vaativia seikkoja tuli ilmi tutkimuksen aikana: kiinnityshitsien kapasiteettitarkastelu, pintalevyn lokaalinen pistekuorman kestävyys, kennolevyn väsymiskestävyys ja värähtelykäyttäytyminen sekä vaihtoehtoisten kennolevyjen prototyypitys ja kestävyysmittaukset.

ABSTRACT

Mechanical properties of steel sandwich panel with corrugated core

Aim of this study was to assess the strength of the steel sandwich panel with a corrugated core, as manufactured currently by HT-Laser. This assessment was done with analytical calculations, FEM and laboratory tests. There were six research questions: 1) What is the static strength of corrugated core sandwich panel? 2) How loading direction and type affect the strength? 3) How possible manufacturing defects affect the strength? 4) What is the risk of local buckling? 5) What kind of enhancements can be made to increase strength? 6) How well do analytical and finite element calculations match laboratory tests? FEM and analytical calculations can predict global behaviour of the corrugated core sandwich panel when compared with experimental results. Maximum allowable transverse load for the panel was 21.2 kN/m^2 for end-support, and 22.9 kN/m^2 for all-round support. Other loading directions or types were not tested, but type of support has an effect on strength. Local buckling happens on the upper faceplate. FEM nonlinear analysis did not predict the upper faceplate buckling. There was however no catastrophic failure such as multiple weld failures or sudden drop in load carrying capacity, and the panel had a lot of plastic capacity. Manufacturing defects were not observed to affect strength. Four different options to better strength were tested in FEM. All of them increased the strength and require modifications to the manufacturing process to varying extend. 1 mm faceplate requires only modification of laser parameters. This study left room for further research: Capacity assessment of welds, local point load capacity of faceplate, fatigue strength and vibration behaviour of the panel, prototyping of panel alternatives and conducting strength tests.

TABLE OF CONTENTS

LIST OF SYMBOLS AND ABBREVIATIONS

Roman

$\bar{a}$ Length of the plate [mm]

$\bar{b}$ Appropiate width of the plate [mm]

a Width of the panel [mm]

a_1 Dimension of corrugation cross-section [mm]

a_2 Dimension of corrugation cross-section [mm]

A_c Area of the corrugation, per unit width [mm^2/mm]

A_f Area of the faceplates, per unit width [mm^2/mm]

A_{brutto} Brutto cross-sectional area of the plate [mm^2]

A_{eff} Effective cross-sectional area of the plate [mm^2]

$A_{i,eff}$ Individual effective cross-sectional area [mm^2]

A_{ij} In-plane stiffness coefficients [N/mm]

a_{ij} Inverse values of in-plane stiffness coefficients [mm/N]

A_{mn} Coefficient of the slope in xz-plane

b Length of the panel [mm]

b_1 Dimension of corrugation cross-section [mm]

b_2 Dimension of corrugation cross-section [mm]

B_{mn} Coefficient of the slope in yz-plane

c Length to width ratio of the panel

$C1...C7$ Auxiliary variables for calculation of S

$C_{11}...C_{33}$ Auxiliary variables for stiffness terms matrix [N/mm]

$C_{44}...C_{66}$ Auxiliary variables for stiffness terms matrix [Nmm/mm]

d_1 Dimension of corrugation cross-section [mm]

d_2 Dimension of corrugation cross-section [mm]

d_f Hat width of the corrugation [mm]

D_x, D_y Bending stiffness in x- and y-direction, per unit width [Nmm]

D_{ij} Bending stiffness terms [Nmm/mm]

D_{Qx}, D_{Qy} Transverse shear stiffness in x- and y-direction, per unit width [Nmm]

D_{xy} Torsional stiffness, per unit width [Nmm]

e_1 Dimension of corrugation cross-section [mm]

e_2 Dimension of corrugation cross-section [mm]

E_c Elastic modulus of the core [MPa]

E_c* Elastic stretching modulus of core [MPa]

E_f Elastic modulus of the faceplates [MPa]

E_x, E_y Extensional stiffness in x- and y-direction, per unit width [N/mm]

e_y Placement of new bending axes due to effective areas [mm]

f_1 Dimension of corrugation cross-section [mm]

f_2 Dimension of corrugation cross-section [mm]

f_y Yield strength of the material [MPa]

f_{bv} Shear buckling strength [MPa]

g_1 Dimension of corrugation cross-section [mm]

G_1, G_2 Shear moduli of the lower and upper faceplates, respectively [MPa]

g_2 Dimension of corrugation cross-section [mm]

G_c Shear modulus of the core [MPa]

G_f Shear modulus of the faceplates [MPa]

G_{xy} Shear stiffness in xy-plane, per unit width [Nmm]

h Total height of the panel [mm]

h_c Core height [mm]

h_{EC} Distance between top and bottom surface of core [mm]

I_c Second moment of area of the core, per unit width [mm^4/mm]

I_f Second moment of area of the faceplates, per unit width [mm^4/mm]

I_{eff} Effective second moment of area [mm^4]

$I_{i,eff}$ Individual effective second moment of area [mm^4]

I_{unit} Panel unit cross-section second moment of area [mm^4/mm]

j_1 Dimension of corrugation cross-section [mm]

j_2 Dimension of corrugation cross-section [mm]

k_1 Dimension of corrugation cross-section [mm]

k_2 Dimension of corrugation cross-section [mm]

K_L Non-dimensional integral parameter function of corrugation cross-section geometry

k_y, k_z Non-dimensional parameters, locating origin of y- and z-coordinates

k_σ Buckling factor

K_{A_z} Non-dimensional integral parameter function of corrugation cross-section geometry

k_c Ratio of distance between lower faceplate mid-surface and shear center of corrugation

k_{GJ} Ratio of distance between lower faceplate mid-surface and zero shear plane

K_{I_y} Non-dimensional integral parameter function of corrugation cross-section geometry

K_{I_z} Non-dimensional integral parameter function of corrugation cross-section geometry

$K_{I_{yz}}$ Non-dimensional integral parameter function of corrugation cross-section geometry

K_{L_y} Non-dimensional integral parameter function of corrugation cross-section geometry

K_{L_z} Non-dimensional integral parameter function of corrugation cross-section geometry

$K_{L_{yz}}$ Non-dimensional integral parameter function of corrugation cross-section geometry

l_c Length of the corrugation leg [mm]

L_{ij} Auxiliary variables when solving deflection of panel

m, n Number of half-waves in x- and y-directions

M_{cr} Critical moment [Nmm]

N_i Compressive load in x-, y- and xy-directions [N/mm]

P Matrix of Euler's coefficient

p Length of the half-pitch of corrugation [mm]

q_0 Transverse distributed loading [MPa]

Q_x Transverse shear force in x-plane [N/mm]

Q_{ij} Effective stiffness terms for the faceplates [N/mm]

Q_{ij}^* Effective stiffness terms for the core [N/mm]

q_{mn} Euler's coefficient

R_{C1} Dimension of corrugation cross-section [mm]

R_{C2} Dimension of corrugation cross-section [mm]

R_{i_1} Lower radius of core leg [mm]

R_{i_2} Upper radius of core leg [mm]

S Non-dimensional coefficient

S_i Individual first moment of area [mm^3]

s_w Auxiliary variable for shear buckling strength

t_1, t_2 Thicknesses of the lower and upper faceplates, respectively [mm]

t_c Core plate thickness [mm]

t_f Faceplate thickness [mm]

u_{mn} Coefficient matrix

V_{cr} Critical shear force for corrugated profile [N]

w Deflection of the panel [mm]

W_{eff} Effective section modulus [mm^3]

y_i Individual distance from center of mass to the bending axis [mm]

z_k^b z-coordinate of the lower faceplate

z_k^t z-coordinate of the upper faceplate

z_k^{*b} z-coordinate of the bottom of core

z_k^{*t} z-coordinate of the top of core

Greek

α Factor corresponding to buckling curve

χ_c Reduction factor

ε Stress coefficient

ε_i Strains in x-, y- and xy-directions

γ_{M0} Safety factor

λ_c Slenderness of the beam

λ_p Plate slenderness

λ_w Auxiliary variable for shear buckling strength

v_x' Bending Poisson's ratio in x-direction

v_y' Bending Poisson's ratio in y-direction

v_c Poisson's ratio of the core

v_f Poisson's ratio of the faceplate

v_x Extensional Poisson's ratio in x-direction

v_y Extensional Poisson's ratio in y-direction

ϕ Auxiliary variable for reduction factor

ψ Stress ratio

ρ Reduction factor

ρ_c Final reduction factor

σ_i Stresses in x-, y- and xy-directions

$\sigma_{cr,c}$ Elastic critical column buckling stress of plate [MPa]

$\sigma_{cr,p}$ Critical stress for equivalent orthotropic plate [MPa]

σ_{cr} Elastic critical plate buckling stress [MPa]

σ_E Buckling stress of the equivalent orthotropic plate [MPa]

$\sigma_{x,c,max}$ Maximum core stress in x-direction [MPa]

$\sigma_{x,c}$ Core stress in x-direction [MPa]

$\sigma_{x,f,max}$ Maximum faceplate stress in x-direction [MPa]

$\sigma_{x,f}$ Faceplate stress in x-direction [MPa]

$\sigma_{y,f,max}$ Maximum faceplate stress in y-direction [MPa]

$\tau_{cr,c,xy}$ Critical buckling stress of core considering xy-plane [MPa]

$\tau_{cr,c,xz}$ Critical buckling stress of core considering xz-plane [MPa]

$\tau_{cr,f,xy}$ Critical buckling stress of faceplate considering xy-plane [MPa]

$\tau_{xy,max}$ Maximum faceplate shear stress in xy-plane [MPa]

τ_{xy} Shear tress in xy-plane [MPa]

θ, ϑ Angle of the corrugation diagonal [°]

θ_x, θ_y Slopes of the normal to the middle plane of the sandwich plate about the xz- and yz-planes

ξ Auxiliary variable for the final reduction factor

Abbreviations

$C1$ The first constraint setup

$C2$ The second constraint setup

$KV-1$ The first test sample

$KV-2$ The second test sample

$S1$ The first test cylinder

$S2$ The second test cylinder

1 Introduction

Due to ever rising concerns of saving energy and limit emissions, point of interest is at seeking for light-weight but durable structures. Sandwich panels with corrugated core serve this well, as they are stronger for given weight than solid bulk forms. (Zaid, Rejab & Mohamed 2016, p.3; Järvenpää, Lämsä, Hietala & Mäntyjärvi 2014, p. 781). This allows to use material of less strength or to use stronger material for lesser weight. Panels can be bonded or welded, of which latter has become popular due to advanced laser welding, allowing thin structures to be welded with minimum distortions and heat input. (Caccese & Yorulmaz 2009, p.2 - 3; SANDOCORE 2005, p.159) However, due to their newness within industry, there is little information of mechanical properties of steel sandwich panels, manufactured as mass-scale products, instead of laboratory samples.

Aim of this study is to assess mechanical properties of corrugated core sandwich panel, as manufactured currently by HT-Laser, by making analytical and empirical models. Customers can then use these models as help during their own design work. Research questions are 1) What is the static strength of corrugated core sandwich panel? 2) How loading direction and type affect the strength? 3) How possible manufacturing defects affect the strength? 4) What is the risk of local buckling? 5) What kind of enhancements can be made to increase strength? 6) How well do analytical and finite element calculations match laboratory tests?

2   Methods

To assess the mechanical properties of the corrugated core, both analytical and finite element method (FEM) models were created. Due to their orthotropic nature, analytical solutions for corrugated core sandwich panels are scarce, and are done with many assumptions (SAND-CORE 2005, p.38). Thus, in order to calculate more accurate results, FEM is needed. Analytic and FEM results were then used to estimate the real transverse distributed loading test results in the laboratory.

The figure 1 shows the conduct of this study. It consists of the literature study, findings of which are used to define the Python code used in analytical calculations. Likewise, the literature study is used to define FEM model. Results of FEM model and literature study are used when creating laboratory test procedure. This includes the placement of the strain gauges and design of the test device.
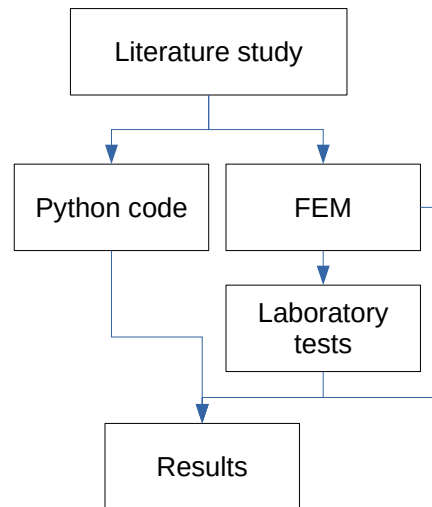

Figure 1. Conduct of the study. Results of finite element method (FEM) were used to design laboratory tests.

2.1   Introduction of model

The current production model of the corrugated core sandwich is presented in the figures 2 and 3. They present schematic sizes of the panel and profile. The table 1 presents the numerical values of the sandwich panel. Manufacturing is done with a disk laser.

Figure 2. Overall dimensions of the current panel.
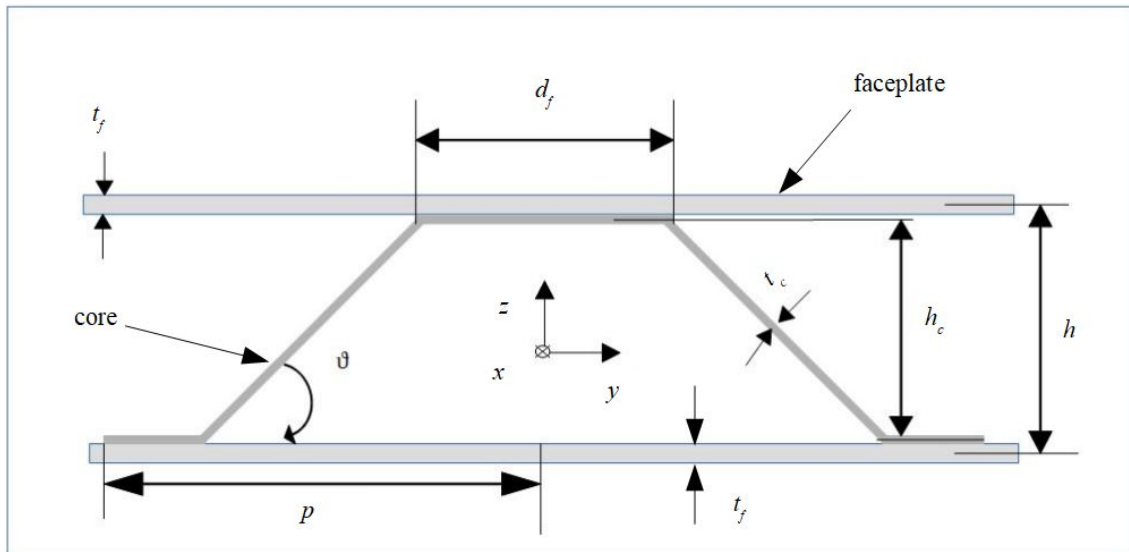
Figure 3. Overall dimensions of the current panel.

2.2 Analytical model

Corrugated core sandwich is highly orthotropic in its nature. This has posed challenges for the designers looking for optimization of construction or to assess initial mechanical properties. Kujala, Romanoff, Salminen, Varis & Vilpas (2003, p. 18 - 23) list designer tools: use of ready made data tables, use of beam theory and analytical solutions, use of plate theory and analytical solutions, and finally using 3D finite element models. They reckon that using the combination of nonlinear geometry and nonlinear material model with 3D FEM yields the most accurate predictions, but in cost of complexity and computation time. The ready-made data-tables are the fastest way for the designer to obtain initial strength of the panel, but unfortunately they are very geometry specific. Utilization of the beam theory gives modestly

Table 1. Dimensions of the current panel.

Parameter	Symbol	Value
Width	a	2000 mm
Length	b	1000 mm
Total height	h	15.3 mm
Core height	h_c	14 mm
Hat width	d_f	6.2 mm
Half-pitch	p	20 mm
Core thickness	t_c	0.5 mm
Faceplate thickness	t_f	0.75 mm
Core angle	ϑ	45 °

accurate initial solutions, but for the accurate predictions it is too restricted to boundary and loading conditions. Plate theory gives the best compromise between accuracy and speed, although it is often restricted to simple-supported panel.

The plate theory can be divided in the case of sandwich plate to the Mindlin-Reissner plate and classical laminate theories (Shaban & Alibeigloo 2017, p. 404 - 405; Lurie, Solyaev, Volkov-Bogorodskiy, Bouznik & Koshurina 2017, p.1011 - 1013; Cheon & Kim 2015, p.1218-1220; Vinson 1999, p.51, 54; Airasmaa, Kokko, Komppa & Saarela 1991, p. 312 - 329) in the way they handle the orthotropic sandwich structure. Homogenization is a way to represent 3D sandwich as 2D plate. The first derivation of the elastic constants for corrugated core sandwich panel specifically was done by Libove & Hubka (1951, p.6 - 10). They utilized Mindlin-Reissner theory by assuming that "[s]traight material lines normal to the middle surface are assumed to remain straight, but not necessarily normal to the middle surface, during distortion of the plate" (Libove & Hubka 1951, p.3). There have been also other derivations of equivalent plate, for example Chang, Ventsel, Krauthammer & John (2005, p. 81 - 89), Buannic, Cartraud & Quesnel (2003, p. 299–312) and Cheon & Kim (2015, p. 1217 - 1223). Chang et al. used Mindlin-Reissner theory, Buannic et al. used Kirchhoff-Love theory and Cheon & Kim used classical laminate theory. Buannic et al. (2003, p.299) notified that Kirchoff-Love theory leads to neglection of transverse shear effect on pure bending and thus more inaccurate results compared to Mindlin-Reissner theory.

Calculations in this study were done using Python 3.7 distribution with numpy, scipy and mpmath libraries. Calculation code is presented in the appendix C.

2.2.1 Classical laminate model

For the analytic calculations of classimal laminate theory, methods listed by Lurie et al. (2017, p.1011 - 1013) were followed, taking into account the lack of insulation layer and difference in coordinate system, and supplementing with Cheon & Kim (2015, p.1218-1220),

Vinson (1999, p.51, 54) and Airasmaa et al. (1991, p. 312 - 329).

Relation between stresses, effective stiffness and strains can be written as $[\sigma] = [Q_{ij}][\varepsilon]$. Relation between normal forces, in-plane stiffness coefficients and strain can also be written as $[N] = [A_{ij}][\varepsilon]$. Thus, it can be written that $[\varepsilon] = [A_{ij}]^{-1}[N]$. Inverse matrix can be replaced so that $[a_{ij}] = [A_{ij}]^{-1}$. This is done in whole in equations 1, 2 and 3. Thus, it can be said that $a_{11} = A_{22}/A$, $a_{12} = -A_{12}/A$, $a_{22} = A_{11}/A$, $a_{66} = 1/(2A_{66})$, and $A = A_{11}A_{22} - A_{12}^2$.(Lurie et al. 2017, p.1011; Cheon & Kim 2015, p.1218; Vinson 1999, p.51, 56.)

$$\begin{bmatrix} \sigma_x \\ \sigma_y \\ \sigma_{xy} \end{bmatrix} = \begin{bmatrix} Q_{11} & Q_{12} & 0 \\ Q_{12} & Q_{22} & 0 \\ 0 & 0 & Q_{66} \end{bmatrix} \begin{bmatrix} \varepsilon_x \\ \varepsilon_y \\ 2\varepsilon_{xy} \end{bmatrix} \tag{1}$$

$$\begin{bmatrix} N_x \\ N_y \\ N_{xy} \end{bmatrix} = \begin{bmatrix} A_{11} & A_{12} & 0 \\ A_{12} & A_{22} & 0 \\ 0 & 0 & A_{66} \end{bmatrix} \begin{bmatrix} \varepsilon_x \\ \varepsilon_y \\ 2\varepsilon_{xy} \end{bmatrix} \tag{2}$$

$$\begin{bmatrix} \varepsilon_x \\ \varepsilon_y \\ \varepsilon_{xy} \end{bmatrix} = \begin{bmatrix} a_{11} & a_{12} & 0 \\ a_{12} & a_{22} & 0 \\ 0 & 0 & a_{66} \end{bmatrix} \begin{bmatrix} N_x \\ N_y \\ N_{xy} \end{bmatrix} \tag{3}$$

The effective stiffness terms $Q_{11} = Q_{22} = E/(1 - v^2)$, $Q_{12} = vQ_{11}$ and $Q_{66} = G$ are for the faceplates. The effective stiffness terms for the core can be written as $Q_{22}^* = Q_{12}^* = Q_{66}^* = 0$ and $Q_{11}^* = Et_c(d_f + h_c/cos\vartheta)/(ph_c)$. (Lurie et al. 2017, p.1011; Cheon & Kim 2015, p.1220; Vinson 1999, p.41.) It should be noted that Q_{11}^* and Q_{22}^* are swapped compared to original, due to the difference in coordinate system.

In-plane stiffness terms can be assessed with the help of effective stiffness terms in general form as in equation 4 and in particular form as in equation 5 (Lurie et al. 2017, p.1011; Cheon & Kim 2015, p.1220; Vinson 1999, p.54):

$$A_{ij} = Q_{ij}(z_k^t + z_k^b) + Q_{ij}^*(z_k^{*t} + z_k^{*b}) \tag{4}$$

$$A_{ij} = 2Q_{ij}t_f + Q_{ij}^*h_c \tag{5}$$

Bending stiffness terms can also be assessed in a general form with effective stiffness terms as in equation 6 and in a particular form in equation 7 (Lurie et al. 2017, p.1011; Cheon & Kim 2015, p.1220; Vinson 1999, p.54):

$$D_{ij} = \frac{1}{3}\left[Q_{ij}\left((z_k^t)^3 + (z_k^b)^3\right) + Q_{ij}^*\left((z_k^{*t})^3 + (z_k^{*b})^3\right)\right] \tag{6}$$

$$D_{ij} = \frac{1}{3}\left[Q_{ij}\left(2(h/2)^3 + 2(h/2 - t_f)^3\right) + 2Q_{ij}^*(h/2 - t_f)^3\right] \tag{7}$$

Maximum shear stress in xy-plane can be assessed as in the equation 8. This can be contrasted with critical buckling stresses for the faceplate and core, as presented in equations 9 and 10. Assumptions are infinite plates with simple supports. (Lurie et al. 2017, p.1012.)

$$\tau_{xy} = \frac{Q_{66}N_{xy}}{A_{66}} \tag{8}$$

$$\tau_{cr,f,xy} = \frac{\pi^2\sqrt{2}}{3}\frac{E}{1-v^2}\left(\frac{t_f}{2p - d_f}\right)^2 \tag{9}$$

$$\tau_{cr,c,xy} = \frac{\pi^2\sqrt{2}}{3\sin\vartheta}\frac{E}{1-v^2}\left(\frac{t_c\cos\vartheta}{h_c}\right)^2 \tag{10}$$

Combining above mentioned, it can be written that $[\sigma] = [Q_{ij}][a_{ij}][N]$. Thus, x-direction compressive stresses under compressive loading can be assessed as in equation 11 and 12, for the faceplates and core, respectively. Note the different notation compared to the original due to the difference of coordinate system (Lurie et al. 2017, p.1012.)

$$\sigma_{x,f} = (Q_{11}a_{11} + Q_{12}a_{12})N_x \tag{11}$$

$$\sigma_{x,c} = Q_{11}^* a_{11}N_x \tag{12}$$

Critical local buckling stresses due to compressive loading for the faceplate and core can be assessed by using theory of isotropic plate with simple supports.(Lurie et al. 2017, p.1012; Vinson 1999, p.248-249.)

$$\sigma_{cr,f} = \frac{\pi^2}{3}\frac{E}{1-v^2}\left(\frac{t_f}{2p - d_f}\right)^2 \tag{13}$$

$$\sigma_{cr,c} = \frac{\pi^2}{3}\frac{E}{1-v^2}\left(\frac{t_c\cos\vartheta}{h_c}\right)^2 \tag{14}$$

Critical compression load in relation to global buckling is assessed as in equation 15 for orthotropic plate with simple supports. It should be noted that $c = b/a$ and m is number of half-waves due to buckling (Lurie et al. 2017, p.1012.)

$$N_{cr} = \frac{\pi^2\sqrt{D_{22}D_{11}}}{a^2}\left[\sqrt{\frac{D_{11}}{D_{22}}}\left(\frac{m}{c}\right)^2 + \frac{2(D_{12} + 2D_{66})}{\sqrt{D_{11}D22}} + \sqrt{\frac{D_{22}}{D_{11}}}\left(\frac{c}{m}\right)^2\right] \tag{15}$$

Bending stresses in x- and y-directions and shear stresses in xy-plane for the upper faceplate due to the transverse uniformly distributed load q_0 can be calculated as presented in the equations 17, 18 and 19, whereas bending stress in x-direction for core is the equation 19. (Lurie et al. 2017, p.1012; Vinson 1999, p.138-139.) To simplify presentation, Lurie et al. (2017, p.1012) has used simplification as follows in equation 16. It should be noted that a and b are swapped in equations 16, 17 and 18 compared to original.

$$D = D_{11}\left(\frac{m}{b}\right)^4 + 2(D_{12} + 2D_{66})\left(\frac{mn}{ab}\right)^2 + D_{22}\left(\frac{n}{a}\right)^4 \tag{16}$$

$$\sigma_{x,f,max}(z) = \frac{16q_0 z}{\pi^4} \sum_{m=1,3...}^{\infty} \sum_{n=1,3...}^{\infty} \frac{(-1)^{m+n}}{mnD}\left(Q_{11}\left(\frac{m}{b}\right)^2 + Q_{12}\left(\frac{n}{a}\right)^2\right) \tag{17}$$

$$\sigma_{y,f,max}(z) = \frac{16q_0 z}{\pi^4} \sum_{m=1,3...}^{\infty} \sum_{n=1,3...}^{\infty} \frac{(-1)^{m+n}}{mnD}\left(Q_{12}\left(\frac{m}{b}\right)^2 + Q_{22}\left(\frac{n}{a}\right)^2\right) \tag{18}$$

$$\tau_{xy,max}(z) = \frac{32q_0 z}{\pi^4} \sum_{m=1,3...}^{\infty} \sum_{n=1,3...}^{\infty} \frac{1}{abD}Q_{66} \tag{19}$$

$$\sigma_{x,c,max}(z) = \frac{16q_0 z}{\pi^4} \sum_{m=1,3...}^{\infty} \sum_{n=1,3...}^{\infty} (-1)^{m+n}\frac{nQ_{11}^*}{mDb^2} \tag{20}$$

To attain transverse shear forces, Lurie et al. (2017, p.1012) has used approximation of the classical theory in equation 21. It should be noted that a and b are swapped in equation 21 compared to original. By attaining shear force, transverse shear stress in core walls can be calculated in equation 21. The critical transverse shear stress for the core is presented in equation 23.

$$Q_x(x,y) = \frac{16q_0}{\pi^3} \sum_{m=1}^{\infty} \sum_{n=1}^{\infty} \frac{1}{mbD}\left(-(2D_{66} + D_{12})\left(\frac{m}{b}\right)^2 - D_{11}\left(\frac{n}{a}\right)^2\right)\sin\frac{m\pi x}{b}\cos\frac{n\pi y}{a} \tag{21}$$

$$\tau_{xz} = \frac{Q_x(d_f + h_c(\cos\vartheta)p}{2t_c h_c h} \tag{22}$$

$$\tau_{cr,c,xz} = \frac{\pi^2\sqrt{2}}{3}\frac{E}{1-v^2}\left(\frac{t_c\cos\vartheta}{h_c}\right)^2 \tag{23}$$

The equations presented in this section are used in the CLT module in Python code.

2.2.2 Elastic constants for corrugated core sandwich

Next follows the axial and bendings stiffnesses developed by Libove and Hubka (1951, p. 6 - 10). A_f and A_c are faceplate and corrugation core areas per unit width, respectively. l_c is the length of corrugation leg. t_1 and t_2 denote the thicknesses of the lower and the upper faceplates, respectively. E_x and E_y are extensional stiffness terms in x- and y–directions per

unit width, respectively. v_x and v_y are extensional Poisson's ratios. E_f and E_c are faceplate and core material elastic moduli.

$$A_f = t_2 + t_1 \tag{24}$$

$$A_c = \frac{l_c t_c}{p} \tag{25}$$

$$E_x = E_f A_f + E_c A_c \tag{26}$$

$$E_y = \frac{E_f A_f}{1 - v_f^2 (1 - \frac{E_f A_f}{E_x})} \tag{27}$$

$$v_x = v_f \tag{28}$$

$$v_y = v_x \frac{E_y}{E_x} \tag{29}$$

D_x and D_y are bending stiffness terms in x- and y-directions per unit width, respectively. I_f and I_c are second moment of area for faceplates and core per unit width. $v_{\prime x}$ and $v_{\prime y}$ are bending Poisson's ratios.

$$D_x = E_f I_f + E_c I_c \tag{30}$$

$$D_y = \frac{E_f I_f}{1 - v_f^2 (\frac{E_f I_f}{D_x})} \tag{31}$$

$$v_{\prime x} = v f \tag{32}$$

$$v_{\prime y} = v_{\prime x} \frac{D_y}{D_x} \tag{33}$$

D_{xy} is torsional stiffness term per unit width. G_f is shear modulus of the faceplate material, G_c is shear modulus of the core material. $k_c = \frac{1}{2}(1 + \frac{A_1 - A_2}{2ph})$ is ratio of distance between lower faceplate mid-surface and shear center of corrugation. $k_{GJ} = \frac{\frac{G_c t_c^2}{A_c} k_c + G_2 t_2}{GA}$ is ratio of distance between lower faceplate mid-surface and zero shear plane. $GA = G_1 t_1 + \frac{G_c t_c^2}{A_c} + G_2 t_2$ is unit shear stiffness in respect of x- and y-directions. G_1, t_1 refer to the lower faceplate and G_2, t_2 to the upper faceplate (Libove and Hubka 1951, p. 26 - 28.)

$$D_{xy} = 2 \left[G_1 t_1 k_{GJ}^2 + \frac{G_c t_c^2}{A_c} (k_{GJ} - k_c)^2 + G_2 t_2 (1 - k_{GJ}^2) \right] h^2 \tag{34}$$

G_{xy} is shear stiffness in xy-plane per unit width.

$$G_{xy} = \frac{G_c t_c^2}{A_c} + G_f A_f \tag{35}$$

D_{Qy} is transverse shear stiffness in y-direction per unit width.

$$D_{Qy} = Sh \left(\frac{E_c}{1 - v_c^2} \right) \left(\frac{t_c}{h_c} \right)^3 \tag{36}$$

The non-dimensional coefficient S can be derived in general form in the equation 37. It can be presented with help of auxiliary variables C_1-C_7. (equations 38 - 44). K_{I_z}, $K_{I_{yz}}$, K_{I_y}, K_{A_z}, K_L, K_{L_y}, $K_{L_{yz}}$ and K_{L_z} are non-dimensional integral parameter functions of corrugation cross-section geometry. E_c^* is elastic stretching modulus of core. It can be assumed to be equal to the E_c. Parameters k_y and k_z are non-dimensional, locating origin of y- and z-coordinates. (Libove and Hubka 1951, p. 27; 58; 61-62.)

$$S = \frac{3 \frac{h_c}{p} C_7 (C_2^2 - C_1 C_3) - C_3 + \frac{p}{h_c}(2C_2 - \frac{p}{h_c}C_1)}{12[2\frac{p}{h_c}[\frac{p}{h_c}(C_1 C_4 - C_2 C_5) - (C_2 C_4 - C_3 C_5)] + \frac{h_c}{p}[3C_7[(C_4(C_1 C_4 - 2C_2 C_5) + C_3 C_5^2 - C_6(C_1 C_3 - C_2^2)] + \frac{p}{h_c}(C_4^2 - C_3 C_6) + 2(\frac{p}{h_c})^2(C_2 C_6 - C_4 C_5) + (\frac{p}{h_c})^3(C_5^2 - C_1 C_6)] + \frac{h}{h_c}\frac{p}{h_c}(C_2^2 - C_1 C_3))]} \tag{37}$$

$$C_1 = K_L + \frac{1}{3}\frac{E_c(1-v_2^2)}{E_2(1-v_c^2)}(\frac{t_c}{t_2})^3\frac{p}{h_c} \tag{38}$$

$$C_2 = K_{A_z} + \frac{k_y}{2}\frac{p}{h_c}K_L \tag{39}$$

$$C_3 = K_{I_z} + k_y\frac{p}{h_c}(K_{A_z} + \frac{k_y}{4}\frac{p}{h_c}K_L) + \frac{1}{12}\frac{E_c}{E_c^*}(\frac{t_c}{h_c})^2 K_{L_z} \tag{40}$$

$$C_4 = K_{I_z} + \frac{1}{2}[k_z + (1+\frac{t_2}{t_c})\frac{t_c}{h_c}](K_{A_z} + \frac{k_y}{2}\frac{p}{h_c}K_L) + \frac{k_y}{2}\frac{p}{h_c}K_{A_y} - \frac{1}{12}\frac{E_c}{E_c^*}(\frac{t_c}{h_c})^2 K_{L_{yz}} \tag{41}$$

$$C_5 = K_{A_y} + \frac{1}{2}[k_z + (1+\frac{t_2}{t_c})\frac{t_c}{h_c}]K_L \tag{42}$$

$$C_6 = K_{I_y} + [k_z + (1+\frac{t_2}{t_c})\frac{t_c}{h_c}](K_{A_y} + \frac{1}{4}[k_z + (1+\frac{t_2}{t_c})\frac{t_c}{h_c}]K_L) + \frac{1}{12}\frac{E_c}{E_c^*}(\frac{t_c}{h_c})^2 K_{L_y} \tag{43}$$

$$C_7 = \frac{E_1}{E_c}\frac{1-v_c^2}{1-v_1^2}(\frac{t_1}{t_c})^3 \tag{44}$$

However, if considering the common type of sandwich with symmetrical core and symmetric sandwich as a whole, then $k_z = k_y = 1$, thus K_{A_y} and K_{A_z} can be eliminated. Also, because

of common factor in the numerator and denominator, S can be simplified as in equation 45. (Libove and Hubka 1951, p.63.)

$$S = \frac{6\frac{h_c}{p}B_3 B_7 + (\frac{p}{h_c})^2}{12[-2(\frac{p}{h_c})^2 B_4 + \frac{h_c}{h}[6B_7(B_3 B_6 - B_4^2) + (\frac{p}{h_c})^3 B_6] + \frac{h}{h_c}\frac{p}{h_c}B_3]} \tag{45}$$

$$B_3 = K_{L_z} + \frac{1}{12}\frac{E_c}{E_c^*}(\frac{t_c}{h_c})^2 K_{L_z} \tag{46}$$

$$B_4 = K_{L_{yz}} - \frac{1}{12}\frac{E_c}{E_c^*}(\frac{t_c}{h_c})^2 K_{L_{yz}} \tag{47}$$

$$B_6 = K_{L_y} + \frac{1}{12}\frac{E_c}{E_c^*}(\frac{t_c}{h_c})^2 K_{L_y} \tag{48}$$

$$B_7 = C_7 = \frac{E_1}{E_c}\frac{1-v_c^2}{1-v_1^2}(\frac{t_1}{t_c})^3 \tag{49}$$

Parameters K_{I_z}, $K_{I_{yz}}$, K_{I_y}, K_{A_z}, K_L, K_{L_y}, $K_{L_{yz}}$ and K_{L_z} can be simplified, if corrugation leg is deemed symmetric and origin of x and y is the middle point of the corrugation leg. They are expressed with help of dimensions of corrugation cross-section R_{C1}, R_{C2}, a_1, a_2, e_1, e_2, g_1, g_2, j_1, j_2, k_1, k_2, d_1, d_2, b_1, b_2, f_1 and f_2. (Libove and Hubka 1951, p.66.)

$$K_{I_z} = \frac{2}{3}(\frac{k_1}{h_c})^2\frac{d_1}{h_c} + \frac{2}{3}[\frac{1}{8}(\frac{p}{h_c})^3 - (\frac{b_1}{h_c})^3)] + 2\frac{R_{C1}}{h_c}(\frac{b_1}{h_c}[\theta\frac{b_1}{h_c} - 2(\frac{R_{C1}}{h_c} - \frac{e_1}{h_c})] + \frac{1}{2}[\theta(\frac{R_{C1}}{h_c} - \frac{g_1}{h_c}\frac{e_1}{h_c})]) \tag{50}$$

$$K_{I_{yz}} = \frac{2}{3}\frac{j_1}{h_c}\frac{k_1}{h_c}\frac{d_1}{h_c} + \frac{1}{2}[\frac{1}{4}(\frac{p}{h_c})^2 - (\frac{b_1}{h_c})^2] + 2\frac{R_{C1}}{h_c}[\frac{a_1}{h_c}(\theta\frac{b_1}{h_c} + \frac{e_1}{h_c} - \frac{R_{C1}}{h_c}) + \frac{g_1}{h_c}(\frac{b_1}{h_c} - \frac{1}{2}\frac{g_1}{h_c})] \tag{51}$$

$$K_{I_y} = \frac{2}{3}(\frac{j_1}{h_c})^2\frac{d_1}{h_c} + \frac{1}{4}\frac{f_1}{h_c} + 2\frac{R_{C1}}{h_c}(\frac{a_1}{b_1}(\theta\frac{a_1}{b_1} + 2\frac{g_1}{h_c}) + \frac{1}{2}[\theta(\frac{R_{C1}}{h_c})^2 + \frac{g_1}{h_c}\frac{e_1}{h_c}]) \tag{52}$$

$$K_{A_z} = K_{A_y} = 0 \tag{53}$$

$$K_L = 2\frac{d_1}{h_c} + 2\theta\frac{R_{C1}}{h_c} + \frac{f_1}{h_c} \tag{54}$$

$$K_{L_y} = \frac{f_1}{h_c} + 2\frac{d_1}{h_c}\cos\theta^2 + \frac{R_{C1}}{h_c}(\theta + \sin\theta\cos\theta) \tag{55}$$

$$K_{L_{yz}} = 2\frac{d_1}{h_c}\sin\theta\cos\theta + \frac{R_{C1}}{h_c}\sin\theta^2 \tag{56}$$

$$K_{L_z} = 2\frac{d_1}{h_c}\sin\theta^2 + \frac{R_{C1}}{h_c}(\theta - \sin\theta\cos\theta) \tag{57}$$

Finally, dimensions needed in equations 50-57 can obtained with p, distance between top and bottom surface of core h_{EC}, lower radius of core leg R_{i_1}, upper radius of core leg R_{i_2}, corrugation angle θ and t_c (Libove & Hubka 1951, p. 69).

$$h_c = h_{EC} - t_c$$

$$R_{C1} = R_{i_1} + \frac{t_c}{2} \qquad\qquad R_{C_2} = R_{i_2} + \frac{t_c}{2}$$

$$a_1 = (1 - \frac{k_z}{2})h_c - R_{C_1} \qquad\qquad a_2 = k_z\frac{h_c}{2} - R_{C_2}$$

$$e_1 = R_{C_1}\cos\theta \qquad\qquad e_2 = R_{C_2}\cos\theta$$

$$g_1 = R_{C_1}\sin\theta \qquad\qquad g_2 = R_{C_2}\sin\theta$$

$$j_1 = a_1 + e_1 \qquad\qquad j_2 = a_2 + e_2$$

$$k_1 = j_1\cot\theta \qquad\qquad k_2 = j_2\cot\theta$$

$$d_1 = j_1\csc\theta \qquad\qquad d_2 = j_2\csc\theta$$

$$b_1 = k_1 + g_1 \qquad\qquad b_2 = k_2 + g_2$$

$$f_1 = 2[(1 - \frac{k_y}{2})p - b_1] \qquad\qquad f_2 = 2(\frac{k_y}{2}p - b_2)$$

D_{Qx} is transverse shear stiffness in x-direction, per unit width. I_{unit} is second moment of area per unit width of cross-section. Q is static moment of area of cross-section. Figure 4 shows the area used in its calculation. (Libove and Hubka 1951, p.11.)

$$D_{Qx} = \frac{G_c I_{unit} t_c h}{p \int_0^{l_c} Q\,ds} \tag{58}$$
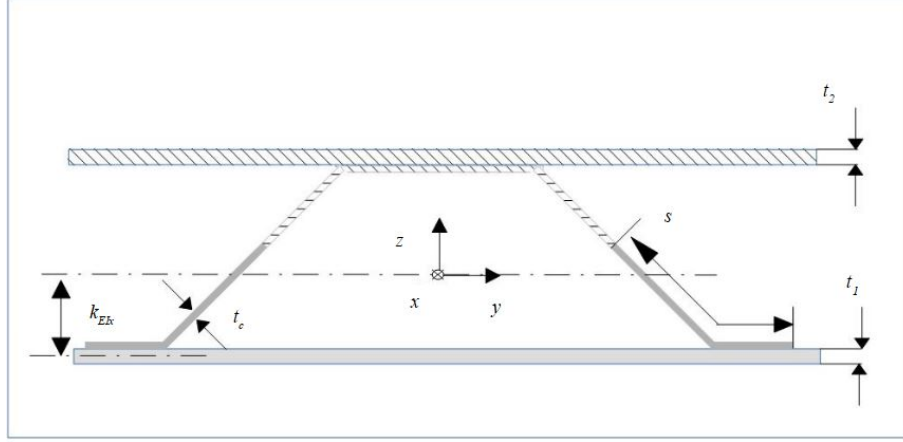
Figure 4. Hatched area is used when calculation static moment of area for D_{Qx} (adapted from Libove and Hubka 1951, p. 70).

If it is considered that only faceplates carry bending loads, D_{Qx} can be simplified, by approximating centroidal axis location $k_{EIx} h$ and thus I_{unit} and $\int_0^{l_c} Q \, ds$.

$$k_{EIx} \approx \frac{\frac{E_2}{E_1} t_2}{t_1 + \frac{E_2}{E_1} t_2} \tag{59}$$

$$I_{unit} \approx 2pt_1(k_{EIx}h)^2 + \frac{E_2}{E_1}(2p)t_2(1 - k_{EIx})^2 h^2 \tag{60}$$

$$\int_0^{l_c} Q \, ds \approx \left[\frac{E_2}{E_1}(2p)t_2(1 - k_{EIx})h \right] l_c \tag{61}$$

Thus, D_{Qx} can be approximately written as in equation 62. Further simplification can be made by inserting $A_c = l_c t_c / p$

$$D_{Qx} \approx \frac{G_c t_c h^2}{l_c p} = \frac{G_c t_c^2}{A_c} \left(\frac{h}{p} \right)^2 \tag{62}$$

These elastic constants are utilized on the next section. With them, deflection of an all-round supported panel can be estimated.

2.2.3   Mindlin-Reissner theory

Classical Kirchhoff plate theory assumes thin plates and thus that transverse shear stress effects are negligible. However, like Buannic et al. (2003, p.299) notified, classical Kirchhoff is not necessarily viable option for corrugated core sandwich plates. Mindlin-Reissner in its assumption of transverse shear effects, should yield better results. Elastic constants can be utilized in following way (Dackman & Ek 2015, p. 13;15). Equation 63 presents the matrix form for compressive loads. Extensional stiffnesses are presented in equations 64-68.

$$\begin{bmatrix} N_{xx} \\ N_{yy} \\ N_{xy} \end{bmatrix} = \begin{bmatrix} C_{11} & C_{12} & 0 \\ C_{21} & C_{22} & 0 \\ 0 & 0 & C_{33} \end{bmatrix} \begin{bmatrix} \varepsilon_x \\ \varepsilon_y \\ \varepsilon_{xy} \end{bmatrix} \tag{63}$$

$$C_{11} = \frac{E_x}{1 - v_x v_y} \tag{64}$$

$$C_{12} = \frac{v_y E_x}{1 - v_x v_y} \tag{65}$$

$$C_{21} = \frac{v_x E_y}{1 - v_x v_y} \tag{66}$$

$$C_{22} = \frac{E_y}{1 - v_x v_y} \tag{67}$$

$$C_{33} = \frac{E_y}{1 - v_x v_y} \tag{68}$$

Equation 69 presents the matrix form for bending moments. Bending stiffeness are presented in equations 70 -74.

$$\begin{bmatrix} M_x \\ M_y \\ M_{xy} \end{bmatrix} = \begin{bmatrix} C_{44} & C_{45} & 0 \\ C_{54} & C_{55} & 0 \\ 0 & 0 & C_{66} \end{bmatrix} \begin{bmatrix} \kappa_x \\ \kappa_y \\ \kappa_{xy} \end{bmatrix} \tag{69}$$

$$C_{44} = \frac{D_x}{1 - v'_x v'_y} \tag{70}$$

$$C_{45} = \frac{v'_y D_x}{1 - v'_x v'_y} \tag{71}$$

$$C_{54} = \frac{v'_x D_y}{1 - v'_x v'_y} \tag{72}$$

$$C_{55} = \frac{D_y}{1 - v'_x v'_y} \tag{73}$$

$$C_{66} = \frac{D_{xy}}{1 - v'_x v'_y} \tag{74}$$

Model employed to calculate uniform lateral load stresses by Lurie et al. (2017, p.1012) is based on classical plate theory. However, it does not consider transverse shear effects. To assess the effects, Vinson (1999, p.153 - 155) shows general solutions for sandwich panels. Chang et al. (2005, p.82 - 83) employs exact solution for corrugated core sandwich panel with elastic constants provided by Libove & Hubka (1951).

$$\frac{\delta M_x}{\delta x} + \frac{\delta M_{xy}}{\delta y} - Q_x = 0 \tag{75}$$

$$\frac{\delta M_{xy}}{\delta x} + \frac{\delta M_y}{\delta y} - Q_y = 0 \tag{76}$$

$$\frac{\delta Q_x}{\delta x} + \frac{\delta Q_y}{\delta y} + q = 0 \tag{77}$$

If previous is written in terms of bending moments M_x, M_y, M_{xy} and shear forces Q_x and Q_y, we get following:

$$M_x = C_{44}\frac{\delta \theta_x}{\delta x} + C_{45}\frac{\delta \theta_y}{\delta y} \tag{78}$$

$$M_y = C_{54}\frac{\delta \theta_x}{\delta x} + C_{55}\frac{\delta \theta_y}{\delta y} \tag{79}$$

$$M_{xy} = C_{66}(\frac{\delta \theta_x}{\delta y} + \frac{\delta \theta_y}{\delta x}) \tag{80}$$

$$Q_x = D_{Q_x}(\theta_x + \frac{\delta w}{\delta x}) \tag{81}$$

$$Q_y = D_{Q_y}(\theta_y + \frac{\delta w}{\delta y}) \tag{82}$$

For simply supported edges, $w = 0$, $\delta \theta_x/\delta x = 0$ when $x = 0, y = a$, and $\delta \theta_y/\delta y = 0$ when $y = 0, x = b$. (Vinson 1999, p.153 - 155; Chang et al. 2005, p.83). By applying Navier solution, deflection w, slopes θ_x and θ_y and distributed load function q can be written as:

$$w = \sum_{m=1,3...}^{\infty} \sum_{n=1,3...}^{\infty} w_{mn} \sin(\frac{m\pi x}{b}) \sin(\frac{n\pi y}{a}) \tag{83}$$

$$\theta_x = \sum_{m=1,3...}^{\infty} \sum_{n=1,3...}^{\infty} A_{mn} \cos(\frac{m\pi x}{b}) \sin(\frac{n\pi y}{a}) \tag{84}$$

$$\theta_y = \sum_{m=1,3..}^{\infty} \sum_{n=1,3...}^{\infty} B_{mn} \sin(\frac{m\pi x}{b}) \cos(\frac{n\pi y}{a}) \tag{85}$$

$$q = \sum_{m=1,3...}^{\infty} \sum_{n=1,3...}^{\infty} q_{mn} \sin(\frac{m\pi x}{b}) \sin(\frac{n\pi y}{a}) \tag{86}$$

The Euler coefficient q_{mn} can be written for uniformly distributed lateral load (Vinson 1999, p.155) as :

$$q_{mn} = \frac{4q}{mn\pi^2}(1 - \cos(m\pi))(1 - \cos(n\pi)) \tag{87}$$

When previous terms are re-arranged, they can be written in matrix for as $[L][u_{mn}] = [P]$. L_{ij} are auxiliary variables, $[u_{mn}]$ is matrix of coefficients and $[P]$ matrix of Euler's coefficient.

$$[L] = \begin{bmatrix} L_{11} & L_{12} & L_{13} \\ L_{21} & L_{22} & L_{23} \\ L_{31} & L_{32} & L_{33} \end{bmatrix} \tag{88}$$

$L_{11} = C_{44}(\frac{m\pi}{b})^2 + C_{66}(\frac{n\pi}{a})^2 - D_{Q_x}$ $\quad L_{12} = (C_{45} + C_{66})(\frac{mn\pi^2}{ab})$ $\qquad L_{13} = -D_{Q_x}(\frac{m\pi}{b})$

$L_{21} = L_{12}$ $\qquad\qquad\qquad\qquad\qquad L_{22} = C_{55}(\frac{n\pi}{a})^2 + C_{66}(\frac{m\pi}{b})^2 - D_{Q_y}$ $\quad L_{23} = -D_{Q_y}(\frac{n\pi}{a})$

$L_{31} = -L_{13}$ $\qquad\qquad\qquad\qquad\qquad L_{32} = -L_{23}$

$L_{33} = D_{Q_x}(\frac{m\pi}{b})^2 + D_{Q_y}(\frac{n\pi}{a})^2$

$$[u_{mn}] = \begin{bmatrix} A_{mn} \\ B_{mn} \\ w_{mn} \end{bmatrix} \tag{89}$$

$$[P] = \begin{bmatrix} 0 \\ 0 \\ q_{mn} \end{bmatrix} \tag{90}$$

Using above equations, coefficients A_{mn}, B_{mn} and w_{mn} can be solved as $[u_{mn}] = [L]^{-1}[P]$. Then w, θ_x and θ_y can be solved, in addition to M_x, M_y and M_{xy}. Vinson (1999, p.155) offers two ways to calculate stresses in the face sheets: using simple equation $\sigma_{ij} = M_{ij}/t_f/h_c$ or by using laminated plate method, also employed by Lurie et al. Calculations of this section are under Mindlin-Reissner-module in Python code.

2.2.4 Critical loadings

The national version of Eurocode 3 is utilized to assess critical loading cases, namely SFS-EN 1993-1-1 for general, SFS-EN 1993-1-3 for corrugated core and SFS-EN 1993-1-5 for faceplates. Because of the thinness of the faceplates and core, the profile is deemed as cross-section class 4. Thus, its effective widths have to be calculated accordingly.

According to SFS-EN 1993-1-5 (p.16), for unstiffened plates, effective area can be calculated with help of brutto cross-sectional area A_{brutto} and the final reduction factor ρ_c as follows:
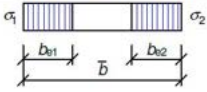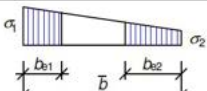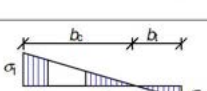
$$A_{eff} = \rho_c A_{brutto} \tag{91}$$

Reduction factor ρ can be calculated as follows:

$$\rho = 1.0, \lambda_p \leq 0.673$$

$$\rho = \frac{\lambda_p - 0.055(3+\psi)}{\lambda_p^2}, \lambda_p \geq 0.673, (3+\psi) \geq 0 \tag{92}$$

where $\lambda_p = \sqrt{\frac{f_y}{\sigma_{cr}}} = \frac{\overline{b}/t}{28.4\varepsilon\sqrt{k_\sigma}}$. $\overline{b}$ is appropriate width of the plate, t is thickness, $\varepsilon = \sqrt{235/f_y}$, ψ is stress ratio and k_σ is corresponding buckling factor. Both ψ and k_σ are presented in the figure 5.

Stress distribution (compression positive)				Effective^P width b_{eff}		
				$\psi = 1$: $b_{eff} = \rho \, \overline{b}$ $b_{e1} = 0,5 \, b_{eff}$ $\qquad b_{e2} = 0,5 \, b_{eff}$		
				$1 > \psi \geq 0$: $b_{eff} = \rho \, \overline{b}$ $b_{e1} = \frac{2}{5-\psi} b_{eff}$ $\quad b_{e2} = b_{eff} - b_{e1}$		
				$\psi < 0$: $b_{eff} = \rho \, b_c = \rho \, \overline{b}/(1-\psi)$ $b_{e1} = 0,4 \, b_{eff}$ $\qquad b_{e2} = 0,6 \, b_{eff}$		
$\psi = \sigma_2/\sigma_1$	1	$1 > \psi > 0$	0	$0 > \psi > -1$	-1	$-1 > \psi > -3$
Buckling factor k_σ	4,0	$8,2/(1,05+\psi)$	7,81	$7,81 - 6,29\psi + 9,78\psi^2$	23,9	$5,98(1-\psi)^2$

Figure 5. Stress ratio ψ, buckling factor k_σ and effective widths, according to SFS-EN 1993-1-5 (p.17)

Behaviour of the plate can vary between plate and beam, as shown in figure 6, depending on support, and relation between the plate width and length. Because of characteristics of sandwich panel, faceplates per unit width can be handled as beams.
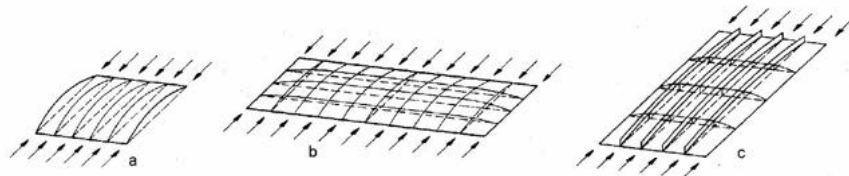
Figure 6. Beam-like behaviour of the plate, when a) no side supports, b) length-to-width-ratio is small c) longitudinally stiffened plate with high length-to-width-ratio (SFS-EN 1993-1-5, p.17)

Critical stress as beam-like behaviour can be calculated as follows:

$$\sigma_{cr,c} = \frac{\pi^2 E t^2}{12(1-v^2)\overline{a}^2} \tag{93}$$

where $\bar{a}$ is length of the plate (SFS-EN 1993-1-5, p. 20). Critical stress for equivalent orthotropic plate (SFS-EN 1993-1-5, p. 42) can be calculated as follows:

$$\sigma_{cr,p} = k_\sigma \sigma_E \tag{94}$$

$$\sigma_E = \frac{\pi^2 E t^2}{12(1-v^2)\bar{b}^2} \tag{95}$$

Slenderness of the beam λ_c (SFS-EN 1993-1-5, p. 21) can be calculated as:

$$\lambda_c = \sqrt{\frac{f_y}{\sigma_{cr,c}}} \tag{96}$$

Reduction factor χ_c for beam (SFS-EN 1993-1-1, p.61) can be calculated as follows:

$$\chi_c = \frac{1}{\phi + \sqrt{\phi^2 - \lambda_c^2}} \tag{97}$$

where $\phi = 0.5[1 + \alpha(\lambda_c - 0.2) + \lambda_c^2]$ and $\alpha = 0.21$. Final reduction factor ρ_c can be calculated as follows:

$$\rho_c = (\rho - \chi_c)\xi(2 - \chi) + \chi_c \tag{98}$$

where $\xi = \frac{\sigma_{cr,p}}{\sigma_{cr,c}} - 1$, $0 \leq \xi \leq 1$. With the final reduction factor, effective areas of the cross-section can be assessed. It should be noted that effective areas are different depending on loading case, normal or bending load. Figure 7 shows the effective areas in respect of loading case.
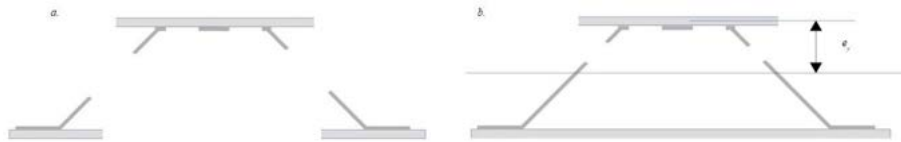
Figure 7. Demonstration of effective areas of the panel cross-section, when loaded with a. normal load and b. bending load. e_y is placement of new bending axes due to effective areas.

Placement of the new bending axis can be calculated with help of individual the first moment of areas S_i and individual effective cross-sectional areas $A_{i,eff}$ as follows:

$$e_y = \frac{\sum S_i}{\sum A_{i,eff}} \tag{99}$$

With the newly established e_y, a new stress ratio ψ can be calculated, and above described process continued. The iteration is continued until $\rho = 1.0$ and the placement of the axis does not change.

When the final A_{eff} is established, the critical load (SFS-EN 1993-1-1, p.53) can be assessed as follows:

$$N_{cr} = \frac{A_{eff}f_y}{\gamma_{M0}} \tag{100}$$

where γ_{M0} is safety factor given nationally as 1.0. Similarly, the critical moment can be calculated as follows:

$$M_{cr} = \frac{W_{eff}f_y}{\gamma_{M0}} \tag{101}$$

where W_{eff} is effective section modulus. It can be calculated as:

$$W_{eff} = \frac{I_{eff}}{e_y} = \frac{\sum I_{i,eff} + \sum A_{i,eff}y_i^2}{e_y} \tag{102}$$

where $I_{i,eff}$ are individual second moment of areas of cross-section parts and y_i are individual distances from center of masses of the individual cross-section parts to the e_y.

Shear is deemed to be carried solely by the core. For the corrugated profile, it can be assessed from SFS-EN 1993-1-3 (p.45) as follows:

$$V_{cr} = \frac{A_c f_{bv}}{\gamma_{M0}} \tag{103}$$

where A_c is core area, and shear buckling strength f_{bv} is given in the table 2

*Table 2. Shear buckling strength f_{bv} (SFS-EN- 1993-1-5, p45).*

| $\lambda_w = 0.346 s_w/t \sqrt{f_y/E}$	f_{bv}
$\lambda_w \leq 0.83$	$0.58 f_y$
$0.83 \leq \lambda_w \leq 1.40$	$0.48 f_y/\lambda_w$
$\lambda_w \geq 1.40$	$0.67 f_y/\lambda_w^2$
s_w	$(h - 2t_f - t_c)/sin(\vartheta)$

2.3   Finite element model

Due to its thin faceplates and core, 0.75 and 0.5 mm, respectively, main concern of failure in the sandwich structure is buckling under load (Vinson 1999, p.245). To assess the buckling load, FEM was created with Femap NX Nastran 2020.1 -software.

Faceplates and core were modelled with CQUAD4 elements. Element lengths were set to 7 mm in both the core and the faceplates. Eight elements were used along one wavelength in faceplates in order to capture the buckling form. For the same reason, six elements were created on web. (NX Nastran User's Guide 2016, p.632.) On the connection between faceplate and core, two and three elements were used on the single-weld and double-weld models, respectively. These are presented in the figures 8, 9 and 10. The effect of welds were captured
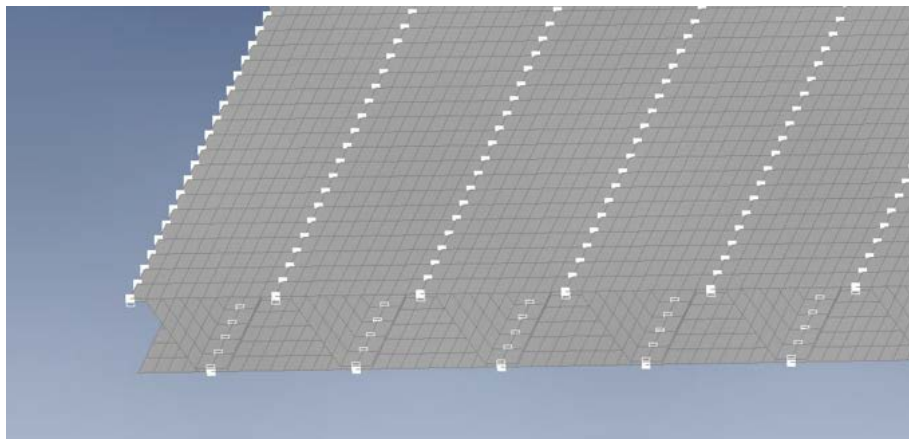
by using rigid elements between faceplates and the core. RBE2 elements were used, with translations and rotations locked in relation to source node (Caccese & Yorulmaz 2009, p.25; SANDCORE 2005, p.40).
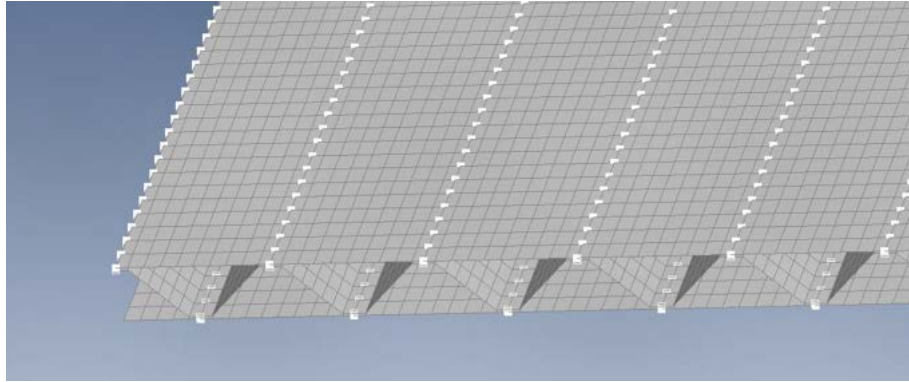
Figure 8. Arrangement of the elements in the single-weld model.
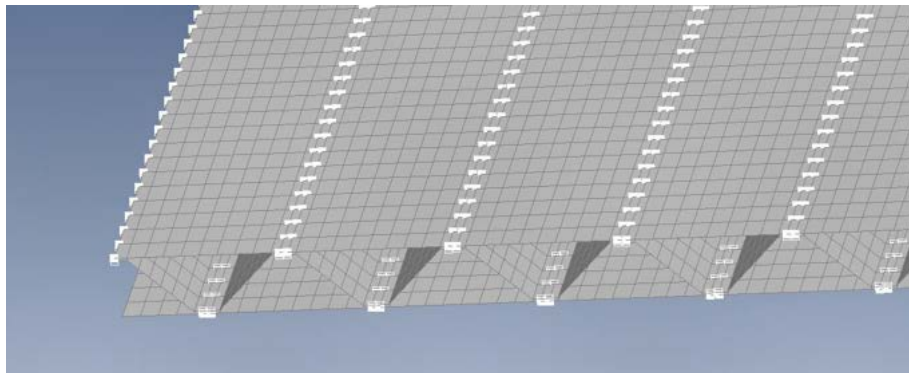
Figure 9. Arrangement of the elements in the double-weld model.

Figure 10. Arrangement of the elements in 60 °core model

Material properties used in the model are listed in the table 3. For linear elastic buckling, only E and ν were used. For nonlinear analysis, Femap bi-linear material model was used with

the help of said material properties. For DC01, nominal value of 220 MPa was used for both yield and ultimate strength. This was due to the large variety in both values. DC01 is a deep-drawing steel. Vinco (2020, p.1) recommends using 235 MPa value for design purposes. Lower value was chosen due to safety concerns (SFS-EN 1993-1-1, p.42). Calculations were done also with the true tensile test values of both 0.5 mm and 0.75 mm sheets, as provided by the manufacturer (TATA Steel 2019, p.2). Calculations were also done with S355 to assess effect of strength to the results. Its values were provided by ThyssenKrupp (2019, p.2).

*Table 3. Material properties of the different models.*

Material	E [GPa]	ν	f_y [MPa]	f_u [MPa]	A_{80} [%]
$S355$	210	0.3	355	470	18
$DC01(true)_{0.75}$	-	-	200	330	34
$DC01(true)_{0.5}$	-	-	192	324	39
$DC01(nom.)$	-	-	220	220	28

In the table 4, there are chemical compositions listed. They are taken from the sheets of 0.5 mm and 0.75 mm, provided by the manufacturer (TATA Steel 2019, p.2). Variation of chemical composition can affect mechanical properties of the material.

*Table 4. Chemical composition of the sheets.*

Material	C	Mn	P	S	Si	Al	Cu	Cr	Ni
$DC01_{0.75}$	0.043	0.222	0.006	0.005	0.020	0.038	0.017	0.031	0.024
$DC01_{0.5}$	0.044	0.212	0.007	0.009	0.013	0.041	0.013	0.019	0.023
	Mo	Nb	V	N	B	Ti	Al-Zq	Sn	
$DC01_{0.75}$	0.003	0	0.001	0.0043	0	0.002	0.037	0.001	
$DC01_{0.5}$	0.004	0	0.002	0.003	0	0.001	0.039	0.001	

Constraints were applied nodally. The figures 11 and 12 present the constraint setups for the two cases. In the first case, only edges along y-axis were constrained, one edge as pinned and the other as simply supported. The panel behaves like a beam.
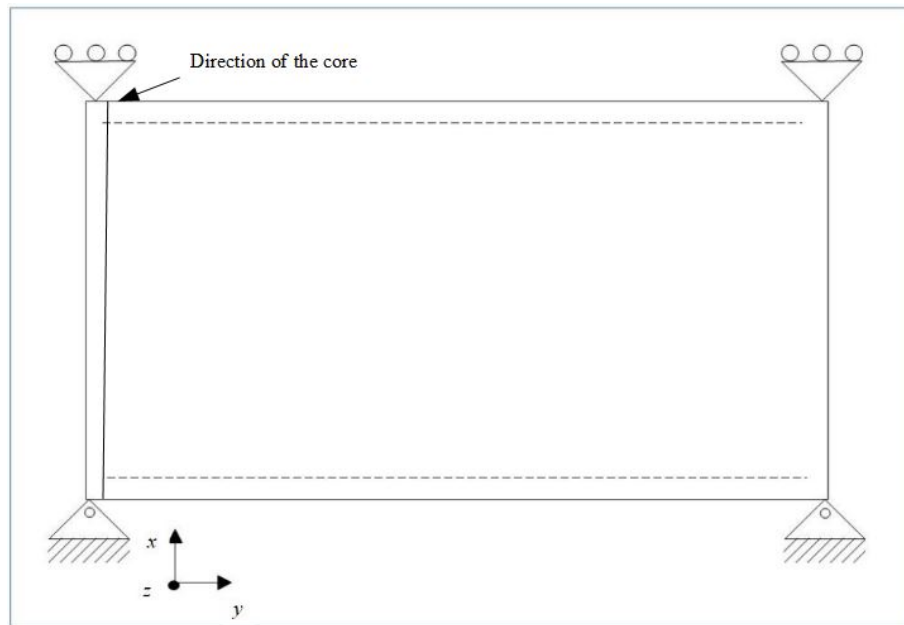
Figure 11. The first constraint setup (C1). One end along y-axis is pinned, the other one is simply supported. Edges along x-axis are unsupported.

In the second case, edges along the y-axis were constrained similarly to the first case, but also the edges along the x-axis were simply supported. Models were simulated as corrugation leg upwards, and constraint applied to the edge of the lower faceplate. This is not optimum design as there is no end plate, however panels are tested as-built.
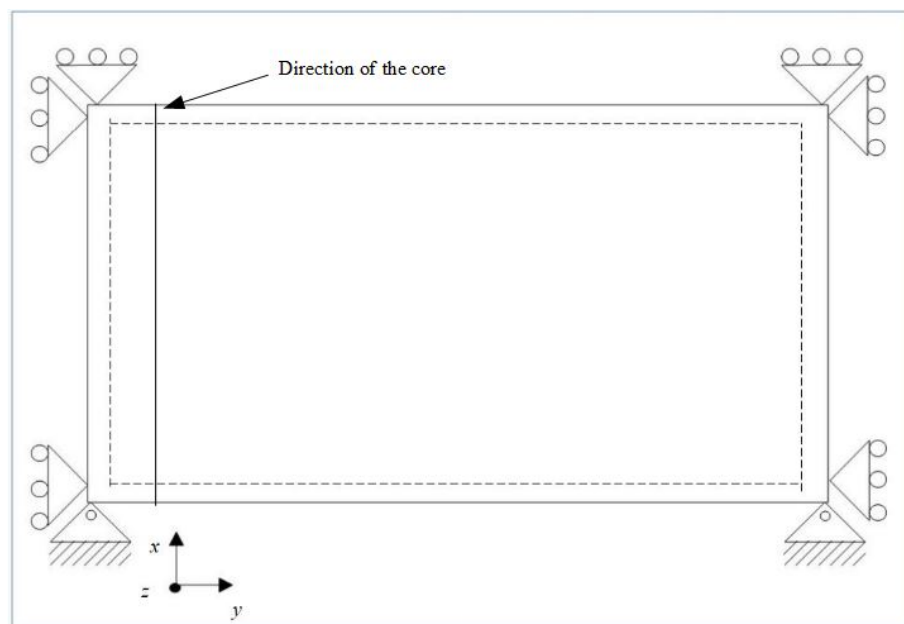
Figure 12. The second constraint setup (C2). One end along y-axis is pinned, the other one is simply supported. Edges along x-axis are simply supported.

2.4 Design of welds

Design of the welds of the corrugated core sandwich panel were checked. According to EN 1993-1-3 (p. 69), because of the total thickness being $t_{total} = t_c + t_f \leq 4$ mm, clause given by said standard can be followed. In general, the resistance of the connection should be fulfilled by the structure and not by the weld. This can be accomplished by ensuring that the throat size of the weld is at least as much as the thickness of the structure. This means at the narrowest 0.5 mm throat size, due to the thickness of the core. If the partial safety factor $\gamma_{M2} = 1.25$ is employed, this means around 0.63 mm weld throat thickness.

2.5 Laboratory experiments

Two panels were bending tested in the laboratory, in as-built condition from HT-Laser production. There are many different ways to test the bending behaviour of the sandwich panel: patch load, three-point, four-point and uniform load (Kozak 2003, p. 62; Frank, Romanoff & Remes 2013, p. 727; Lange & Nelke 2013, p. 902; Valdevit, Wei, Mercer, Zok & Evans 2006, p. 4895; Wennhage & Zenkert 1998, p. 2-3; Järvenpää, Mäntyjärvi & Hietala 2014, p. 783; Estrada-Martínez, Mollón & Bonhomme 2016, p. 284; SANDCORE 2005, p. 47; Kujala et al. 2003, p. 44).

For this case, uniform-type load was applied. Three possible ways were considered: pressurized waterlines by Kujala et al (2003, p.44), water bag and inverted pressing by Wennhage & Zenkert (1998, p. 2-3) and multiple line loads simulating uniform load by Estrada-Martínez, Mollón & Bonhomme (2016, p. 284). Due to equipment concerns, method employed by Estrada-Martínez, Mollón & Bonhomme was chosen.

Figures 13 and 14 present the 3D sketch of the test device. Edge along the x-axis was divided to eight segments. Similarly, edge along y-axis was divided to 16 segments. As design load, 96 kN was used, as it exceeds maximum linear buckling load calculated with FEM including safety margin of 1.5. Square hollow section tubes of 100x100x6 were used as levers to distribute two concentrated loads to more uniform-like load. Solid bars of diameter 30 mm were used, both as axles to allow the pivoting of the test device, as well as to distribute the load finally to the upper plate as pressing components. Those used as pressing components were machined so that the middle section was narrowed to diameter of 25 mm. Under the pressing components, 6 mm thick plywood was used to distribute the load on the upper plate. Supports were made of 60 mm diameter steel bars. For the first constraint setup, they were situated 30 mm inward from the end of the panel. For the second constraint setup, they were situated 30 mm inward from the end of the panel, and 30 mm inward from the edge of the panel. It should be noted that the laboratory supports differ from supports used in FEM in this regard, as in FEM, supports were at farthest ends and edges of the panel.
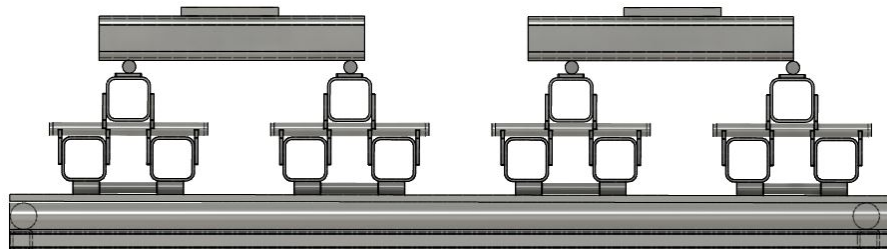
Figure 13. 3D sketch of the test arrangement, long side.
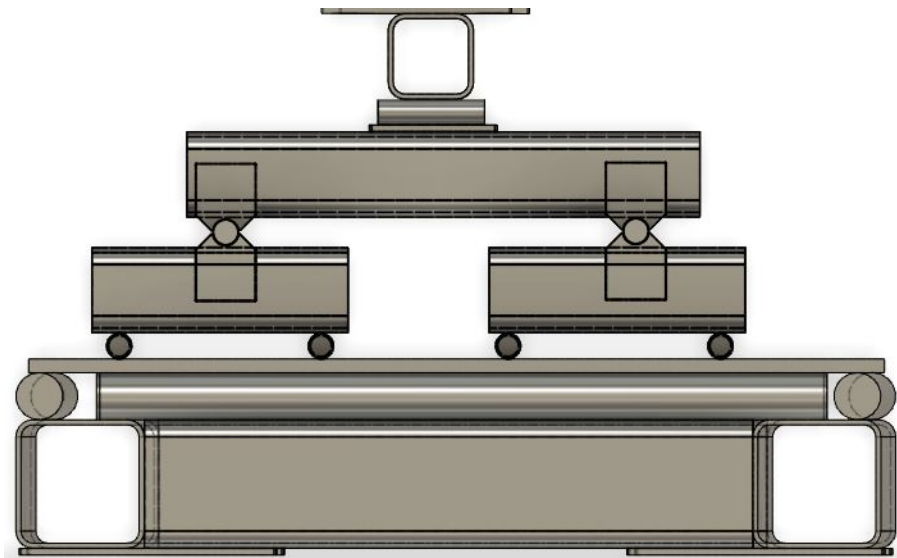
Figure 14. 3D sketch of the test arrangement, short side.

The proofing of the test device is presented in the figure 15. As the figure shows, the behaviour of the test device was proofed for both constraint setups with 8 mm thick steel plate of S235, before the actual tests with the panels. Test device was pressed down up to 8 mm as true displacement of the steel plate. As there were no adverse movement, the device was deemed safe for the actual tests.

Figure 15. Proofing the test device with 8 mm steel plate of S235. Cylinder support is missing.

Tested panels were straight from manufacturer, with possible manufacturing errors. The figures 16 and 17 present these errors, most notably that core is not in line with the upper and the lower plates. This error is present in both panels. Also, because of this, there are marks of laser cutting on the core before the laser has come on top of the upper plate. Their initial shapes were measured, and are presented in the appendices A and B. Both panels were a bit arched. The panels were named KV-1 and KV-2, depending whether the panel was used in the first test with the first constraint arrangement or in the second test with the second constraint arrangement.

Figure 16. Manufactured panels.

Figure 17. Manufactured panels.

2.5.1 Test procedure for the first test

Test logs for the first test with the sample KV-1 is shown in the appendix A. There are also presented the placement and type of the strain gauges used in the test. Test was conducted in phases, some planned and some unexpected, such as exceeding available capacity of the cylinders . Forces and displacements of the both cylinders were recorded. The actual displacement was recorded with a laser sensor. There were four strain gauges installed: SG1A & B, SG2A & B, SG3A & B and SG4. The first strain gauge (SG1A & B) was placed on top of the nearest weld to the midsection of the panel. The second (SG2A & B) and the third gauges (SG3A & B) were placed in the middle of the plate field, near the midsection of the panel, the second on the upper and the third on the lower faceplate. The fourth (SG4) strain gauge was placed on the web plate near the edge of the panel, on top of support. These placements were chosen according to the highest stress fields from FEM calculations. Gauges SG1 - SG3 on upper and lower plates were biaxial Rosette-type items, thus they measured both x- and y-strains. Gauge SG4 was measuring only y-strains. It was placed to capture core crushing effect.

The test was done via displacement control of the cylinders. This was deemed safer than force-control, as the stability of panel was still somewhat unknown. The actual control of loading was manual. Loading rate was 1 mm/min. First, the control was done by following the displacement of the cylinders. After around 11 mm displacement of the cylinders, the control was carried out by following the laser sensor displacement. The distance of the laser sensor from the upper plate during start was 6.958 mm. This distance includes the displacement due to the weight of the loading grid. During the first phase, the cylinders were driven to displacement of around 7 mm, after which load was reset to zero, but not the strain gauges. This was done to observe the behaviour of the test setup. After resetting of forces, cylinders were driven to the displacements of the around 8 mm and 10 mm, after which the test had to be started over again precipitously, as the available capacity of the cylinders (20 kN) was exceeded. The strain gauge SG2A was re-zeroed, as it had already reached its limit

of 5000 μstrains. After the available capacity of cylinders was raised, the cylinders were driven back to the 10 mm, and further to 11 mm. After this, displacement of the laser sensor was followed instead of the cylinders. Between displacements of around 22 mm - 32 mm, the load increments were done by around 1 mm at the time. After that, bigger increments up to 5 mm were taken, as the panel had clearly reached its maximum load capacity. After reaching the maximum displacement threshold of the laser (50 mm), the laser sensor was reinstalled so the the distance to the upper faceplate was 33.1 mm. The panel was then driven again so that laser threshold was once again reached at new 50 mm, true displacement being around 88 mm. Test was stopped here.

2.5.2 Test procedure for the second test

The test logs and placements of the strain gauges of the test sample KV-2 are presented in the appendix B. As with the first test, cylinders were displacement-controlled. The loading rate was set to 1 mm/min. Due to the limits of 5000 μstrains of the first test being too small, the strain gauges were calibrated up to 10 000 μstrains for the second test. Placement of the strain gauges on the upper and lower plates was similar to the first test. The placement of the web plate gauge was changed to the nearest diagonal at the middle-end of the panel. The laser displacement sensor was at the same spot as with the first test, and its zero-level was 1.099 mm.

Cylinders were driven to 4 mm, then to 7 mm, after which 1 mm load increments were taken up to 11 mm of cylinder displacement. Then, displacement recorded by the laser displacement sensor was followed. Load increments of 2 mm were taken. At 22 mm displacement, coefficient of SG2A strain gauge was changed, as it was near its threshold. After 30 mm displacement, load increments of 5 mm were taken to speed up the testing. Coefficient of SG1A strain gauge was changed at 40 mm of displacement. Test was continued until around 50 mm of displacement, when one of the axels was nearly slipping from the loading grid, which made the continuation of the test unsafe. However, the plastic capacity of the panel was achieved.

3   Results

In this chapter, analytical, FEM and laboratory test results are presented and they are compared to each other. From FEM, linear, elastic buckling and nonlinear results are presented. Also, three different variations of the corrugated core sandwich panel and their results are presented and compared.

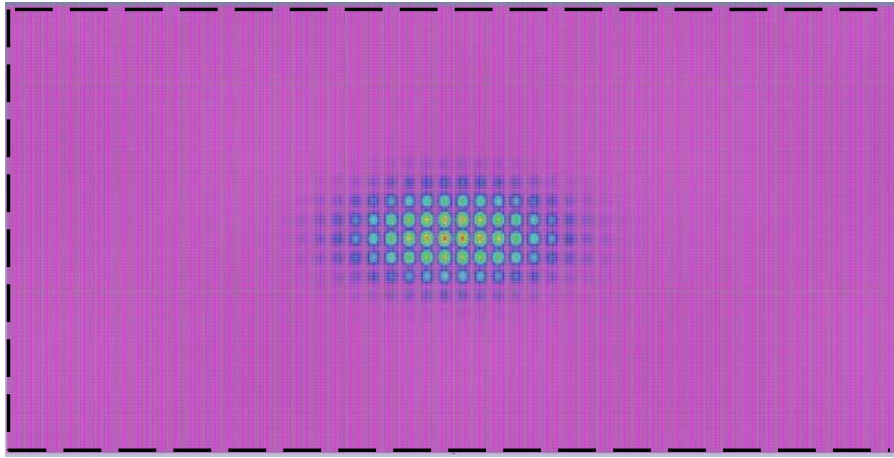### 3.1   Linear elastic buckling of the panel

The figure 18 presents elastic buckling behaviour of the single weld panel. The constraints are according to the first constraint arrangement, demonstrated by the dashed lines. It can be seen that the upper faceplate is critical for linear buckling, with buckling modes taking place at the center of the panel.
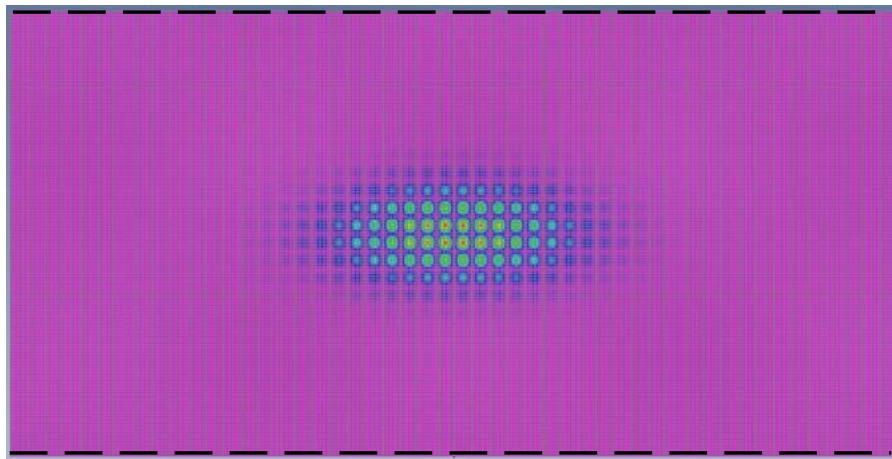
Figure 18. Buckling of the single weld panel, with the first constraint arrangement. Dashed lines demonstrate the constraint. Critical buckling load is 31.8 kN/m^2

Linear elastic buckling of the single weld panel, with the second constraint arrangement, demonstrated by the dashed lines, is presented in the figure 19. As with the first constraint arrangement, the buckling modes take place at the upper faceplate, at the center.
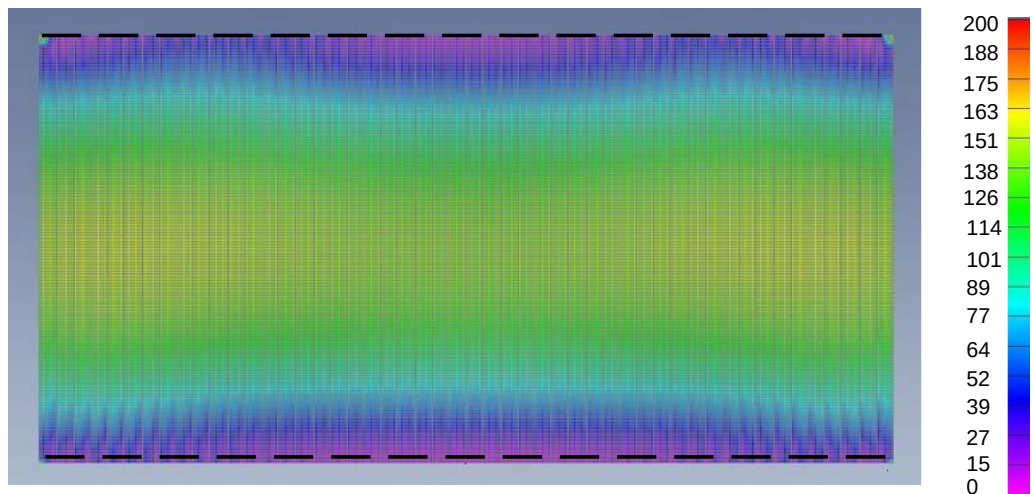
Figure 19. Buckling of the single weld panel, with the second constraint arrangement. Dashed lines demonstrate the constraint. Critical buckling load is 31.79 kN/m^2.

Linear elastic buckling modes of the the panel with 1 mm thick faceplates their location do not differ from the single weld panel. Linear elastic buckling modes of the double-weld panel, with the first and the second constraint arrangements, there is a little difference compared to the previous panels on the location of the modes. However, there is a size difference. With the first constraint arrangement, the buckled area is a bit smaller, whereas with the second constraint arrangement, the buckled area is distinctively larger. 60-degree core angle exhibits no difference in location nor size of the buckled area, compared to the single-weld panel, with either constraint arrangement.
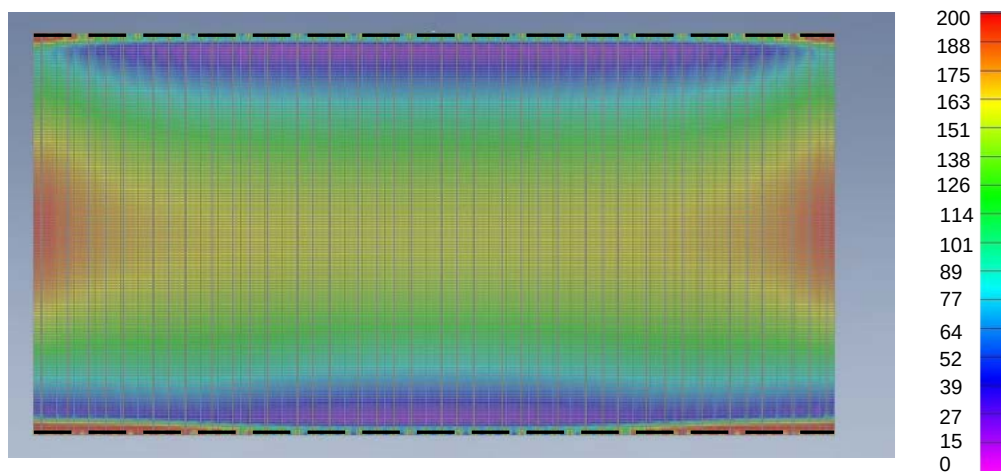
3.2   Nonlinear behaviour

The figure 20 presents the results of nonlinear FEM for the single weld panel, from the top of the panel. The constraints are according to the first constraint arrangement. Colors present Von Mises stress distribution. The upper faceplate is stressed, but the stresses do not equate the nominal yield strength of the DC01.

Figure 20. Nonlinear behaviour of the single-weld panel, with the first constraint arrangement, top view.

From the figure 21, which presents the bottom view of the panel, it can be seen that the highest stresses in the lower faceplate take place at the edges and ends of the panel. These stresses equate to the nominal yield strength of the DC01.

Figure 21. Nonlinear behaviour of the single-weld panel, with the first constraint arrangement, bottom view.
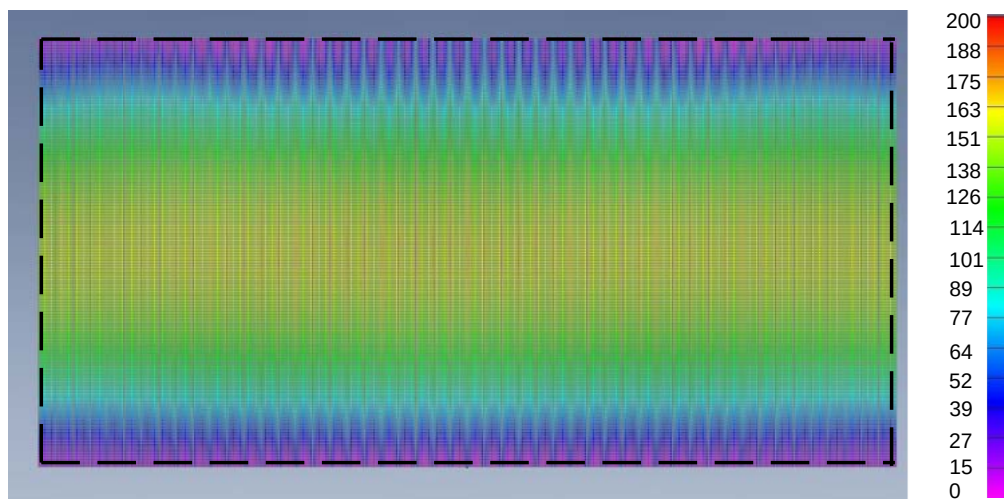
Figure 22 present above mentioned panel from isometric view. It can be seen that the core is heavily stressed towards the edges of the panel. These stresses equate to the nominal yield strength of the DC01.
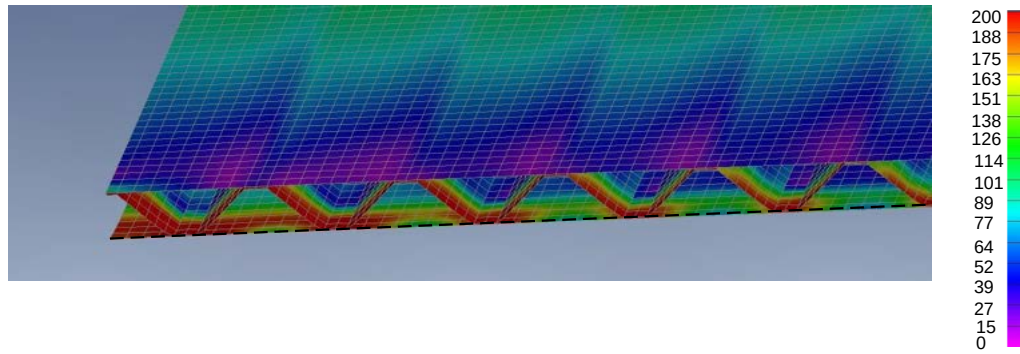
Figure 22. Nonlinear behaviour of the single-weld panel, with the first constraint arrangement, isometric view.

For the second constraint arrangement, the figure 23 presents the top view of the single-weld panel. It can be seen that the stresses do not equate to the nominal strength of the DC01.

Figure 23. Nonlinear behaviour of the single-weld panel, with the second constraint arrangement, top view.

The figure 24 presents the bottom view of the panel. It can be seen that edges of the lower faceplate are heavily stressed. The stresses equate to the nominal yield strength of the DC01.

Figure 24. Nonlinear behaviour of the single-weld panel, with the second constraint arrangement, bottom view.

The isometric view in the figure 25 reveals that the core is heavily stressed. The highest stresses in the core concentrate at the center-end of the panel. Those stresses are equal to the nominal yield strength of the DC01.
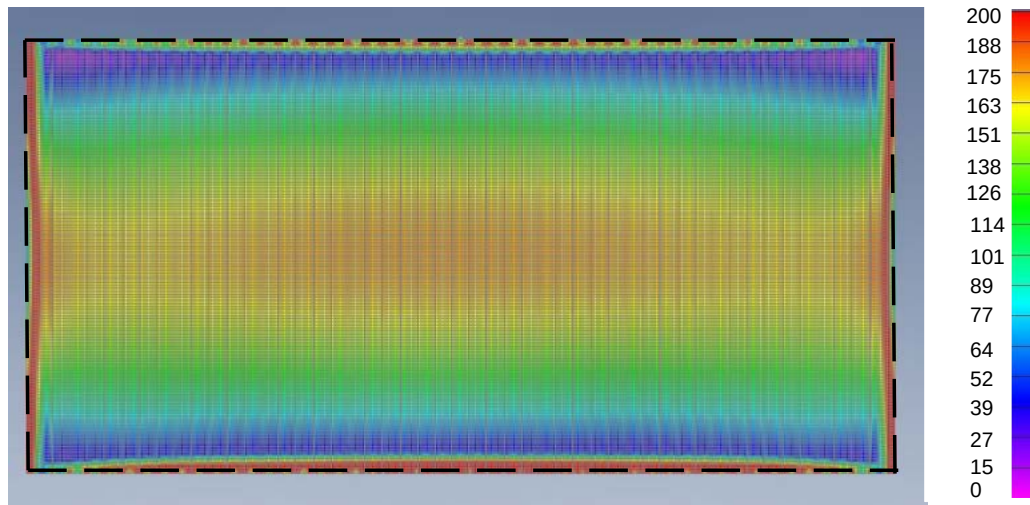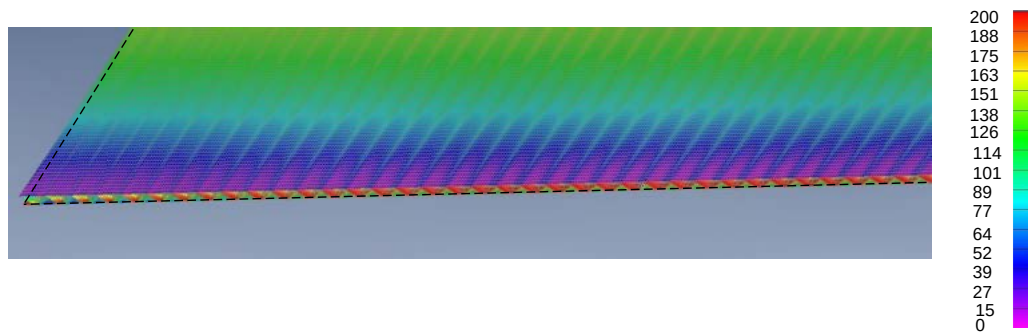

Figure 25. Nonlinear behaviour of the single-weld panel, with the second constraint arrangement, isometric view.

There is little difference on the location nor size of the stress areas with true DC01 values, compared to the nominal DC01 values, in either constraint arrangement. However, the maximum stress values themselves are lower than with nominal DC01, as expected.

To assess the effect of the strength of the material, S355 was simulated for the single-weld panel, for both the core and faceplates. Thicknesses remained the same. There is little difference in location and sizes of the stress areas compared to the DC01 panel in the first constraint arrangement, however, their values do not reach the yield strength of S355. Thus, it can be said that faceplates are not critical. With the second constraint arrangement, again, there is little difference on the size and placement of stress areas compared to the DC01

panel. However, stresses at the lower faceplate are not as high in relation to yield strength, as with DC01 panel. Highest stress areas in the core are at the edges of the panel. These stresses reach the yield strength of the S355. Stress concentrates on the center-end of the core, and to the edge side of the lower faceplate. These stresses equate to the yield strength of the S355.

To assess the effect of faceplates to the strength of the sandwich panel, 1 mm thick faceplates were introduced. The core thickness was not altered. The material was nominal DC01. The constraints are according to the first constraint arrangement. Once again, the stress areas do not change. Faceplate stresses are however lower than yield stress of DC01. This is not the case in the core, where stresses reach the nominal yield strength of the DC01 towards the edges of the panel. With the second constraint arrangement, again, no difference in the stress areas compared to the normal panel. Lower faceplate is the most heavily stressed from the faceplates, although the stresses do not reach the nominal yield strength of the DC01. In the core, the peak stresses and the center-end reach the yield strength of the DC01.

Double-weld was considered, due to its assumed simplicity production flow-wise. The spacing of the welds was not optimized through manufacturability nor load carrying capacity - the goal was to see if double-welds ave any effect on the behaviour of the panel. No geometry nor material changes were implemented on the panel itself. Stress areas do not differ from normal panel, however the lower faceplate is clearly more heavily stressed. Once again, the core stresses are the most at the edges of the panel. Those stresses reach nominal yield stress of the DC01. Stress areas of double-weld panel with the second constraint arrangement do not differ from the single weld panel. However, areas of max stress, equating to the nominal yield strength of DC01, are much larger in both the upper and lower faceplates. The core exhibits the same behaviour as in previous cases, where the highest stresses take place at the center-end of the panel.

Another variation of the panel was one with the core angle of 60 degrees. This was done to shorten the unsupported length of the faceplates, to rise the threshold for buckling. Thicknesses were kept the same as in the normal panel, as well as the height of the panel was unaltered. With the first constraint arrangement, the stress areas do not differ from normal panel. However, the upper and lower faceplates are highly stressed, as the areas of stress equal to the nominal yield strength of DC01 are larger. Core is, once again, stressed towards the edges of the panel, as well as at the center of the panel.

Thus far, behaviours of the panels have not differed from each. However, when the panel with the 60 °core was simulated with the second constraint arrangement, its behaviour distinguished remarkably from the others. Figures 26 and 27 show the behaviour unscaled, from

top and bottom view, respectively. There is clear signs of catastrophic failure, occurring at the edges of the panel.
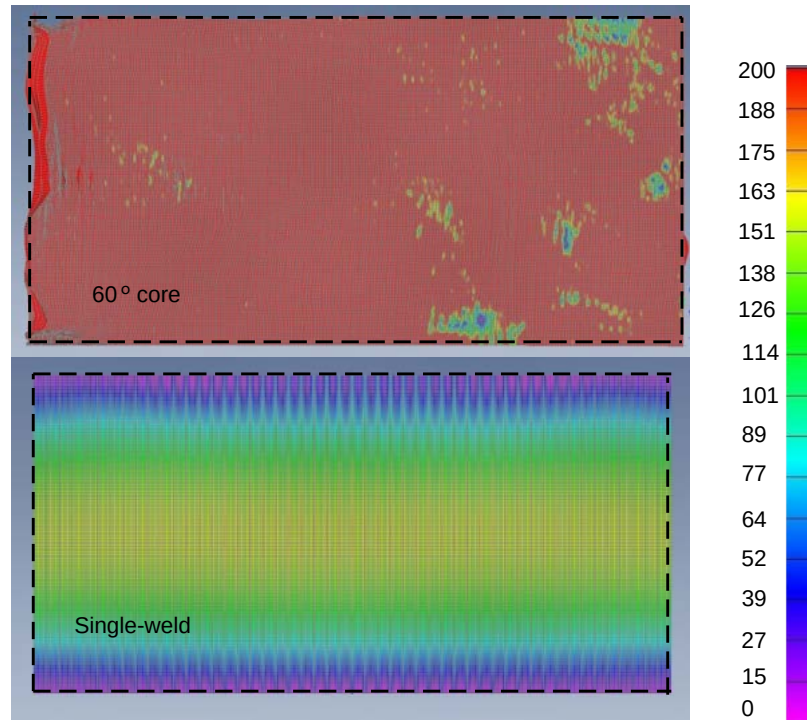
Figure 26. Nonlinear behaviour of panel with 60 °core, with the second constraint arrangement, top view.
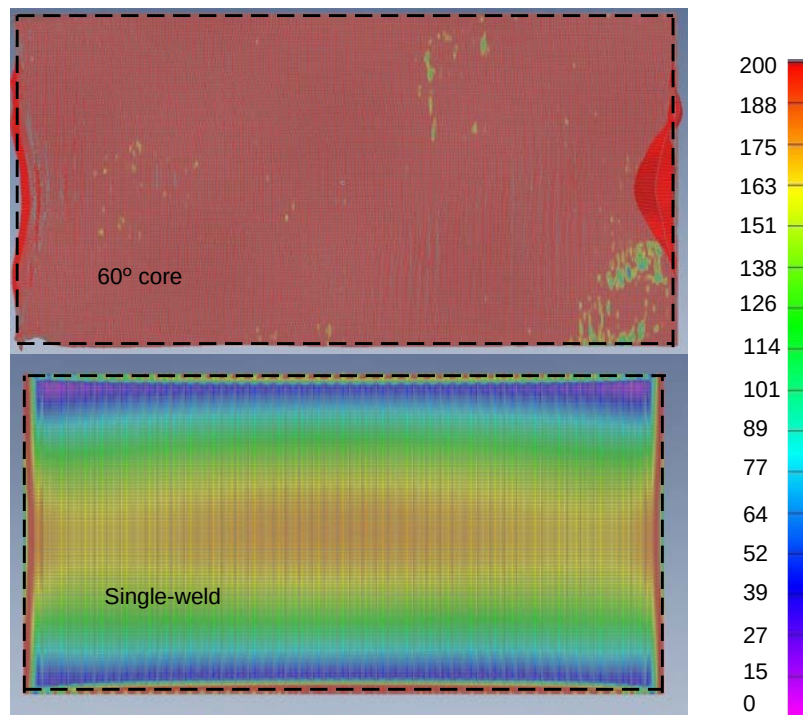
Figure 27. Nonlinear behaviour of panel with 60 °core, with the second constraint arrangement, bottom view.

In figure 28, top images are scaled down to 0.1 times, to get better view on the behaviour of the panel. It can be clearly seen that the edge of the lower faceplate has crumbled inwards, which have led to the catastrophic failure. This is further implicated by the size of stress areas where stress equals to the nominal yield strength of the DC01.
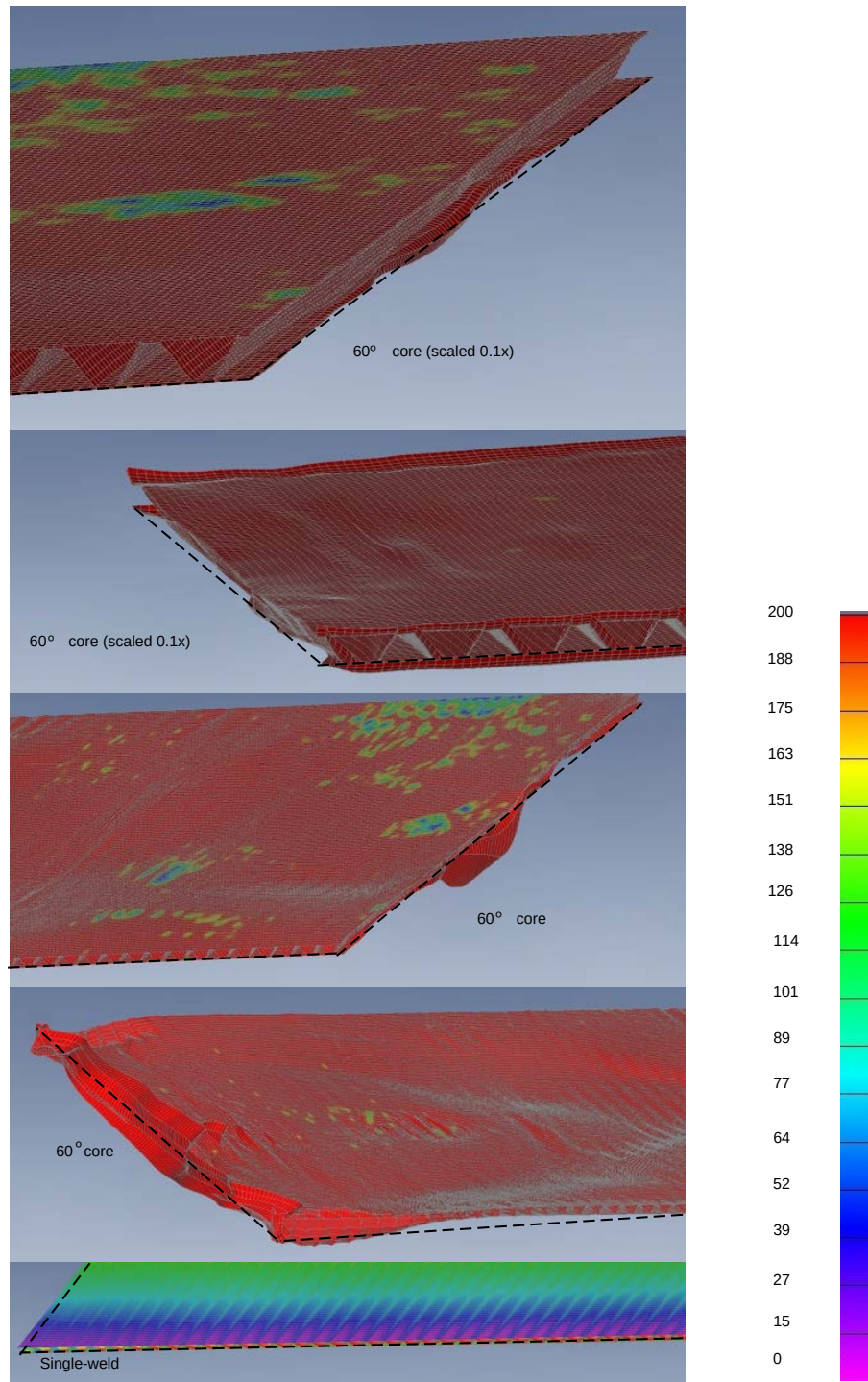
Figure 28. Nonlinear behaviour of panel with 60 °core, with the second constraint arrangement, isometric view.

3.3   Results of the laboratory tests

Laboratory tests were conducted according to the procedures, introduced in the section 2.5. The results will be presented in the form of force-displacement for both test samples KV-1 and KV-2. Stress-displacement charts are presented in appendices I and J. Photos of defor-

mations are presented in appendices D and E.

Figure 29 and 30 present the force-displacement charts of the first cylinder (S1), the second cylinder (S2) of KV-1 and comparison with results obtained by FEM. Charts are presented for both cylinders, because there was asymmetry between them in forces, due to slight asymmetry in stiffness of the panel. Displacement is the true displacement of the midsection of the panel, according to the laser sensor. For reference, force-displacement results of FEM are drawn on the same charts. These results are those with true DC01 material values.
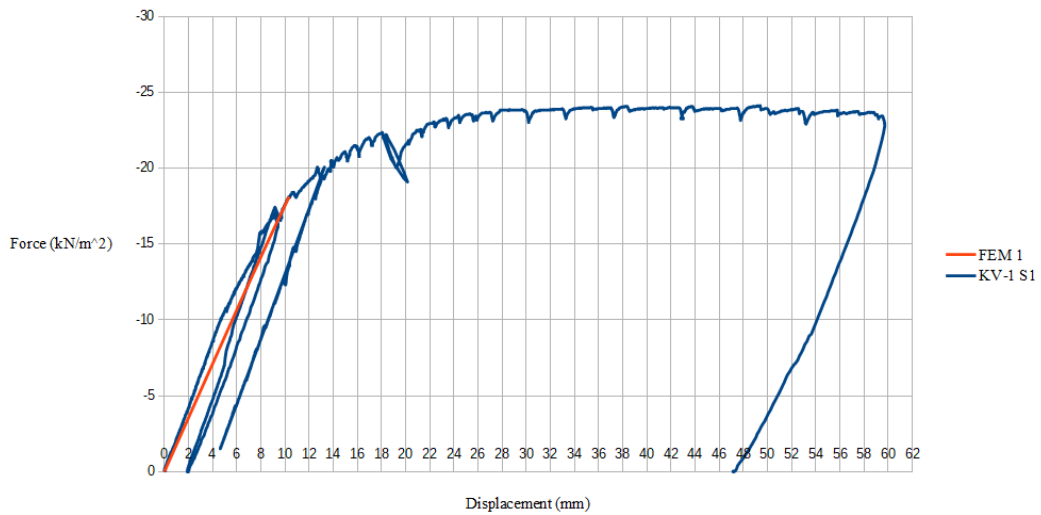
Figure 29. Force-displacement of the first cylinder. FEM results are drawn as a reference.
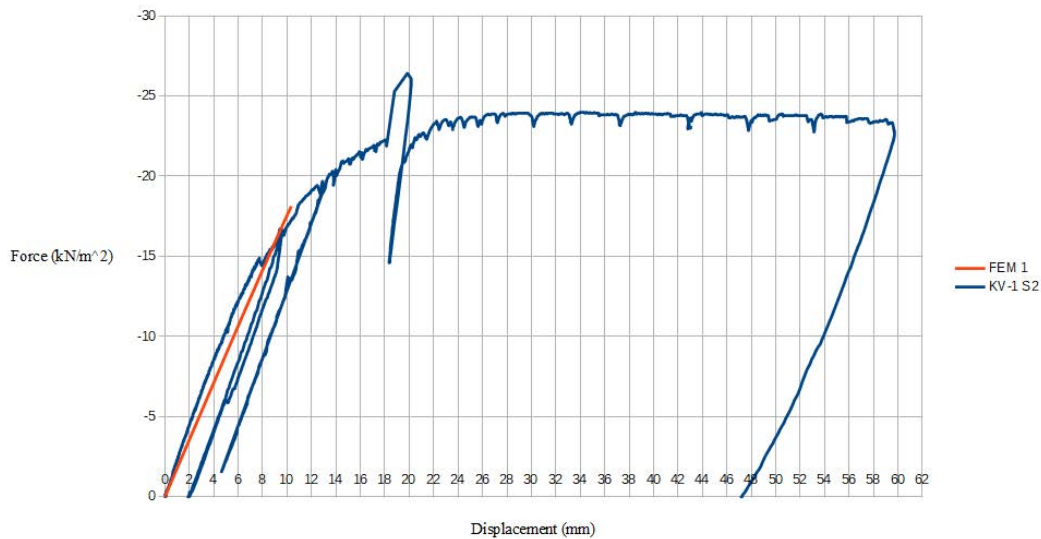
Figure 30. Force-displacement of the second cylinder. Spike around 18 mm is due to the right said of the panel losing resistance suddenly. FEM results are drawn as a reference.

Figures I.1 and I.2 present the x- and y-direction stress-displacements of KV-1. These were

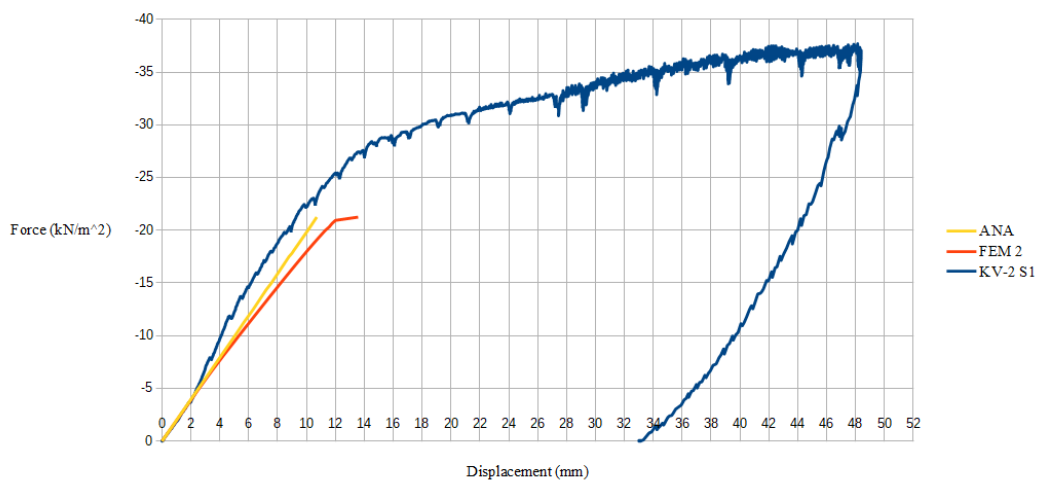calculated by the strains measured by SG1A and SG1B strain gauges. Displacement is the true displacement, according to the laser sensor. FEM results from corresponding spots are drawn as a reference.

Stresses to the x- and y-directions on the upper plate of KV-1 are presented in the figures I.3 and I.4. These were calculated from the strains of SG2A and SG2B strain gauges, respectively. Displacements are panel midsection displacements according to laser sensor. FEM results are presented as a reference.

Lower faceplate stress-displacement charts of KV-1 in x- and y-directions are presented in the figures I.5 and I.6. Stresses are calculated from the strains of SG3A and SG3B strain gauges. Again, displacements are midsection displacements by laser sensor. FEM results are for a reference.

Stress-displacement of core diagonal of KV-1 is presented in the figure I.7. Stresses are calculated from SG4 strain gauge strains. Displacement is according to midsection laser sensor.

Similar charts were drawn for the KV-2. Figures 31 and 32 present the force-displacement charts for S1 and S2. FEM results and analytical results are drawn as a reference. FEM results are those with true DC01 material values. Displacement is according to the true displacement by laser sensor.

Figure 31. Force-displacement of S1 of KV-1. FEM and analytical results are drawn as a reference.
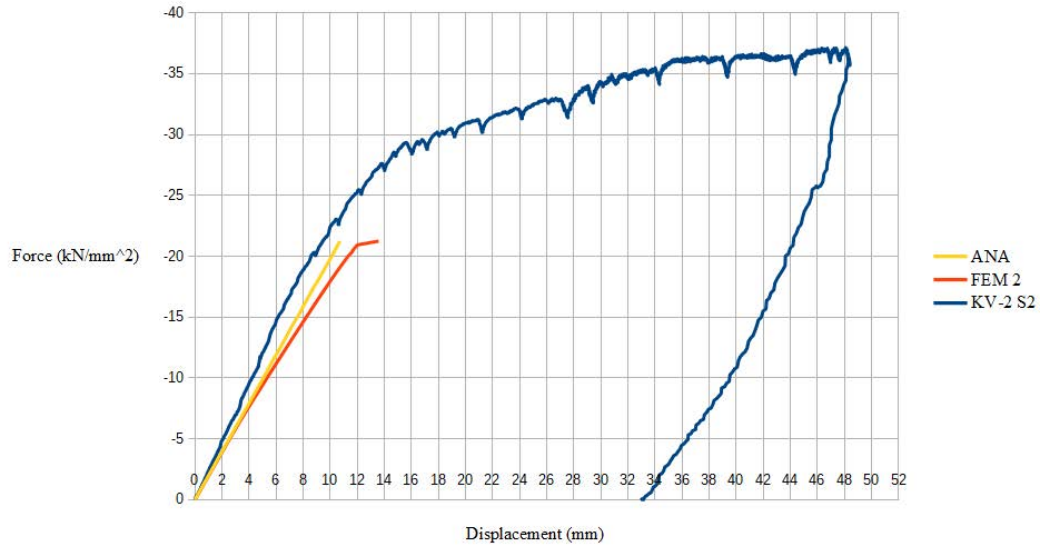
Figure 32. Force-displacement of S2 of KV-1. FEM and analytical results are drawn as a reference.

Figures J.1 and J.2 present the stress-displacement of weld of KV-2 in x- and y-directions. Stresses were calculated according to strains obtained by SG1A and SG1B strain gauges. Displacement is the true displacement measured by laser sensor.

Stress-displacements of the upper faceplate of KV-2 in x- and y-directions are shown in the figures J.3 and J.4. Stresses were calculated from the measurements of the gauges SG2A and SG2B. Displacements are from the midsection laser sensor.

Stress-displacements of the lower faceplate of KV-2 in x- and y-directions are shown in the figures J.5 and J.6. Stresses were calculated from the measurements of the gauges SG3A and SG3B. Displacements are from the midsection laser sensor.

Figure J.7 shows the stress-displacement chart of the core diagonal. Stresses were calculated from the strains measured by SG4, displacements are from the midsection laser sensor. FEM results are drawn as a reference.

The panel has a great deal of plastic capacity. There is no catastrophic failure such as multiple simultaneous failure of welds or sudden drop in load capacity, and deformations are happening safely. Part of the deformation capabilities are explained by the material, DC01 is deep-drawing steel grade.

3.4   Numerical assessment of the results

In previous sections, the behaviour of the different panel models were assessed visually from FEM results. In this section, different results - analytical, FEM and laboratory tests - are compared together numerically.

In the table 5, there are comparison of the results of FEM linear elastic buckling and non-linear simulations of each panel model, and laboratory test of KV-1. In order to give better understanding of the performance of each different panel model, their cross-sectional areas and multiple coefficients are introduced. Area (A_{coeff}), linear elastic buckling (LN_{coeff}) and nonlinear (NL_{coeff}) coefficients are calculated by dividing the particular value by the value of the base model. In essence, they illustrate how many times greater or smaller is the performance of the particular model compared to the base model. Because sandwich structures are often used in applications where weight-savings are important, mass-efficiency coefficients are introduced as well. Mass-efficiency for linear buckling (ME_{LN}) and nonlinear (ME_{NL}) is calculated by taking the particular coefficient and dividing it by the particular area coefficient. Thus, it is possible to compare how much performance different options yield in relation to the mass. For the KV-1, as there was not a clear breaking point, the point of max load is determined by the point of visual deformations, or buckling of the upper plate.

Table 5. Maximum allowable loadings and coefficients of different panels, the first constraint arrangement.

Profile	Area [mm^2]	LN$_{bckl}$ [kN/m^2]	NL [kN/m^2]	KV-1 [kN/m^2]	A$_{coeff}$	LN$_{coeff}$	NL$_{coeff}$	ME$_{LN}$	ME$_{NL}$
60°core	4574	65.95	28.75	N/A	1.07	2.07	1.44	1.95	1.35
Double-weld	4290	38.36	24.06	N/A	1	1.21	1.20	1.21	1.20
1 mm FP	5290	62.55	23.13	N/A	1.23	1.97	1.16	1.6	0.94
Single-weld	4290	31.8	20	21.2	1	1	1	1	1

The table 6 presents similar comparison, as the previous table. It should be noted that for the panel with 60 °core, the nonlinear result is the value that equates to the catastrophic failure, as discussed in the previous section. Here is also presented the analytical results, as they presume constraints equal to the second constraint arrangement. For the double-weld panel, analytical calculation was not done, as there are few suitable formulas for the specific case. For the KV-2, the maximum allowable load was determined as with KV-1, to the load that causes visual deformations, or buckling of the edge and upper plate.

Table 6. Maximum allowable loadings and coefficients of different panels, the second constraint arrangement.

Profile	Area [mm^2]	LN$_{bckl}$ [kN/m^2]	NL [kN/m^2]	ANA [kN/m^2]	KV-2 [kN/m^2]	A$_{coeff}$	LN$_{coeff}$	NL$_{coeff}$	ME$_{LN}$	ME$_{NL}$
60°core	4574	65.06	14.06	25.3	N/A	1.07	2.05	0.6	1.92	0.56
Double-weld	4290	37.73	28.13	N/A	N/A	1	1.19	1.2	1.19	1.2
1 mm FP	5290	61.26	26.88	31.7	N/A	1.23	1.93	1.15	1.56	0.93
Single-weld	4290	31.79	23.44	21.4	22.9	1	1	1	1	1

The effect of the material strength was investigated on the calculation model. There were three models: the nominal DC01, the true DC01 based on the real tests for the sheets, and S355. Thicknesses stayed the same. These results are presented in the table 7.

Table 7. Effect of material strength on nonlinear FEM results of single-weld panel.

Material	C1 [kN/m^2]	C2 [kN/m^2]	Coeff	Coeff
S355	27.81	32.19	1.39	1.37
DC01 (true)	18.13	21.3	0.91	0.91
DC01	20	23.44	1	1

It should be noted that the selection of S355 is not based on the supply from the supplier, as their selection of materials did not include S355, but high strength materials, like S700. Also, those materials were not available on the thicknesses necessary. Thus, the selection of S355 was done from principle, rather than from practicality.

4 Discussion

In this section, the results of analytical calculations, FEM and laboratory tests are discussed and compared. Both the first constraint (end-supported) and the second constraint (all-round supported) are compared. For the laboratory test, comparison between the first test sample KV-1 and the second test sample KV-2 is made. Also, recommendations for improving the design of the panel are given. In the end, critical assessment of the methodology is done, to sure that the results are valid.

4.1 Criticality of the core in FEM

By considering the results presented in the previous sections, it can be said that there are multiple failure mechanisms. From the linear elastic buckling point of view, the upper faceplate is expectedly critical. As the slenderness of the plate is a main factor - meaning the unsupported length of the plate in relation to its thickness - changes that affect the slenderness will affect the maximum linear buckling load. This is supported by the results in tables 5 and 6. Both the panel with 1 mm faceplates and the panel with 60 °core achieved top performance. It should be noted that the 60 °core panel was intendedly designed so that the faceplates would fall to the Class 3 category in Eurocode 3, instead of the Class 4 as originally. As the results in linear elastic buckling show, this goal was achieved. There are very small differences when comparing the linear elastic buckling results between the first and the second constraint arrangement, probably due to the a/b-ratio of the panel being so high.

When considering faceplates and nonlinear results, the lower faceplate proves to be more critical than the upper. It should be noted that this is most likely due to lack of dislocation strengthening in FEM model, which caused numerical converge to end when reaching yield strength, thus before the upper plate could buckle. This is especially true with the high-performance panels as 60 °core panel and double-weld panel. As expected, the edges of the lower faceplate are highly stressed on the first constraint arrangement. The stresses on edges on the second constraint arrangement are mostly due to non-optimal, unsupported part of the lower faceplate. The location of the stress areas in the lower faceplate indicates that they are due to moments and transverse shear in x-direction on the first constraint arrangement. On the second constraint arrangement, the stresses in the faceplates seem to be mostly moment induced.

Obviously, the most stressed component of the panel is the core near the support. Even in cases when neither the upper nor the lower faceplates reach yield strength of the material, the stresses in the core did. The location of the peak stresses are dependant of the constraint arrangement. On the first constraint arrangement, the stresses take place at the edges of the panel. On the second constraint arrangement, the location of stresses is at the center of the

panel. This indicates that the stresses are due to the transverse shear in x-direction. For the second constraints arrangement, this is supported by the analytical results (see appendix F), although the absolute values according to the analytical results does not reach to the yield strength.

The behaviour of the 60 °core panel on the second constraint arrangement is not readily explainable. Chang et al. (2005, p. 84) remark that experimental evidence collected by Tan et al. (1989) showed that M_y can be opposite of the FEM and analytical solutions under transverse distributed load. This means instead of the lower faceplate being in tension and upper faceplate being in compression, the negative moment causes the upper faceplate to be in tension and the lower faceplate to be in compression. In the solution of Tan et al., the both moments M_x and M_y were positive; in the solution provided by Chan get al., the M_x is positive and M_y is negative, coinciding thus with the experimental data. Analytical solution employed in this paper is based on the one of Chang et al, as previously discussed, and the solution is validated with the panel geometry used by Tan et al. and Chang et al. Chang et al. notifies that because M_y being substantially smaller than M_x, and because transverse shear deformation is greater than bending deformation, the lower faceplate did not move inwards. The panel used in their experiment was longer than it was wide (6 m x 2.1 m), thus explaining the disparity of the moments. In the case of this paper, the disparity between the moments exists in analytical results (see appendix H for 60°core, for other panels see appendices F & G), but it is not as high as with Chang et al. It should be noted that M_y is still positive, not negative, but the behaviour of the 60 °core panel in FEM on the second constraint arrangement suggests that M_y in reality is negative. Why it does not happen with other panel models, it can be speculated that due to more vertical angle, the panel gains more resistance against M_x but at the same time becomes less resistant against M_y. This is implied also by the tests conducted by SANDCORE (2005, p. 44-50) with various support and load type combinations for V-core and I-core sandwich panels. I-core can be thought as special case of V-core with 90°core angle. I-core possesses better stiffness (SANDCORE 2005, p. 51) compared to the V-core, at least in x-direction.

4.2   How do the laboratory results compare to FEM and analytical findings?
When comparing the the force-displacement charts 29 and 30 for the first test sample KV-1, it can be seen that the KV-1 is a bit stiffer than the FEM model. However, this difference is minor, and can be somewhat explained by the shorter support distance compared to the FEM. The constraints in FEM model are applied on the ends of the panel, whereas for practical reasons the KV-1 supports, each is 30 mm inward from the end of the panel, thus the support distance is 60 mm overall shorter than in FEM model.

Stress of the weld of KV-1 in x-direction follows very close to the FEM model. However, there is a noticeable difference in y-direction. Y-stress in FEM remains on compression,

whereas the stress in KV-1 shifts from compression to tension. This can be explained by formation of the waves due to the buckling of the upper plate. The top of sin wave occurs where the strain gauge SG1B was situated, thus giving superficial increase in stresses.

Establishing of the buckling waves explain also the rapid increase in x- and y-stresses in the upper faceplate (figures I.3 and I.4). The placement of the SG2A and SG2B gauges falls into bottom of the sin wave, thus giving excessive stress calculations based on the strains. Strain gauges capture the establishing of buckling waves before they are clear visually.

As the lower faceplate did not go through buckling, the stresses should match better between FEM and KV-1. Stress along x-direction match very well. However, in y-directions there is a minor difference. The strain gauge SG3B seems to have been suffering from noise on data. It can be said though that FEM stresses are on the safe side. Shifting of y-stresses from tension to compression can be explained by formation of "saddle" shape, where the edges of the panel are lower than the midsection.

The biggest difference between FEM and KV-1 occur on the stresses of core diagonal. FEM model assumes nearly three times higher stresses than KV-1 experiences. This may be due to the fact that the loading did not extend on top of the supports, and that SG4 gauge was situated on the end of the panel, behind the supports, due to practical reasons.

When comparing S1 and S2 force-displacement charts of the second test sample KV-2 to the FEM model and analytical results, it can be seen that KV-2 is clearly stiffer than the FEM model or analytical model predicts. Analytical model is a bit stiffer than the FEM model. For FEM model, the difference is again likely due to the support distances. The supports were situated at the edges and ends of the panel in FEM, whereas for practical reasons in KV-2 they were situated 30 mm inwards from the edges and ends of the panel. This means that support distances for both directions were 60 mm shorter than in FEM. More importantly, the supports in x-direction (edge of the panel) were partially below the last corrugation of the core, giving them much more support than being just below the lip of the lower plate.

In the weld x- and y-stresses, it can be seen that stresses follow the same path for both FEM model and KV-2, before differentiating rapidly, especially y-stresses. Stress in y-direction in FEM model stays at compression, whereas in KV-2 the stress changes from compression to tension. As with KV-1, this can be explained by the formation of the buckling waves at the upper plate. The top of sin wave occurs on the weld, thus increasing strains measured by the SG1A and SG1B gauges, without increase in actual stresses compared to the calculation.

This is also demonstrated by the x- and y-stresses on the upper faceplate. Stresses follow the same pace initially, but formation of buckling waves increases strains rapidly. Bottom of sin

wave is where the strain gauges SG2A and SG2B were situated, thus giving a large amount of compression.

Because there was no buckling at the lower faceplate, the stresses should follow more closely each other. There is a minute difference in x-stresses between FEM model and KV-2 at lower faceplate. However, the y-stresses follow each other perfectly. Because there is no saddle shape formation like with KV-1, stresses remain on tension.

As with KV-1, the core diagonal stresses differ vastly. Stresses in FEM model are over three times as high as in KV-2. Again, this may be because of the supports and load points being situated away from the placement of SG4. The placement of SG4 gauges in both KV-1 and KV-2 was done for practical reasons, as the height of the core was too small to fit the gauges, the upper faceplate had to be cut open and welded close after placing the gauge.

It can be concluded that FEM model and laboratory tests support each other at global level. The biggest difference is that FEM model lacks the nonlinear buckling mechanism occurring in the test samples, thus throwing off the stress readings in the upper faceplate. However, stresses in the lower faceplates match each other. Neither of core diagonal stresses match, this can be traced back to the placement of the gauges in relation to the supports and loading points.

4.3 Feasibility of the alternative panels

Originally, the alternative panel designs were intended to go from the least modifications required to the manufacturing process, to the most modifications required in this order: double-weld, new material, 1 mm faceplate and 60°core. However, during the panel manufacturing process, it came apparent that all of the alternatives would require modifications to the existing manufacturing process.

In practise, double-weld panel design would need widening of the hat of the core corrugation, in order to fit in two welds. New material would require to change tooling with which the core corrugation is made, as there is no stronger material available with the same thicknesses as the original panel from the supplier. The 1 mm faceplate requires least modifications, as only the laser parameters have to be changed. 60°core panel would also require a new tooling for the corrugation core.

If there is desire to increase performance of the panel without changing tooling or material, 1 mm faceplate design would be optimal. It also helps against buckling of the upper faceplate. However, it is not the best option mass-efficiency-wise. When considering purely mass-efficiency, the 60°core is superior. It requires nevertheless tooling change, and its catastrophic failure on the second constraint arrangement would assure the need for prototyping and real-world strength tests. If no new material and only slight tooling change is desired,

the double-weld is a good option. Lastly, there is the option to change material. Although this seems to increase greatly the strength of panel, when moving from DC01 to the S355, it does not remove the tendency for the upper plate to buckle. In fact, when looking at ε (SFS-EN 1993-1-5, p.15), the upping of the strength of the material would also shorten the allowable plate field length. The loading capacity of deformed panel would increase, but buckling tendency would nevertheless increase.

4.4   Reliability and validation of the results

In this study, triangulation was used to assure reliable results. This means using different sources to collect the results. In this study, analytical calculations, FEM and lastly laboratory tests were used. As the results correspond each other with some margin, it can be concluded that the study is reliable. As for validity of methods, FEM and analytical formulas are established in the field. There is no standard procedure method for distributed loading on sandwich panel, but the method employed in this study was applied from Estrada-Martínez,Mollón Bonhomme (2016), who reported it being succesful. Thus, it can be concluded that research methods were valid.

5 Conclusions

Aim of this study was to assess the strength of the steel sandwich panel with a corrugated core, as manufactured currently by HT-Laser. This assessment was done with analytical calculations, FEM and laboratory tests. There were six research questions: 1) What is the static strength of corrugated core sandwich panel? 2) How loading direction and type affect the strength? 3) How possible manufacturing defects affect the strength? 4) What is the risk of local buckling? 5) What kind of enhancements can be made to increase strength? 6) How well do analytical and finite element calculations match laboratory tests? Below, the findings of this study are encapsulated by bullet points.

- FEM and analytical calculations can predict global behaviour of the corrugated core sandwich panel when compared with experimental results.

- Maximum allowable transverse load for the panel is 21.2 kN/m^2 for end-support, and 22.9 kN/m^2 for all-round support. Other loading directions or types were not tested, but type of support has an effect on strength.

- Local buckling happens on the upper faceplate. FEM nonlinear analysis did not predict the upper faceplate buckling. There is however no catastrophic failure such as multiple weld failures or sudden drop in load carrying capacity, and the panel has a lot of plastic capacity.

- Manufacturing defects were not observed to affect strength.

- Four different options to better strength were tested in FEM. All of them increase the strength and require modifications to the manufacturing process to varying extend. 1 mm faceplate requires only modification of laser parameters.

- This study leaves room for further research: Capacity assessment of welds, local point load capacity of faceplate, fatigue strength and vibration behaviour of the panel, prototyping of panel alternatives and conducting strength tests.

References

Airasmaa, I., Kokko, J., Komppa, V., Saarela, O. 1991. Muovikomposiitit. Helsinki: Muoviyhdistys. 556 p.

Buannic, N., Cartraud, P., Quesnel, T. 2003. Homogenization of corrugated core sandwich panels. Composite structures. Volume 59. Issue 3. pp. 299-312.

Caccese, V., Yorulmaz, S. 2009. Laser welded steel sandwich panel bridge deck development: finite element analysis and stake weld strength tests. No. 42987. Maine. Dept. of Transportation.

Chang, W. S., Ventsel, E., Krauthammer, T., John, J. 2005. Bending behavior of corrugated-core sandwich plates. Composite structures. Volume 70. Issue 1. pp. 81-89.

Cheon, Y. J., Kim, H. G. 2015. An equivalent plate model for corrugated-core sandwich panels. Journal of Mechanical Science and Technology. Volume 29. Issue 3. pp. 1217-1223.

Dackman, D., Ek, W. 2015. Steel sandwich decks in medium span bridges. Master's Thesis. Chalmers University of Technology.

Estrada-Martínez, S., Mollón, V., Bonhomme, J. 2016. Improvements to the procedure for flexural testing, on two spans, of full wood-based sandwich panel subject to uniform load. Construction and Building Materials. Volume 102. pp. 281-296.

Frank, D., Romanoff, J., Remes, H. 2013. Fatigue strength assessment of laser stake-welded web-core steel sandwich panels. Fatigue Fracture of Engineering Materials Structures. Volume 36. Issue 8. pp. 724-737.

Järvenpää, A., Lämsä, J., Hietala, M., Mäntyjärvi, K. 2014. Mechanical Properties of a Metal Sandwich Panel Manufactured Using Longitudinally Laminated Forming Tools. In Key Engineering Materials. Vol. 611. pp. 781-785. Trans Tech Publications Ltd.

Järvenpää, A., Lämsä, J., Hietala, M., Mäntyjärvi, K. 2014. Mechanical Properties of a Metal Sandwich Panel Manufactured Using Longitudinally Laminated Forming Tools. Key Engineering Materials. Trans Tech Publications Ltd. Volume 611. pp. 781-785.

Kozak, J. 2003. Fatigue tests of steel sandwich panel. WIT Transactions on The Built Environment. Volume 68.

Kujala, P., Romanoff, J., Salminen, A., Varis, J., Vilpas, M. 2003. Teräksiset kerroslevyrakenteet. Helsinki: Metalliteollisuuden keskusliitto MET.

Libove, C., Hubka, R. E. 1951. Elastic constants for corrugated-core sandwich plates.

Lurie, S. A., Solyaev, Y. O., Volkov-Bogorodskiy, D. B., Bouznik, V. M., Koshurina, A. A. 2017. Design of the corrugated-core sandwich panel for the arctic rescue vehicle. Composite Structures. Vol 160. pp. 1007-1019.

Nelke, H., Lange, J. 2013. Experiments on fatigue behaviour of sandwich panels. Research and Applications in Structural Engineering, Mechanics and Computation. CRC Press. pp. 359-360.

NX Nastran User's Guide. 2016. Siemens Product Lifecycle Management Software Inc. 776 p.

SANDCORE. 2005. Best Practice Guide for Sandwich Structures in Marine Applications. Coordination Action on Advanced Sandwich Structures in the Transport Industries, Under European Commission Contract No. FP6-506330. SAND. CORe.

SFS-EN-1993-1-1. Eurocode 3: Design of Steel Structures. Part 1-1: General Rules and Rules for Buildings.

SFS-EN-1993-1-3.Eurocode 3. Design of steel structures. Part 1-3: General rules. Supplementary rules for cold formed members and sheeting.

SFS-EN-1993-1-5. Eurocode 3. Design of steel structures. Part 1-5: Plated structural elements.

Shaban, M., Alibeigloo, A. 2017. Three-dimensional elasticity solution for sandwich panels with corrugated cores by using energy method. Thin-Walled Structures. Vol 119. pp. 404-411.

Tan, K. H., Montague, P., Norris, C. 1989. Steel sandwich panels: finite element, closed solution, and experimental comparisons, on a 6 mx 2. 1 m panel. Structural Engineer. Volume 67. pp. 159-66.

TATA Steel. 2019. LPR-29 ainetodistus 0,5 mm.

TATA Steel. 2019. LPR-29 ja 7 ainetodistus 0,75 mm.

ThyssenKrupp. 2019. Product information for hot-rolled precision strip made in Hohenlimburg. Version 8/19. 2 p.

Valdevit, L., Wei, Z., Mercer, C., Zok, F. W., Evans, A. G. 2006. Structural performance of near-optimal sandwich panels with corrugated cores. International Journal of Solids and Structures. Volume 43. Issue 16. pp. 4888-4905.

Vinco. 2020. Low Carbon Steel strip: cold rolled [web document]. [Cited: 25.10.2020]. Available: https://www.vinco.es/en/strip/low-carbon-steel/cold-rolled/

Vinson, J. R. 1999. The behavior of sandwich structures of isotropic and composite materials. CRC Press. 377 p.

Wennhage, P., Zenkert, D. 1998. Testing of sandwich panels under uniform pressure. Journal of testing and evaluation. Volume 26. Issue 2. pp. 101-108.

Zaid, N. Z. M., Rejab, M. R. M., Mohamed, N. A. N. 2016. Sandwich structure based on corrugated-core: a review. In MATEC Web of Conferences.Vol. 74. p. 00029. EDP Sciences.

A   KV-1 strain gauge setup, form and test log

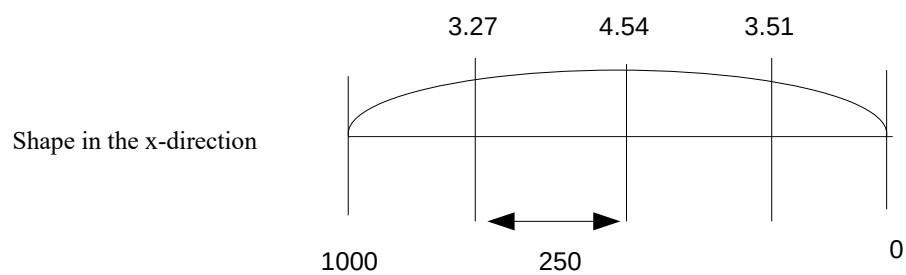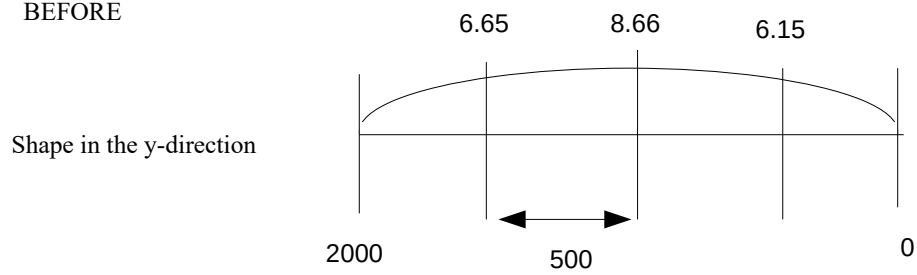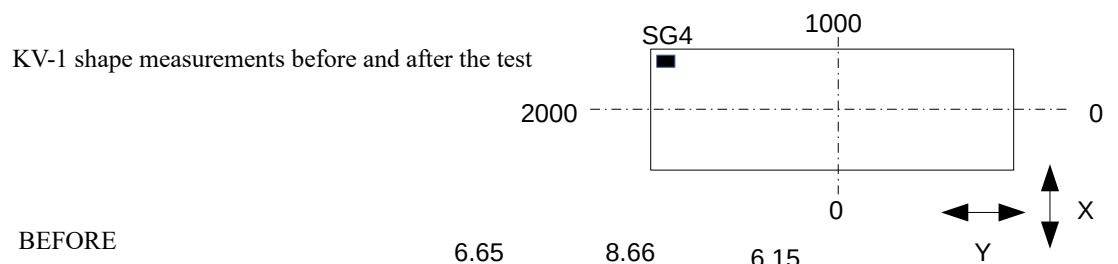Setup for the strain gauges KV-1   date: 7.10.2020
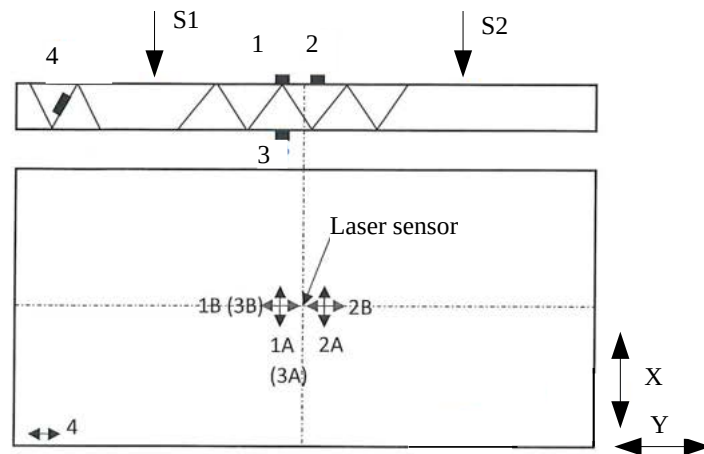
CH0 - Force cylinder S1   = 1V – 10kN   CH1 – Force cylinder S2   = 1V -10kN

CH2 – Displ cylinder S1   = 1V – 15mm   CH3 –Displ cylinder S2   = 1V – 15mm

CH4 – Laser sensor   = 1V – 5mm   CH5 – Gauge 1A (upper)   = 1V – 500yStr

CH6 – Gauge 1B (upper)   = 1V - 500yStr   CH7 – Gauge 2A (upper)   = 1V – 500yStr

CH8 – Gauge 3A (lower)   = 1V – 500yStr   CH9 –Gauge 3B (lower)   = 1V – 500yStr
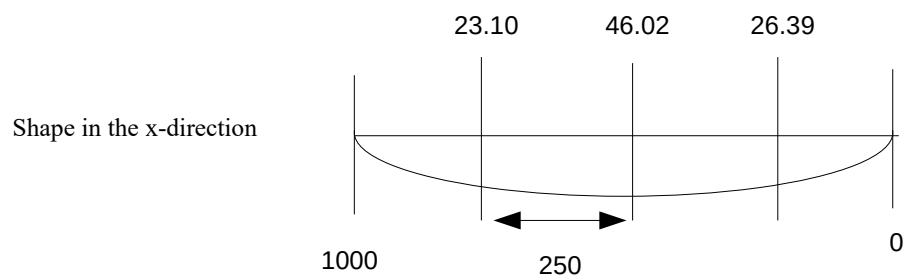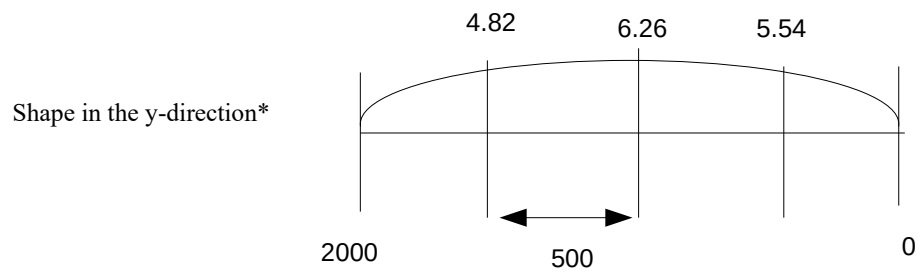
CH10 –Gauge 4 (diagonal)   = 1V – 500yStr

Gauges 1-3: type 3/120XY91. K-values: A-gauges K=2.00 & B-gauges K=1.98

Gauge 4: type 3/120LY41-3L-2M. K-value = 2.00

Calibration values: K=1.98 = 5000 yStr – 12.001 kohm. K=2.00 = 5000 yStr – 11.880 kohm

KV-1 shape measurements before and after the test

SG4

1000

2000

0

X

Y

0

BEFORE

Shape in the y-direction

6.65   8.66   6.15

2000   500   0

Shape in the x-direction

3.27   4.54   3.51

1000   250   0

AFTER

Shape in the y-direction*

4.82   6.26   5.54

2000   500   0

Shape in the x-direction

23.10   46.02   26.39

1000   250   0

* Because of the saddle shape, the measurement was taken from the bottom of the panel.

KV-1   07.10.20
Laser sensor zero: -6,958 mm

| Force | | Siirtymä | | | Order | Remarks |
S1	S2	S1	S2	Laser		
-10,7	-10,5	-4,48	-4,2	-12,1	1.	
-16,3	16,7	-7,5	-7,2	-16,3	2.	
-0,1	-0,2	-1,3	-1,2	-8,98		zeroing
-16,7	-16,6	-7,8	-7,5	-16,7	3.	
-19,4	-19,4	-9,8	-9,6	-19,9	4.	safety limit exceeded
-20,2	-20,2	-10,5	-10,3	-20,97	5.	
-20,8	-20,9	-11,1	-11	-22	6.	
-21,3	-21,2	-11,7	-11,6	-23	7.	buckling of upper plate, photographed
-21,7	-21,6	-12,4	-12,2	-24,2	8.	
-22,1	-21,9	-12,9	-12,8	-25,1	9.	S2 force dropped 8 kN, right edge failed
-20	-20,2	-13	-13,9	-26,2	10.	equalization of cylinders
-21,7	21,8	-13,8	-14,6	-27,2	11.	
-22,5	-22,3	-14,6	-15	-28,4	12.	
-22,9	-23	-15,3	-15,5	-29,4	13.	
-22,8	-23	-15,9	-16	-30,5	14.	
-23,1	-23,1	16,5	-16,6	-31,4	15.	
-23,3	-23,2	-17,1	-17,1	-32,6	16.	
-23,4	-23,5	-17,9	-17,9	-34,1	17.	
-23,1	-23,1	-19,4	-19,3	-37,2	18.	
-23,3	-23,3	-21	-20,9	-40,2	19.	
-23,4	-23,2	-23	-23,9	-44,2	20.	photographed
-23,4	-23,1	-25,8	-25,8	-49,9	21.	zeroing of laser sensor (33,1 mm)
-23,2	-22,9	-28,2	-28,3	-37,9	22.	
-23,1	-22,9	-30,8	-31,1	-43,3	23.	
-22,9	-22,7	-33,8	-34,3	-49,9	24.	
0	0	-24,5	-25,2	-37,3	25.	Zero force

Aimed displacement

| According to the cylinder displacement		
1mm	0.	
5 mm	1.	
8 mm	2.	
zeroing		(according to forces, gauges not zeroed)
8 mm	3.	
10 mm	4.	(20 kN safety limit exceeded, back to start, gauge SG2A zeroed to 1150 yStr)
11 mm	5.	
According to the laser sensor displacement		
22 mm	6.	
23 mm	7.	(upper plate buckling, photographed)
24 mm	8.	
25 mm	9.	(S2 force dropped 8 kN, right edge failed)
26 mm	10.	(equalization of cylinders)
27 mm	11.	
28 mm	12.	
29 mm	13.	
30 mm	14.	
31 mm	15.	
32 mm	16.	
34 mm	17.	
37 mm	18.	
40 mm	19.	
44 mm	20.	(photographed)
50 mm	21.	(lowering of laser sensor)
37.9 mm	22.	
43.3 mm	23.	
49.9 mm	24.	
zero forces	25.	

B   KV-2 strain gauge setup, form and test log

Strain gauge setup KV-2   date: 15.10.2020
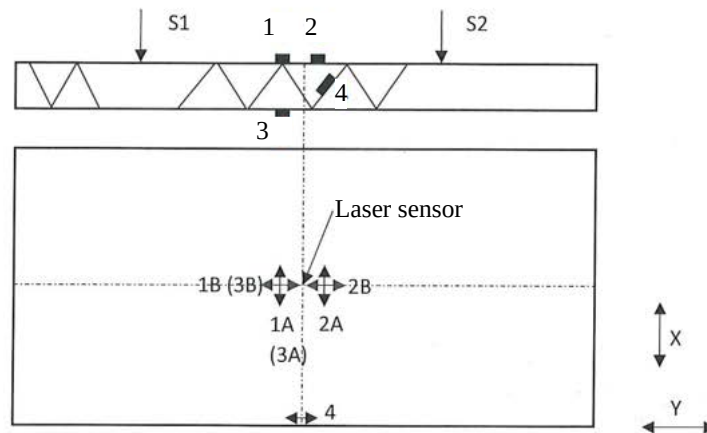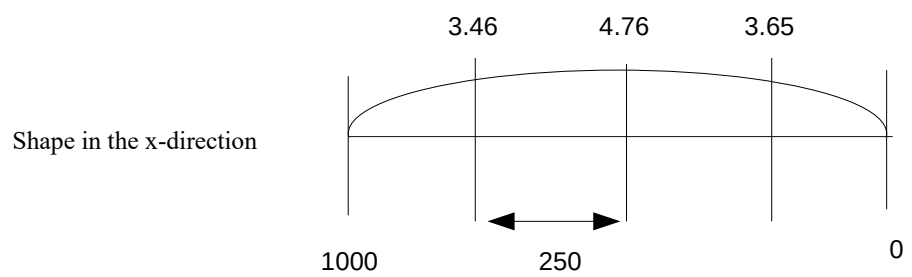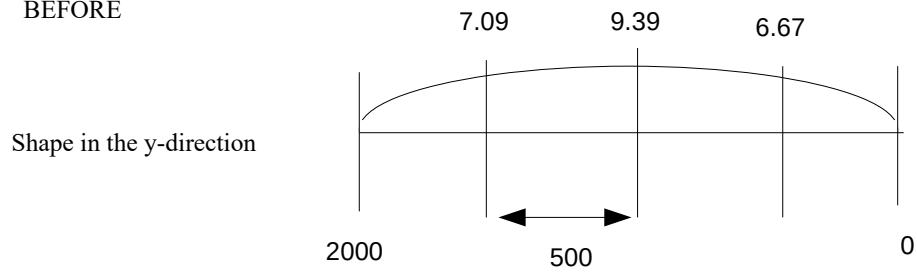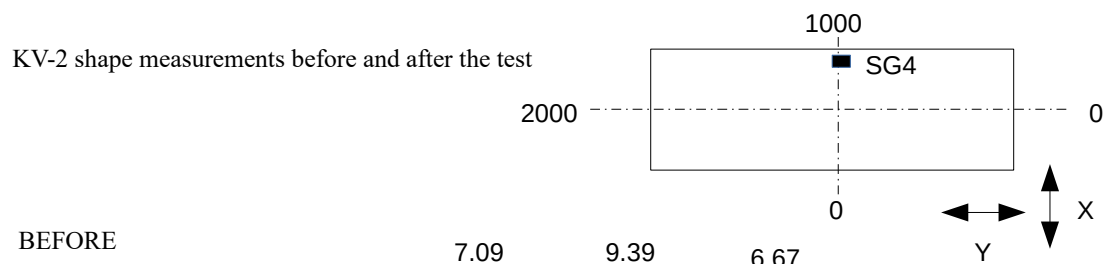

CH0 - Force cylinder S1   = 1V – 10kN   CH1 – Force cylinder S2   = 1V -10kN

CH2 – Displ cylinder S1   = 1V – 15mm   CH3 – Displ cylinder S1   = 1V – 15mm

CH4 – Laser sensor   = 1V – 5mm   CH5 – Gauge 1A (upper)   = 1V – 1000yStr

CH6 – Gauge 1B (upper)   = 1V - 1000yStr   CH7 – Gauge 2A (upper)   = 1V – 1000yStr

CH8 – Gauge 3A (lower)   = 1V – 1000yStr   CH9 –Gauge 3B (lower)   = 1V – 1000yStr

CH10 – Gauge 4 (diagonal)   = 1V – 1000yStr

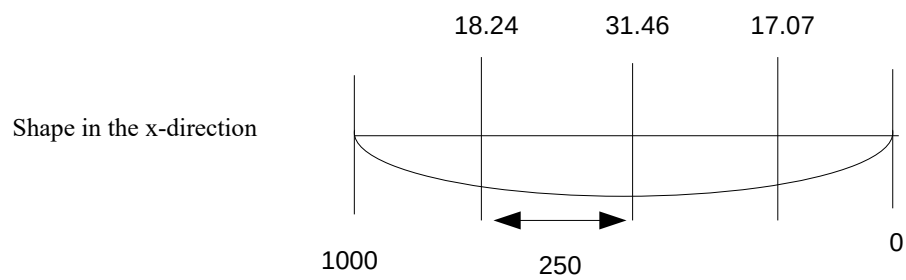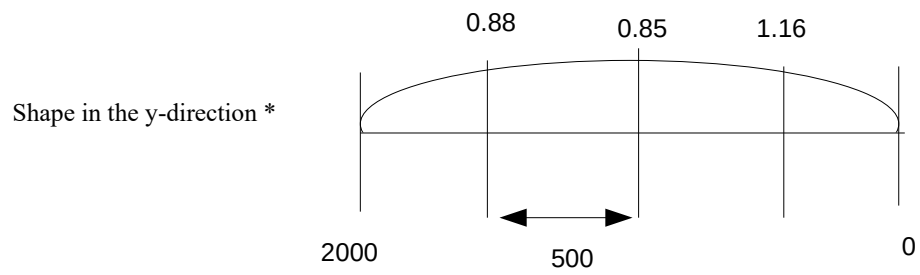Gauges 1-3: type 3/120XY91. K-values: A-gauges K=2.00 & B-gauges K=1.98

Gauge 4: type 3/120LY41-3L-2M. K-value = 2.0

Calibration values: K=1.98 = 10 000 yStr – 5.941 kohm. K=2.00 = 10 000 yStr – 5.880 kohm

KV-2 shape measurements before and after the test

1000

■ SG4

2000

0

0

X

Y

BEFORE

7.09   9.39   6.67

Shape in the y-direction

2000   0

500

3.46   4.76   3.65

Shape in the x-direction

1000   0

250

AFTER

0.88   0.85   1.16

Shape in the y-direction *

2000   0

500

18.24   31.46   17.07

Shape in the x-direction

1000   0

250

* Edges of the panel had folded up, so measurements were taken from the bottom of the panel

KV-2 15.10.20
Laser sensor zero: -1.099 mm

Force		Siirtymä			Order	Remarks
S1	S2	S1	S2	Laser		
-11,7	-11,7	-4,1	-4,2	-6	1.	
-20,1	-20,1	-6,5	-7,1	-10	2.	
-22,9	-23	-7,4	-8,1	-11,7	3.	edge buckling, photographed
-25,1	-25,2	-8,3	-9,1	-13,4	4.	
-27,4	-27,3	-9,2	-10,1	-15,1	5.	photographed, more buckling
-28,6	-28,6	-10,5	-11,1	-17,1	6.	
-29,1	-29,2	-11,3	-11,6	-18,1	7.	
-30	-29,9	-12,7	-12,7	-20,3	8.	
-30,7	-30,8	-13,9	-13,8	-22,2	9.	SG2A coefficient change
-31,6	-31,4	-15,8	-15,3	-25,2	10.	
-32,3	-32,2	-17,7	-16,8	-28,4	11.	
-32,6	-32,8	-19	-17,7	-30,4	12.	
-33,8	-34,4	-21,8	-20	-35,4	13.	photographed, snapping heard
-34,8	-35,3	-24,5	-22,6	-40	14.	SG1A coefficient change
-35,5	-25,3	-27,2	-25,3	-45,4	15.	
-36,4	-36,2	-29,3	-27,4	-49,4	16.	photographed
0	0	-18,5	-17,1	-34,1	17.	zero forces

Aimed displacement

According to the cylinder displacement		
4 mm	1.	
7 mm	2.	
8 mm	3.	(edge buckling, photographed)
9 mm	4.	
10 mm	5.	(photographed, buckling waves denser)
11 mm	6.	(plastic hinge at the left edge)
According to the laser sensor displacement		
18 mm	7.	(edge photographed)
20 mm	8.	
22 mm	9.	(SG2A coefficient from 9600 yStr to 4600 yStr)
25 mm	10.	
28 mm	11.	
30 mm	12.	
35 mm	13.	(snapping sounds, photographed)
40 mm	14.	(SG1A coefficient changed)
45 mm	15.	
49 mm	16.	(photographed)
zero forces	17.	

C   Python code used in analytical calculations

```python
import numpy as np

import scipy as sp

from mpmath import *

from scipy.interpolate import interp1d


#upper face
t1, E1, v1, G1 = 0.75, 210*10**3,0.3,78*10**3
#lower face
t2, E2, v2, G2 = t1, E1, v1, G1

#panel measures
a, b = 2000, 1000
h, df, p =15.25, 6.2, 20
fy = 220
gammaM0,gammaM1,gammaM2 = 1.0,1.0,1.25
#core
tc, Ec, theta, Gc, vc = 0.5, E1, 45*pi/180, G1, v1
##length of corrugation leg
l=(h-2*t1-tc)/sin(theta)+df



#Loading cases
Nx, Ny, Nxy=[0,0,0]

N=matrix([[Nx],[Ny],[Nxy]])

Mx, My, Mxy=[0,0,0]
M=matrix([[Mx],[My],[Mxy] ])

q=0.1*0.1406


res_file = "file_name.txt" #name of the log file
```

```python
def loads():
    Nx, Ny, Nxy=float(input("Give_Nx:_")),float(input("Give_
        Ny:_")),float(input("Give_Nxy:_"))

    N=matrix([[Nx],[Ny],[Nxy]])

    Mx, My, Mxy=float(input("Give_Mx:_")),float(input("Give_
        My:_")),float(input("Give_Mxy:_"))
    M=matrix([[Mx],[My],[Mxy] ])

    q=float(input("Give_q:_"))

    return N,M,q

def Ac(l,p,tc):
    #core cross section area, per unit width
    Ac=l*tc/p
    return Ac

def Ic(h, p, tc, t1, theta):
    #core moment of inertia per unit width mm^4/mm
    Ix1=2*(df*tc**3/12 + df*tc*(h/2-t1-tc/2)**2)
    #diag ba/12(b^2cos()^2+a^2sin()^2)
    ld=(h-2*t1-tc)/sin(theta)
    Ix2=2*(ld*tc/12*(ld**2*cos(pi/2-theta)**2 + tc**2*sin(pi
        /2-theta)**2))
    Ic=(Ix1+Ix2)/2/p
    return Ic

def Ex(t1, Ac, Ec, E1):
    #axial stiffnesse per unit width [N/m] x-direction
    EAx=Ec*Ac + 2*E1*t1
    Ex=EAx
    return Ex

def Ey(v1, t1, Ac, E1, Ec):
```

```python
    #axial stiffnesse per unit width [N/m] y-direction
    EAx=Ec*Ac + 2*E1*t1
    EAy=2*E1*t1
    Ey=EAy/(1-v1**2*(1-EAy/EAx))
    return Ey


def Dx(h, t1, Ec, E1, Ic):
    #bending stiffnesse per unit width [Nm] x-direction
    EIx=Ec*Ic + 1/2*E1*t1*h**2
    Dx=EIx
    return Dx


def Dy(h, tc, t1, v1, Ec, E1, Ic):
    #bending stiffnesse per unit width [Nm] y-direction
    EIx=Ec*Ic + 1/2*E1*t1*h**2
    EIy=1/2*E1*t1*h**2
    Dy=EIy/(1-v1**2*(1-EIy/EIx))
    return Dy


def Poisson_extension(v1, Ex, Ey):
    vx=v1
    vy=vx*Ey/Ex
    return vx, vy


def Poisson_bending(v1, Dx, Dy):
    v_x=v1
    v_y=v_x*Dy/Dx
    return v_x, v_y


def Dxy(p, h, tc, t1, t2, Gc, G1, G2, Ac):
    #Torsional stiffness per unit meter [Nm]
    #A1 = A2 -> A1-A2=0
    kc=1/2*(1 + (0)/2/p/h)
    GA=G1*t1 + Gc*tc**2/Ac + G2*t2
    k_GJ=(Gc*tc**2*kc/Ac + G2*t2)/GA
    Dxy=2*(G1*t1*k_GJ**2 + Gc*tc/Ac*(k_GJ -kc)**2 + G2*t2*(1-
        k_GJ)**2)*h**2
    return Dxy
```

```python
def Gxy(tc, t1, t2, Ac, Gc, G1, G2):
    #Horizontal shear stiffness per unit meter [N/m]
    Gxy=G1*t1 + Gc*tc**2/Ac +G2*t2
    return Gxy


def DQx(h, p, tc, Gc, Ac):
    #transverse shear stiffness per unit width [N/m] x-
        direction
    DQx=Gc*tc**2/Ac*(h/p)**2
    return DQx



def DQy(p,h_EC, theta, tc):
    #transverse shear stiffness per unit width [N/m] y-
        direction
    kz, ky = 1,1
    EC, E_C = Ec, Ec
    vc=v1
    hc=h_EC-tc
    R_i1, R_i2 = 0.18*hc, 0.18*hc
    R_C1 = R_i1 + tc/2
    R_C2 = R_i2 + tc/2
    a1=(1-kz/2)*hc - R_C1
    a2= kz*hc/2 -R_C2
    e1=R_C1*cos(theta)
    e2=R_C2*cos(theta)
    g1=R_C1*sin(theta)
    g2=R_C2*sin(theta)
    j1=a1+e1
    j2=a2+e2
    k1=j1*cot(theta)
    k2=j2*cot(theta)
    d1=j1*csc(theta)
    d2=j2*csc(theta)
    b1=k1+g1
    b2=k2+g2
    f1=2*((1-ky/2)*p-b1)
```

```python
        f2=2*(ky/2*p-b2)


        K_Iz=2/3*(k1/hc)**2*d1/hc  +  2/3*(1/8*(p/hc)**3-(b1/hc)
            **3)+2*R_C1/hc*(b1/hc*(theta*b1/hc  -2*(R_C1/hc-e1/hc))
            +1/2*(theta*(R_C1/hc)**2-g1/hc*e1/hc))
        K_Iyz=2/3*j1/hc*k1/hc*d1/hc  +  1/2*(1/4*(p/hc)**2 - (b1/hc
            )**2)  +2*R_C1/hc*(a1/hc*(theta*b1/hc+e1/hc-R_C1/hc)  +
            g1/hc*(b1/hc -1/2*g1/hc))
        K_Iy=2/3*(j1/hc)**2*d1/hc  +  1/4*f1/hc  +  2*R_C1/hc*(a1/hc
            *(theta*a1/hc  +2*g1/hc)  +  1/2*(theta*(R_C1/hc)**2 + g1
            /hc*e1/hc))
        K_Az,K_Ay  =0,0
        K_L=2*d1/hc  +2*theta*R_C1/hc  +  f1/hc
        K_Ly=f1/hc  +  2*d1/hc*cos(theta)**2  +  R_C1/hc*(theta  +  sin
            (theta)*cos(theta))
        K_Lyz=2*d1/hc*sin(theta)*cos(theta)  +  R_C1/hc*sin(theta)
            **2
        K_Lz=2*d1/hc*sin(theta)**2  +  R_C1/hc*(theta  -  sin(theta)*
            cos(theta))


        B3=K_Iz  +  1/12*EC/E_C*(tc/hc)**2*K_Lz
        B4=K_Iyz  -  1/12*EC/E_C*(tc/hc)**2*K_Lyz
        B6=K_Iy  +  1/12*EC/E_C*(tc/hc)**2
        B7=E1/EC*(1-vc**2)/(1-v1**2)*(t1/tc)**3


        S=(6*hc/p*B3*B7  +  (p/hc)**2)/12/(-2*(p/hc)**2*B4  +  hc/h
            *(6*B7*(B3*B6-B4**2)  +(p/hc)**3*B6)  +  h/hc*p/hc*B3)
        DQy=S*h*EC/(1-vc**2)*(tc/hc)**3
        return DQy


def w(q,D,  D_Qx,D_Qy ):

    z=h/2
    m,n=1,1
    qmn = 4*q/m/n/np.pi**2*(1-np.cos(m*np.pi))*(1-np.cos(n*np
        .pi))
    L11 = D[0,0]*(m*np.pi/b)**2 + D[2,2]*(n*np.pi/a)**2 +
        D_Qx
```

```python
L12 = (D[0,1] + D[2,2])*(m*n*np.pi**2/a/b)
L13 = D_Qx*(m*np.pi/b)
L21 = L12
L22 = D[1,1]*(n*np.pi/a)**2 + D[2,2]*(m*np.pi/b)**2 +
    D_Qy
L23 = D_Qy*(n*np.pi/a)
L31 = L13
L32 = L23
L33 = D_Qx*(m*np.pi/b)**2 + D_Qy*(n*np.pi/a)**2

L_matrix = np.array([[L11,L12,L13],[L21,L22,L23],[L31,L32
    ,L33]],dtype=np.float32)
q_matrix = np.array([[0],[0],[qmn]  ])

Amn,Bmn,wmn = np.dot(np.linalg.inv(L_matrix),q_matrix)
w_ = np.fromfunction(lambda x_0,y_0: wmn*np.sin(np.pi*x_0
    *10/b)*np.sin(np.pi*y_0*10/a), (int(b/10+1),int(a
    /10+1)),dtype=np.float32)
ex_ = np.fromfunction(lambda x_0,y_0: z*np.pi**2*wmn/b
    **2*np.sin(np.pi*x_0*10/b)*np.sin(np.pi*y_0*10/a),(int
    (b/10+1),int(a/10+1)),dtype=np.float32)
ey_ = np.fromfunction(lambda x_0,y_0: z*np.pi**2*wmn/a
    **2*np.sin(np.pi*x_0*10/b)*np.sin(np.pi*y_0*10/a),(int
    (b/10+1),int(a/10+1)),dtype=np.float32)
exy_ = np.fromfunction(lambda x_0,y_0: -z*np.pi**2*wmn/a/
    b*np.cos(np.pi*x_0*10/b)*np.cos(np.pi*y_0*10/a),(int(b
    /10+1),int(a/1+10)),dtype=np.float32)



kx_ = np.fromfunction(lambda x_0,y_0: -Amn*np.pi/b*np.sin
    (np.pi*x_0*10/b)*np.sin(np.pi*y_0*10/a), (int(b/10+1),
    int(a/10+1)),dtype=np.float32)
ky_ = np.fromfunction(lambda x_0,y_0: -Bmn*np.pi/a*np.sin
    (np.pi*x_0*10/b)*np.sin(np.pi*y_0*10/a), (int(b/10+1),
    int(a/10+1)),dtype=np.float32)
kxy_ = np.fromfunction(lambda x_0,y_0: Amn*np.pi/a*np.cos
    (np.pi*x_0*10/b)*np.cos(np.pi*y_0*10/a) + Bmn*np.pi/b*
    np.cos(np.pi*x_0*10/b)*np.cos(np.pi*y_0*10/a), (int(b
```

```python
                /10+1),int(a/10+1)),dtype=np.float32)


        thetax_ = np.fromfunction(lambda x_0,y_0: Amn*np.cos(np.
            pi*x_0*10/b)*np.sin(np.pi*y_0*10/a), (int(b/10+1),int(
            a/10+1)),dtype=np.float32)
        thetay_ = np.fromfunction(lambda x_0,y_0: Bmn*np.sin(np.
            pi*x_0*10/b)*np.cos(np.pi*y_0*10/a), (int(b/10+1),int(
            a/10+1)),dtype=np.float32)

        gammax_ = np.fromfunction(lambda x_0,y_0: Amn*np.cos(np.
            pi*x_0*10/b)*np.sin(np.pi*y_0*10/a) + np.pi*wmn/b*np.
            cos(np.pi*x_0*10/b)*np.sin(np.pi*y_0*10/a),(int(b
            /10+1),int(a/10+1)),dtype=np.float32)
        gammay_ = np.fromfunction(lambda x_0,y_0: Bmn*np.sin(np.
            pi*x_0*10/b)*np.cos(np.pi*y_0*10/a) + np.pi*wmn/a*np.
            sin(np.pi*x_0*10/b)*np.cos(np.pi*y_0*10/a),(int(b
            /10+1),int(a/10+1)),dtype=np.float32)

        return w_,ex_,ey_,exy_,kx_,ky_,kxy_,gammax_, gammay_


def tau_cr_f(E,v,tf,p,df):
    #shear loading face buckling
    tau_cr_f = pi**2*2**0.5/3*E/(1-v**2)*(tf/(2*p-df))**2
    return tau_cr_f


def tau_cr_c(hc, tc, v, theta, E):
    #shear loading core buckling
    tau_cr_c = pi**2*2**0.5/3/sin(pi/2-theta)*E/(1-v**2)*(tc*
        cos(pi/2-theta)/hc)**2
    return tau_cr_c


def sigma_cr_f (p, df, tf, v, E):
    #compression loading face buckling
    sigma_cr_f = pi**2*E/3/(1-v**2)*(tf/(2*p-df))**2
    return sigma_cr_f
```

```python
def sigma_cr_c(hc, tc, v, theta, E):
    #compression loading core buckling
    sigma_cr_c= pi**2*E/3/(1-v**2)*(tc*cos(pi/2-theta)/hc)**2
    return sigma_cr_c


def tau_cr_c_B (hc, tc, v, theta, E):
    #bending loading core buckling
    tau_cr_c_B= pi**2*2**0.5/3*E/(1-v**2)*(tc*cos(pi/2-theta)
        /hc)**2
    return tau_cr_c_B


def tau_xy (Q, A, N):
    #shear loading, face shear stress
    tau_xy = Q[2,2]/A[2,2]*N[2]
    return tau_xy


def sigma_x_f (Q,a_matrix, N):
    #compression loading, face x-dir stress
    sigma_x_f = (Q[0,0]*a_matrix[0,0] + Q[0,1]*a_matrix[0,1])
        *N[0]
    return sigma_x_f


def sigma_x_c (Qc, a_matrix, N):
    #compression loading, core x-dir stress
    sigma_x_c = Qc[0,0]*a_matrix[0,0]*N[0]
    return sigma_x_c


def N_cr (a,b, D):
    #compression loading global stability
    c = b/a
    m = 1
    N_cr = pi**2*(D[0,0]*D[1,1])**0.5/a**2*((D[1,1]/D[0,0])
        **0.5*(m/c)**2 + 2*(D[1,0] + 2*D[2,2])/(D[0,0]*D[1,1])
        **0.5 + (D[0,0]/D[1,1])**0.5*(c/m)**2)
    return N_cr


def sigma_x_max (a,b,h,q, Q, D):
    #bending loading, x-dir stress face max
```

```python
    x,y,z=a/2,b/2,h/2
    sigma_x_max = 16*q*z/pi**4*nsum(lambda m,n: (-1)**(m+n)/m
        /n/(D[0,0]*(m/b)**4+2*(D[0,1]+2*D[2,2])*(m*n/a/b)**2+D
        [1,1]*(n/a)**4)*(Q[0,0]*(m/b)**2+Q[0,1]*(n/a)**2),
        [1,23],[1,23])
    return sigma_x_max


def sigma_y_max (a,b,h,q, Q, D):
    #bending loading, y-dir face stress max
    x,y,z=a/2,b/2,h/2
    sigma_y_max = 16*q*z/pi**4*nsum(lambda m,n: (-1)**(m+n)/m
        /n/(D[0,0]*(m/b)**4+2*(D[0,1]+2*D[2,2])*(m*n/a/b)**2+D
        [1,1]*(n/a)**4)*(Q[0,1]*(m/b)**2+Q[1,1]*(n/a)**2),
        [1,23],[1,23])
    return sigma_y_max


def tau_xy_max (a,b,q,D,Q):
    #bending loading, face shear stress max
    x,y,z=a/2,b/2,h/2
    tau_xy_max = 32*q*z/pi**4*nsum(lambda m,n: 1/a/b/(D
        [0,0]*(m/b)**4+2*(D[0,1]+2*D[2,2])*(m*n/a/b)**2+D
        [1,1]*(n/a)**4)*Q[2,2],[1,23],[1,23])
    return tau_xy_max


def sigma_x_max_c (a,b,q,Qc,D):
    #bending loading, x-dir stress core max
    x,y,z=a/2,b/2,h/2
    sigma_x_max_c = 16*q*z/pi**4*nsum(lambda m,n: (-1)**(m+n)
        *n*Qc[0,0]/m/b**2/(D[0,0]*(m/b)**4+2*(D[0,1]+2*D[2,2])
        *(m*n/a/b)**2+D[1,1]*(n/a)**4), [1,23],[1,23])
    return sigma_x_max_c


def Q_x (a,b,q,D):
    #bending loading, shear force
    x,y,z=a/2,b/2,h/2
    Q_x= 16*q/pi**3*nsum(lambda m, n: 1/m/b/(D[0,0]*(m/b)
        **4+2*(D[0,1]+2*D[2,2])*(m*n/a/b)**2+D[1,1]*(n/a)**4)
        *(-(2*D[2,2]+D[0,1])*(m/b)**2-D[0,0]*(n/a)**2)*sin(m*
```

```python
                pi*x/b)*cos(n*pi*y/a), [1,23],[1,23])
        return Q_x


def tau_xz (hc, tc, theta, Q_x):
    #bending loading, shear stress on corrugated walls
    tau_xz = Q_x*(df + hc/cos(pi/2-theta))*p/2/tc/hc/h
    return tau_xz



def buckling(a,b,tf,tc, p, Ef,Ec,fy):


    def el_buckl_face(t_t,b_b_t,E_t,k):
        #elastic buckling of face plate
        sigma_e_t_memb = 0.9*k*E_t*(t_t/b_b_t)**2
        sigma_e_t_bend = 0.9*k*E_t*(t_t/b_b_t)**2
        tau_e_t = 4.8*E_t*(t_t/b_b_t)**2
        return sigma_e_t_memb,sigma_e_t_bend,tau_e_t

    def pl_buckl_face(b_b_t,t_t,c_y, c_x,sigma_y_t,E_t):
        #plastic buckling of face plate
        beta_t = b_b_t/t_t *(sigma_y_t/E_t)**0.5
        k = 0.8*beta_t**0.04
        neta_xy_t = 1-(tau_XY_t/tau_b_XY_t)**2
        sigma_b_t = sigma_y_t - sigma_y_t**2/4/sigma_e_t
        tau_b_t = tau_y_t - tau_y_t**2/4/tau_e_t
        bi_axial = sigma_X_t/sigma_b_X_t*neta_XY_t-k*
            sigma_X_t*sigma_Y_t/sigma_b_X_t/sigma_b_Y_t/
            neta_XY_t+(sigma_Y_t/sigma_b_Y_t/neta_XY_t)**1.2
            <1
        P_limit = 2*sigma_y_t*t_t**2*c_y/b_b_t*(2+c_x/b_b_t)
            if cy<=b_b_t else 2*sigma_y_t*t_t**2*(2+c_x/b_b_t)
        return sigma_b_t, tau_b_t, P_limit

    def el_buckl_core(b_b_c,t_c,E_c):
        #elastic buckling of core
        sigma_e_c_memb = el_buckl_face(t_c,b_b_c,E_c,k=4)[0]
        sigma_e_c_bend = 21.6*E_c*(t_c/b_b_c)**2
```

```python
        tau_e_c = 3.8*E_c*(t_c/b_b_c)**2
        return sigma_e_c_memb, sigma_e_c_bend, tau_e_c


def pl_buckl_core(sigma_mem_c, tau_c, tau_b_c,
    sigma_bend_c, sigma_b_c):
    #plastic buckling of core
    memb_shear=sigma_mem_c + (tau_c/tau_b_c)**2 <=1
    bend_shear=(sigma_bend_c/sigma_b_c)**2+(tau_c/tau_b_c
        )**2 <=1
    memb_bend_shear=sigma_memb_c/sigma_b_c+(sigma_bend_c/
        sigma_b_c)**2 <=1
    return memb_shear, bend_shear, memb_bend_shear


def pl_coll_core(c_x,c_y, t_t,t_c, p,sigma_y_t, sigma_y_c
    , theta):
    #plastic collapse of core for V-core
    c = min(cx,cy)
    M_t = sigma_y_t*p*t_t**2/2
    M_c=sigma_y_c*t_c**2/4
    I_t = p*t_t**3/6
    k_2 = M_t**2/12/E/I_t/M_c
    phi = atan(2*k_2*sin(theta)**2/sin(theta-k_2**2)**2)
    k_1 = sigma_y_t/40/t_c/sigma_y_c*(sin(theta)**2-sin(
        phi))**0.5/sin(phi)/cos(phi)
    beta = (M_t/4/M_c/k_1)**0.5
    k_3 = (sin(theta)**2 + 27/4*cos(theta)**2)**0.5
    M_w = M_c
    P_plc =(4*M_t/beta+4*M_w/beta*((k_1*beta*c+M_t/2/M_w)
        /(1+k_1*k_3*t_w)))*(1-(sigma_x_t/sigma_y_w)**2)
        **0.5
    return P_plc


def global_beam(b,D):
    k=1
    n=1
    Nx=(n**2*pi**2*D[0,0]/k**2/b**2)/(1+n**2*pi**2*D
        [0,0]/D[0,1]/k**2/b**2)
    return Nx
```

```python
def global_ortho(a,b,D):
    coeff = b/a*(D[1,1]/D[0,0])**(1/4)
    charty =
        (100,80,60,42,31,25,22,20,19.7,20,21,22.5,25,23,22,21,20,

    chartx =
        (0.3,0.35,0.4,0.5,0.6,0.7,0.8,0.9,1.0,1.1,1.2,1.3,1.4,1.5,

    interpol=interp1d(chartx,charty)
    K_0 = interpol(coeff)
    C=2
    Nx = K_0*(D[0,0]*D[1,1])**0.5/a**2+C*pi**2*(D[0,1]+2*
        D[2,2])/a**2
    return Nx


#localized elastic buckling
##face
sigma_face_crit_x_memb = el_buckl_face(tf,2*p,Ef,k=4)[0]
    if el_buckl_face(tf,2*p,Ef,k=4)[0]/fy <=0.5 else fy-fy
    **2/4/el_buckl_face(tf,2*p,Ef,k=4)[0]
sigma_face_crit_y_memb = el_buckl_face(tf,2*p,Ef,k=1)[0]
    + 0.82*Ef*(Ec/Ef*t/h)**0.5
sigma_face_crit_x_bend = el_buckl_face(tf,2*p,Ef,k=4)[1]
    if el_buckl_face(tf,2*p,Ef,k=4)[1]/fy <=0.5 else fy-fy
    **2/4/el_buckl_face(tf,2*p,Ef,k=4)[1]
sigma_face_crit_y_bend = el_buckl_face(tf,2*p,Ef,k=1)[1]
    + 0.82*Ef*(Ec/Ef*t/h)**0.5
tau_face_crit = el_buckl_face(tf,2*p,Ef,k=4)[2]
face = sigma_face_crit_x_memb,sigma_face_crit_y_memb,
    sigma_face_crit_x_bend,sigma_face_crit_y_bend,
    tau_face_crit
##core
sigma_core_crit_x_memb = el_buckl_core((h-2*tf-tc)/sin(
    theta),tc,Ec)[0] if el_buckl_core((h-2*tf-tc)/sin(
    theta),tc,Ec)[0]/fy<=0.5 else fy-fy**2/4/el_buckl_core
    ((h-2*tf-tc)/sin(theta),tc,Ec)[0]
sigma_core_crit_x_bend = el_buckl_core((h-2*tf-tc)/sin(
```

```python
            theta), tc, Ec)[1] if el_buckl_core((h-2*tf-tc)/sin(
                theta), tc, Ec)[1]/fy <=0.5 else fy-fy**2/4/el_buckl_core
                ((h-2*tf-tc)/sin(theta), tc, Ec)[1]
        tau_core_crit = el_buckl_core((h-2*tf-tc)/sin(theta), tc,
            Ec)[2]
        core = sigma_core_crit_x_memb, sigma_core_crit_x_bend,
            tau_core_crit
        #global in-plane buckling
        in_plane_bckl_load = global_beam(b,D) if b/a<4 else
            global_ortho(a,b,D)
        #localized plastic buckling
        ##face
        sigma_face_crit_plas = pl_buckl_face(2*p, tf ,2*p, b, fy, Ef,
            tau_XY_t, tau_b_xy_t, sigma_X_t, sigma_b_x_t, sigma_b_y_t
            , sigma_Y_t)


        return sigma_face_crit_x_memb, sigma_face_crit_y_memb,
            sigma_face_crit_x_bend, sigma_face_crit_y_bend,
            tau_face_crit,


def EC3():
    def roo(a_,b_, t, fy, k_sigma, psi ,E,v):
        epsilon = (235/fy)**0.5
        #behaviour like plate
        lambda_p = b_/28.4/t/epsilon/(k_sigma)**0.5
        roo = 1.0 if lambda_p <=0.673 else (lambda_p
            -0.055*(3+psi))/lambda_p**2
        #behaviour like beam
        sigma_cr_c=pi**2*E*t**2/12/(1-v**2)/a_**2
        lambda_c=(fy/sigma_cr_c)**0.5
        alfa = 0.21
        sigma_cr_p=k_sigma*pi**2*E*t**2/12/(1-v**2)/b_**2
        phi = 0.5*(1 + alfa*(lambda_c-0.2) + lambda_c**2)
        chi = (phi + (phi**2 -lambda_c**2)**0.5)**-1 if (phi
            + (phi**2 -lambda_c**2)**0.5)**-1 <=1.0 else 1.0
        #interpolation of roo_c
        xi = sigma_cr_p/sigma_cr_c -1 if sigma_cr_p/
            sigma_cr_c -1>=0 and sigma_cr_p/sigma_cr_c -1<=1
```

```python
        else 1.0
    roo_c = (roo-chi)*xi*(2-xi)+chi
    return roo_c


def normal(p,tf,tc,theta,fy):
    p_eff_top = roo(a_=b, b_=2*p, t=tf, fy=fy, k_sigma=4,
        psi=1,E=E1,v=v1)*2*p
    p_eff_bot = roo(a_=b,b_=2*p, t=tf, fy=fy, k_sigma=4,
        psi=1,E=E1,v=v1)*2*p
    df_eff_top = roo(a_=b,b_=df, t=tc, fy=fy, k_sigma=4,
        psi=1,E=Ec,v=vc)*df
    df_eff_bot = roo(a_=b,b_=df, t=tc, fy=fy, k_sigma=4,
        psi=1,E=Ec,v=vc)*df
    l_diag_eff = roo(a_=b,b_=(h-2*tf-tc)/sin(theta), t=tc
        , fy=fy, k_sigma=4, psi=1,E=Ec,v=vc)*(h-2*tf-tc)/
        sin(theta)
    A_eff = sum((p_eff_top*tf, p_eff_bot*tf, df_eff_top*
        tc, df_eff_bot*tc, 2*l_diag_eff*tc))/2/p
    N_cr = A_eff*fy/gammaM0
    return A_eff, N_cr


def bending(h,p, df, tc,tf,theta):

    p_eff_top = roo(a_=b,b_=2*p, t=tf, fy=fy, k_sigma=4,
        psi=1,E=E1,v=v1)*2*p
    df_eff_top = roo(a_=b,b_=df, t=tc, fy=fy, k_sigma=4,
        psi=1,E=Ec,v=vc)*df

    A_face_top = p_eff_top*tf
    A_face_bot = 2*p*tf
    A_core_top = df_eff_top*tc
    A_core_diag = 2*(h-2*tf-tc)/sin(theta)*tc
    A_core_bot = df*tc

    ey_eff = sum((A_face_top*(0),A_face_bot*(h-0.5*tf),
        A_core_top*(0.5*tf+0.5*tc), A_core_diag*(h/2-tf),
        A_core_bot*(h-0.5*tf-0.5*tc)))/sum((A_face_top,
        A_face_bot,A_core_top,A_core_diag,A_core_bot))
```

```python
psi = (h-(ey_eff-0.5*tf))/-(ey_eff-0.5*tf)
if psi ==1:
    k_sigma=4
if psi >0 and psi <1:
    k_sigma = 8.2/(1.05+psi)
if psi ==0:
    k_sigma=7.81
if psi <0 and psi >-1:
    k_sigma=7.81-6.29*psi+9.78*psi**2
if psi ==-1:
    k_sigma=23.9
if psi >-3 and psi <-1:
    k_sigma=5.98*(1-psi)**2


if roo(a_=b,b_=(h-2*t1-tc)/sin(theta), t=tc, fy=fy,
    k_sigma=k_sigma, psi=psi,E=Ec,v=v1)!=1.0:
    bc = (h-2*t1-tc)/sin(theta)/2
    b_eff_1 = 0.4*roo(a_=b,b_=(h-2*t1-tc)/sin(theta),
        t=tc, fy=fy, k_sigma=k_sigma, psi=psi,E=Ec,v=
        v1)*bc
    b_eff_2 = 0.6*roo(a_=b,b_=(h-2*t1-tc)/sin(theta),
        t=tc, fy=fy, k_sigma=k_sigma, psi=psi,E=Ec,v=
        v1)*bc
    bl = (h-2*t1-tc)/sin(theta)/2
    A_diag_1 = 2*b_eff_1*tc
    A_diag_2 = 2*b_eff_2*tc
    A_diag_3 = 2*bl*tc
    y1 = b_eff_1*sin(theta)/2+0.5*tc+0.5*tf
    y2 = (bc-b_eff_2/2)*sin(theta)+0.5*tc+0.5*tf
    y3 = ((h-2*t1-tc)/sin(theta)-bl/2)*sin(theta)
        +0.5*tc+0.5*tf
    A_eff = sum((A_face_top,A_face_bot,A_core_top,
        A_diag_1,A_diag_2,A_diag_3,A_core_bot))
    ey_eff = sum((A_face_top*(0),A_face_bot*(h-0.5*tf
        ), A_core_top*(0.5*tf+0.5*tc),A_diag_1*y1,
        A_diag_2*y2,A_diag_3*y3 ,A_core_bot*(h-0.5*tf
        -0.5*tc)))/A_eff
```

```python
I1 = sum((p_eff_top*t1**3/12, df_eff_top*tc
    **3/12, 2*(b_eff_1*tc/12*(b_eff_1**2*cos(pi/2-
    theta)**2 + tc**2*sin(pi/2-theta)**2)),2*(
    b_eff_2*tc/12*(b_eff_2**2*cos(pi/2-theta)**2 +
     tc**2*sin(pi/2-theta)**2)),
            2*(bl*tc/12*(bl**2*cos(pi/2-theta)**2 +
                tc**2*sin(pi/2-theta)**2)),2*p*t1
                **3/12))

Aiyi = sum((A_face_top*(ey_eff-0)**2,A_face_bot*(
    ey_eff-(h-0.5*tf))**2, A_core_top*(ey_eff
    -(0.5*tf+0.5*tc))**2,
            A_diag_1*(ey_eff-y1)**2,A_diag_2*(
                ey_eff-y2)**2,A_diag_3*(ey_eff-y3)
                **2 ,A_core_bot*(ey_eff-(h-0.5*tf
                -0.5*tc))**2))
I_eff = (I1 + Aiyi)/2/p

W_eff = I_eff/ey_eff
M_cr = W_eff*fy/gammaM0
else:
    A_core_diag
    ey_eff
    A_eff = sum((A_face_top,A_face_bot,A_core_top,
        A_core_diag,A_core_bot))
    I1 = sum((p_eff_top*t1**3/12, df_eff_top*tc
        **3/12, 2*(((h-2*tf-tc)/sin(theta))*tc/12*(((h
        -2*tf-tc)/sin(theta))**2*cos(pi/2-theta)**2 +
        tc**2*sin(pi/2-theta)**2)),
                2*p*t1**3/12))
    Aiyi = sum((A_face_top*(ey_eff-0)**2,A_face_bot*(
        ey_eff-(h-0.5*tf))**2, A_core_top*(ey_eff
        -(0.5*tf+0.5*tc))**2,
                A_core_diag*(ey_eff - (h/2-tf))**2,
                    A_core_bot*(ey_eff-(h-0.5*tf-0.5*
                    tc))**2))
    I_eff = (I1 + Aiyi)/2/p
    W_eff = I_eff/ey_eff
```

```python
        M_cr = W_eff*fy/gammaM0

        return A_eff, ey_eff, I_eff, W_eff, M_cr


def normal_weak(p, tf, fy):
    p_eff_top = roo(a_=a, b_=2*p, t=tf, fy=fy, k_sigma=4,
        psi=1,E=E1,v=v1)*2*p
    A_face_top = p_eff_top*tf
    A_face_bot = 2*p*tf
    A_eff = sum((A_face_top, A_face_bot))/2/p
    N_cr = A_eff*fy/gammaM0
    return A_eff, N_cr


def bending_weak(p, tf, fy):
    p_eff_top = roo(a_=a, b_=2*p, t=tf, fy=fy, k_sigma=4,
        psi=1,E=E1,v=v1)*2*p
    A_face_top = p_eff_top*tf
    A_face_bot = 2*p*tf
    A_eff = sum((A_face_top, A_face_bot))
    ey_eff = sum((A_face_top*(0), A_face_bot*(h-0.5*tf)))
        /sum((A_face_top, A_face_bot))
    I1 = sum((p_eff_top*tf**3/12, 2*p*tf**3/12))
    Aiyi = sum((A_face_top*(ey_eff-0)**2, A_face_bot*(
        ey_eff-(h-0.5*tf))**2))
    I_eff = (I1 + Aiyi)/2/p
    W_eff = I_eff/ey_eff
    M_cr = W_eff*fy/gammaM0
    return A_eff, ey_eff, I_eff, W_eff, M_cr


def shear(h,p,tf,tc,theta,fy,Ec):
    hc=h-2*tf-tc
    sw = (h-2*tf-tc)/sin(theta)
    lambda_w = 0.346*sw/tc*(fy/Ec)
    if lambda_w <=0.83:
        f_bv = 0.58*fy
    elif 0.83 < lambda_w < 1.40:
        f_bv = 0.48*fy/lambda_w
    elif lambda_w >=1.40:
```

```python
        f_bv = 0.67*fy/lambda_w**2
      V_b_Rd = hc/sin(theta)*tc*f_bv/gammaM0
      V_cr = Ac(l,p,tc)*f_bv/gammaM0
      return V_cr



    return normal(p,t1,tc,theta,fy), bending(h,p, df, tc,t1,
      theta),normal_weak(p,t1,fy),bending_weak(p,t1,fy),
      shear(h,p,t1,tc,theta,fy,Ec)



def Mindlin_Reissner(N,M,q):
    log = open(res_file, "a+")



    hc = h -t1 -tc
    #Strains and stresses according to Mindlin-Reissner
      theory
    vx,vy=Poisson_extension(v1,Ex(t1, Ac(l,p,tc), Ec, E1),Ey(
      v1, t1, Ac(l,p,tc), E1, Ec))
    A11 = Ex(t1, Ac(l,p,tc),Ec,E1)/(1-vx*vy)
    A12 = vy*Ex(t1, Ac(l,p,tc),Ec,E1)/(1-vx*vy)
    A21 = vx*Ey(v1, t1, Ac(l,p,tc), E1, Ec)/(1-vx*vy)
    A22 = Ey(v1, t1, Ac(l,p,tc), E1, Ec)/(1-vx*vy)
    A66 = Gxy(tc, t1, t2, Ac(l,p,tc), Gc, G1, G2)
    A_matrix = matrix([[A11,A12,0],[A21,A22,0],[0,0,A66]])

    v_x, v_y = Poisson_bending(v1, Dx(h, t1, Ec, E1, Ic(h, p,
       tc, t1, theta)), Dy(h, tc, t1, v1, Ec, E1, Ic(h, p,
      tc, t1, theta)))
    D11 = Dx(h, t1, Ec, E1, Ic(h, p, tc, t1, theta))/(1-v_x*
      v_y)
    D12 = v_y*Dx(h, t1, Ec, E1, Ic(h, p, tc, t1, theta))/(1-
      v_x*v_y)
    D21 = v_x*Dy(h, tc, t1, v1, Ec, E1, Ic(h, p, tc, t1,
      theta))/(1-v_x*v_y)
    D22 = Dy(h, tc, t1, v1, Ec, E1, Ic(h, p, tc, t1, theta))
      /(1-v_x*v_y)
```

```python
D66 = 1/2*Dxy(p, h, tc, t1, t2, Gc, G1, G2, Ac(l,p,tc))
D = np.array([[D11,D12,0],[D21,D22,0],[0,0,D66]],dtype=np
    .float32)

D_Qx=DQx(h, p, tc, Gc, Ac(l,p,tc))
D_Qy=DQy(p,hc, theta, tc)

print("\n Elastic constants:", file=log)
print("Ex:", Ex(t1, Ac(l,p,tc),Ec,E1), file=log)
print("Ey:", Ey(v1, t1, Ac(l,p,tc), E1, Ec), file=log)
print("Gxy:", Gxy(tc, t1, t2, Ac(l,p,tc), Gc, G1, G2),
    file=log)
print("vx:", vx, file=log)
print("vy:", vy, file=log)
print("Dx:", Dx(h, t1, Ec, E1, Ic(h, p, tc, t1, theta)),
    file=log)
print("Dy:", Dy(h, tc, t1, v1, Ec, E1, Ic(h, p, tc, t1,
    theta)), file=log)
print("Dxy:",Dxy(p, h, tc, t1, t2, Gc, G1, G2, Ac(l,p,tc)
    ),file=log)
print("v_x:", v_x, file=log)
print("v_y:", v_y, file=log)

tree=EC3()
effectiveAxialAreaX, criticalAxialX  = tree[0]
effectiveBendingAreaX,CenterLineX,
    effectiveSecondMomentAreaX,SectionModulusX,
    criticalMomentX = tree[1]

effectiveAxialAreaY,criticalAxialY = tree[2]
effectiveBendingAreaY,CenterLineY,
    effectiveSecondMomentAreaY,SectionModulusY,
    criticalMomentY = tree[3]
criticalShear = tree[4]
print("\n Eurocode 3 \n",file=log)
print("Effective area in x-dir of the profile is:",
    effectiveAxialAreaX, file=log)
print("Critical axial load in x-dir is:",criticalAxialX,
```

```python
    file=log)
print("Effective bending area of the profile is:",
    effectiveBendingAreaX , file=log)
print("Centerline in x−dir due to effective widths:",
    CenterLineX , file=log)
print("Effective second moment of area in x−dir of the
    profile is:", effectiveSecondMomentAreaX , file=log)
print("Effective section modulus in x−dir of the profile
    is:",SectionModulusX , file=log)
print("Critical moment in x−dir is:", criticalMomentX ,
    file=log)
print("Effective area in y−dir of the profile is:",
    effectiveAxialAreaY , file=log)
print("Critical axial load in y−dir is:", criticalAxialY ,
    file=log)
print("Effective bending area in y−dir is:",
    effectiveBendingAreaY , file=log)
print("Centerline in y−dir due to effective widths is:",
    CenterLineY , file=log)
print("Effective second moment of area in y−dir is:",
    effectiveSecondMomentAreaY , file=log)
print("Effective section modulus in y−dir is:",
    SectionModulusY , file=log)
print("Critical moment in y−dir is:", criticalMomentY ,
    file=log)
print("Critical shear is:", criticalShear , '\n', file=log)


#compression loading
CompressionSigmaX = N[0]/2/t1
ConmpressionSigmaY = N[1]/2/t1

#shear loading
CompressionSigmaXY = N[2]/t1

#bending loading

w0,ex ,ey ,exy ,kx ,ky ,kxy ,gammax ,gammay=np.fromfunction(
```

```python
    lambda q1: w(q1/10000,D,D_Qx,D_Qy) ,(1001,))
index=int(q*10000)

i0,j0 = w0.shape
x0,y0=int((b/2)/10),int((a/2)/10)
centerDeflection = w0[x0,y0][index]
maxDeflection = max((np.max(w0[i,j][index]),i,j) for i in
    range(i0) for j in range(j0))
centerStrainX = ex[x0,y0][index]
maxStrainX = max((np.max(ex[i,j][index]),i,j) for i in
    range(i0) for j in range(j0))
centerStrainY = ey[x0,y0][index]
maxStrainY = max((np.max(ey[i,j][index]),i,j) for i in
    range(i0) for j in range(j0))
centerStrainXY = exy[x0,y0][index]
maxStrainXY = max((np.max(exy[i,j][index]),i,j) for i in
    range(i0) for j in range(j0))
centerAngleX = kx[x0,y0][index]
maxAngleX = max((np.max(kx[i,j][index]),i,j) for i in
    range(i0) for j in range(j0))
centerAngleY = ky[x0,y0][index]
maxAngleY = max((np.max(ky[i,j][index]),i,j) for i in
    range(i0) for j in range(j0))
centerAngleXY = kxy[x0,y0][index]
maxAngleXY = max((np.max(kxy[i,j][index]),i,j) for i in
    range(i0) for j in range(j0))
centerGammaX = gammax[x0,y0][index]
maxGammaX = max((np.max(gammax[i,j][index]),i,j) for i in
    range(i0) for j in range(j0))
centerGammaY = gammay[x0,y0][index]
maxGammaY = max((np.max(gammay[i,j][index]),i,j) for i in
    range(i0) for j in range(j0))

print('\n',"Mindlin-Reissner theory",file=log)
print("Deflection at the center is:", centerDeflection.
    max(),"mm and max deflections is: ",maxDeflection[0],
    "mm at x:",maxDeflection[1]*10,"y:",maxDeflection
    [2]*10,file=log)
```

```python
print("Strain_in_x-dir_at_the_center_is", centerStrainX.
    max(), "and_max_strain_is:", maxStrainX[0], "at_x:",
    maxStrainX[1]*10, "y:", maxStrainX[2]*10, file=log)
print("Strain_in_y-dir_at_the_center_is", centerStrainY.
    max(), "and_max_strain_is:", maxStrainY[0], "at_x:",
    maxStrainY[1]*10, "y:", maxStrainY[2]*10, file=log)
print("Strain_in_xy-dir_at_the_center_is", centerStrainXY.
    max(), "and_max_strain_is:", maxStrainXY[0], "at_x:",
    maxStrainXY[1]*10, "y:", maxStrainXY[2]*10, file=log)
print("Def._angle_in_x-dir_at_the_center_is", centerAngleX
    .max(), "and_max_angle_is", maxAngleX[0], "at_x:",
    maxAngleX[1]*10, "y:", maxAngleX[2]*10, file=log)
print("Def._angle_in_y-dir_at_the_center_is", centerAngleY
    .max(), "and_max_angle_is", maxAngleY[0], "at_x:",
    maxAngleY[1]*10, "y:", maxAngleY[2]*10, file=log)
print("Def._angle_in_xy-dir_at_the_center_is",
    centerAngleXY.max(), "and_max_angle_is", maxAngleXY[0], "
    at_x:", maxAngleXY[1]*10, "y:", maxAngleXY[2]*10, file=log
    )
print("Shear_strain_in_x-dir_at_the_center_is:",
    centerGammaX.max(), "and_max_strain_is:", maxGammaX[0], "
    at_x:", maxGammaX[1]*10, "y:", maxGammaX[2]*10, file=log)
print("Shear_strain_in_y-dir_at_the_center_is:",
    centerGammaY.max(), "and_max_strain_is:", maxGammaY[0], "
    at_x:", maxGammaY[1]*10, "y:", maxGammaY[2]*10, file=log)

centerMX = D[0,0]*centerAngleX.max() + D[0,1]*
    centerAngleY.max()
centerMY = D[1,0]*centerAngleX.max()+D[1,1]*centerAngleY.
    max()
centerMXY = D[2,2]*centerAngleXY.max()

maxMX = D[0,0]*maxAngleX[0] + D[0,1]*maxAngleY[0]
maxMY = D[1,0]*maxAngleX[0] + D[1,1]*maxAngleY[0]
maxMXY = D[2,2]*maxAngleXY[0]

print("Moment_in_x-dir_at_the_center_is:", centerMX, "and
    _max_moment_is:", maxMX, file=log)
```

```python
    print("Moment in y-dir at the center is:", centerMY, "and
        max moment is:", maxMY, file=log)
    print("Moment in xy-dir at the center is:", centerMXY, "
        and max moment is:", maxMXY, file=log)


centerSigmaX = centerMX/t1/hc
centerSigmaY = centerMY/t1/hc
centerSigmaXY = centerMXY/t1/hc
centerVonMises = (centerSigmaX**2 -(centerSigmaX*
    centerSigmaY)+centerSigmaY**2 +(3*centerSigmaXY))**0.5
maxSigmaX = maxMX/t1/hc
maxSigmaY = maxMY/t1/hc
maxSigmaXY = maxMXY/t1/hc


    print("Stress in x-dir at the center is:", centerSigmaX,"
        and max stress is:", maxSigmaX, file=log)
    print("Stess in y-dir at the center is:", centerSigmaY,"
        and max stress is:", maxSigmaY, file=log)
    print("Stress in xy-dir at the center is:", centerSigmaXY
        ,"and max stress is:", maxSigmaXY, file=log)
    print("Von Mises at the center  is:", centerVonMises, file
        =log)


centerQX = D_Qx*centerGammaX.max()
centerQY =D_Qy*centerGammaY.max()


maxQX = D_Qx*maxGammaX[0]
maxQY = D_Qy*maxGammaY[0]
    print("Shear in x-dir at the center is", centerQX, "and
        max shear is:", maxQX, file=log)
    print("Shear in y-dir at the center is:", centerQY, "and
        max shear is:", maxQY, file=log)


maxTauX = maxQX/tc
maxTauY = maxQY/tc
    print("Shear stress in x-dir is:", maxTauX, file=log)
    print("Shear stress y-dri is:", maxTauY, file=log)
```

```python
        MomentX=D[0,0]*kx[x0,y0] + D[0,1]*ky[x0,y0]
        ind_X=(np.abs(MomentX-criticalMomentX)<=10).argmax()
        criticalUniformLoadX = ind_X/10000
        MomentY=D[1,0]*kx[x0,y0] + D[1,1]*ky[x0,y0]
        ind_Y=(np.abs(MomentY-criticalMomentY)<=10).argmax()
        criticalUniformLoadY=ind_Y/10000
        print("The critical uniform load in x-dir is:",
            criticalUniformLoadX, file=log)
        print("The critical uniforml load in y-dir is:",
            criticalUniformLoadY, file=log)


        if maxQX >= criticalShear or maxQY >= criticalShear:
            log.write("Maximum shear is greater than critical 
                shear")
            Shear = D_Qx*gammax
            ind_X=tuple((np.abs(Shear[i,j]-criticalShear)<=0).
                argmax() for i in range(i0) for j in range(j0) if
                (np.abs(Shear[i,j]-criticalShear)<=0).argmax()!=0)
            criticalUniformLoadShear = ind_X/10000
            print("Critical uniform load is:",
                criticalUniformLoadShear, file=log)
        else: print("Maximum shear is smaller than critical shear
            ",file=log)
        log.close()



def CLT(N,M,q):
    log = open(res_file, "a+")

    print('\n', "Classical laminate theory",file=log)
    hc = h -t1 -tc
    Q11 = E1/(1-v1**2)
    Q12 = v1*Q11
    Q22 = Q11
    Q66 = G1
```

```python
Q11c = E1*tc*(df +hc/cos(pi/2-theta))/(p*hc)
Q12c = 0
Q22c = 0
Q66c = 0


Q = matrix([[Q11,Q12,0],[Q12,Q22,0],[0,0,Q66]])
Qc = matrix([[Q11c,Q12c,0],[Q12c,Q22c,0],[0,0,Q66c]])


A11 = Q11*2*t1 + Q11c*hc
A12 = Q12*2*t1 + Q12c*hc
A22 = Q22*2*t1 + Q22c*hc
A66 = 2*(Q66*2*t1 + Q66c*hc)
A_matrix = matrix([[A11,A12,0],[A12,A22,0],[0,0,A66]])
D = 1/3*(Q*(2*(h/2)**3 -(h/2-t1)**3) + Qc*2*(h/2-t1)**3)
a_matrix = A_matrix**-1


#shear loading
centerShearStress = tau_xy(Q, A_matrix, N)
criticalShearStressFace = tau_cr_f(E1,v1,t1,p,df)
criticalShearStressCore = tau_cr_c(hc, tc, vc, theta, Ec)

print("Max shear stress in xy-dir of the face is:",
    centerShearStress, file=log)
print("Critical shear stress in xy-dir of the face is:",
    criticalShearStressFace, file=log)
print("Critical shear stress in xy-dir of the core is:",
    criticalShearStressCore, file=log)


#compression loading

CompressionFaceSigmaX = sigma_x_f (Q,a_matrix, N)
CompressionCoreSigmaX = sigma_x_c(Qc, a_matrix, N)
criticalCompressionStressFace = sigma_cr_f (p, df, t1, v1
    , E1)
criticalCompressionStressCore= sigma_cr_c(hc, tc, vc,
    theta, Ec)
criticalCompressionLoad = N_cr (a,b, D)
print("Max compression stress of the face is:",
```

```python
        CompressionFaceSigmaX , file=log )
    print ( "Max_compression_stress_of_the_core_is:",
        CompressionCoreSigmaX , file=log )
    print ( "Critical_compression_stress_of_the_face_is:",
        criticalCompressionStressFace , file=log )
    print ( "Critical_compression_stress_of_the_core_is:"   ,
        criticalCompressionStressCore , file=log )
    print ( "Critical_compression_load_is:",
        criticalCompressionLoad , file=log  )


    #bending loading
    maxBendingStressFaceX = sigma_x_max (a,b,h,q, Q, D)
    maxBendingStressFaceY = sigma_y_max (a,b,h,q, Q, D)
    maxBendingShearStressFace = tau_xy_max (a,b,q,D,Q)
    maxBendingStressCoreX = sigma_x_max_c (a,b,q,Qc,D)
    ShearX = Q_x (a,b,q,D)
    ShearStressCoreXZ = tau_xz (hc, tc, theta, ShearX)
    criticalBendingShearStressCore = tau_cr_c_B (hc, tc, vc,
        theta, Ec)

    print ( "Max_bending_stress_in_x−dir_of_the_face_is:",
        maxBendingStressFaceX , file=log )
    print ( "Max_bending_stress_in_y−dir_of_the_face_is:",
        maxBendingStressFaceY , file=log )
    print ( "Max_bending_stress_in_x−dir_of_the_core_is:",
        maxBendingStressCoreX , file=log )


    log.close()

def Main():

    Mindlin_Reissner(N,M,q)
    CLT(N,M,q)
```

Main ( )

D Photos of KV-1 test
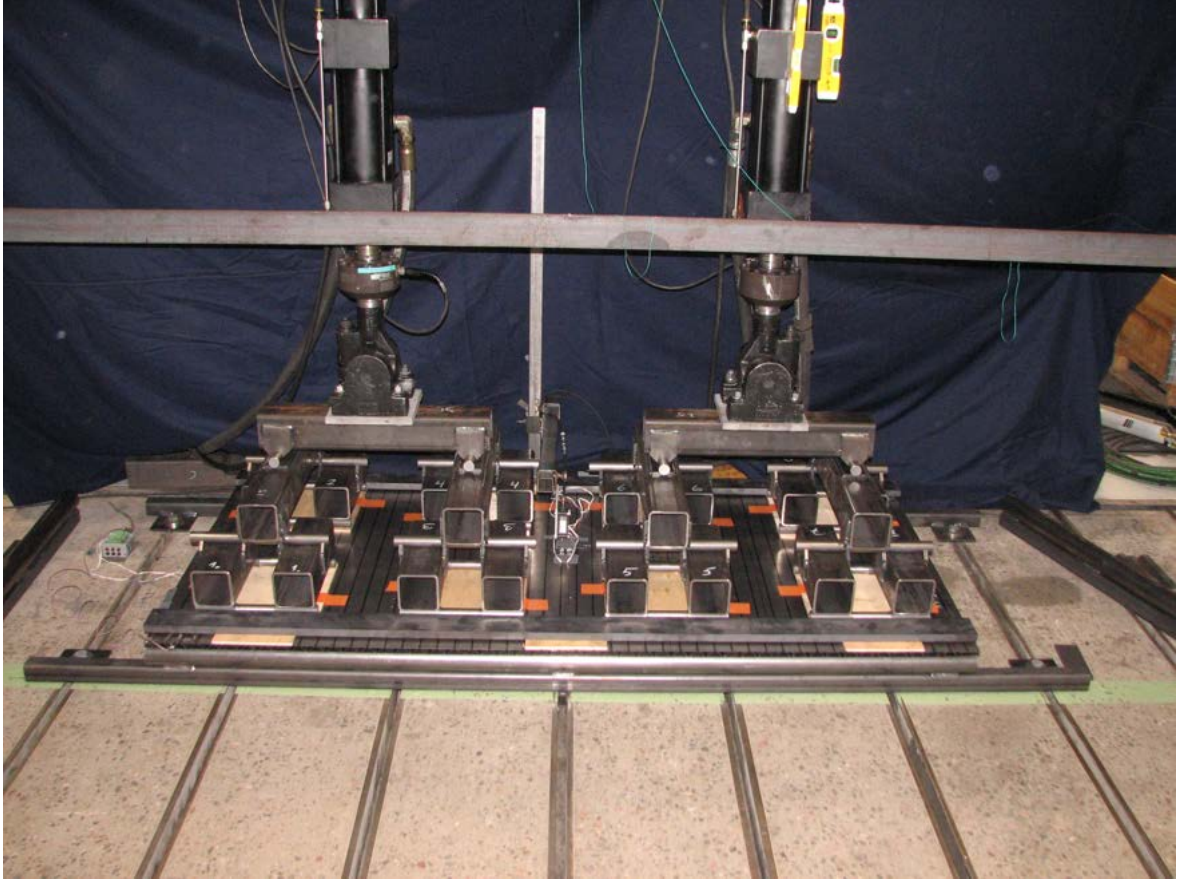
Figure D.1. KV-1 test setup.
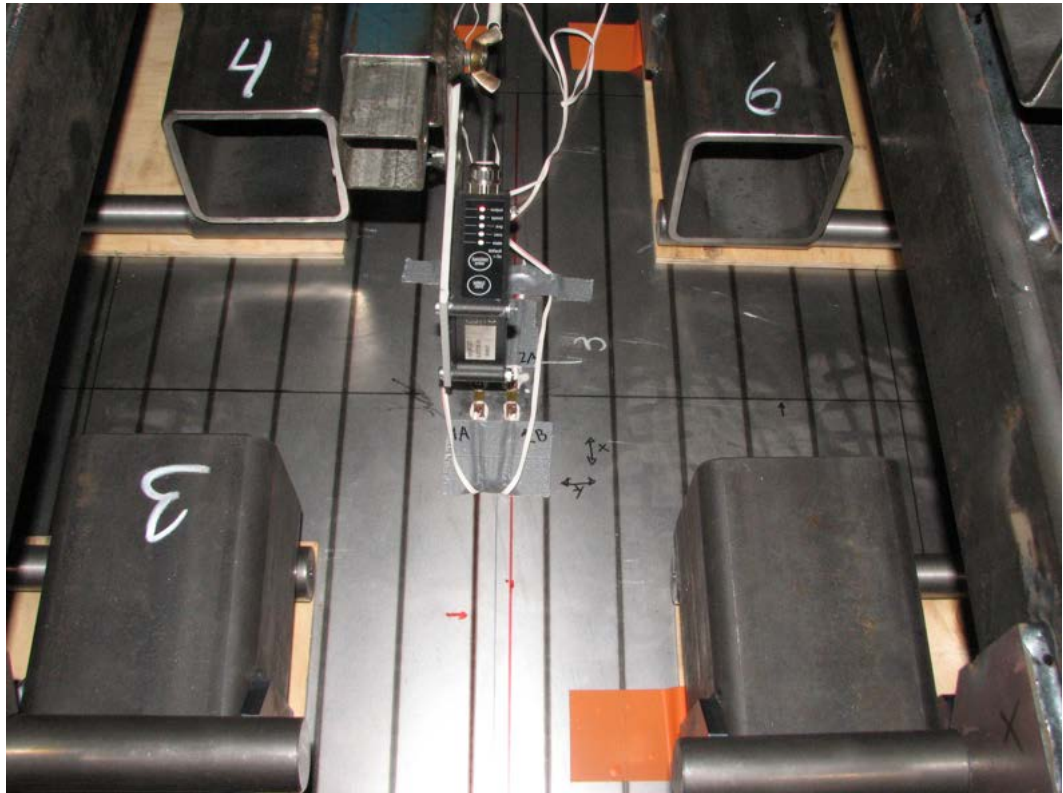
Figure D.2. Placement of SG1A & B, SG2A & B and laser sensor in KV-1.
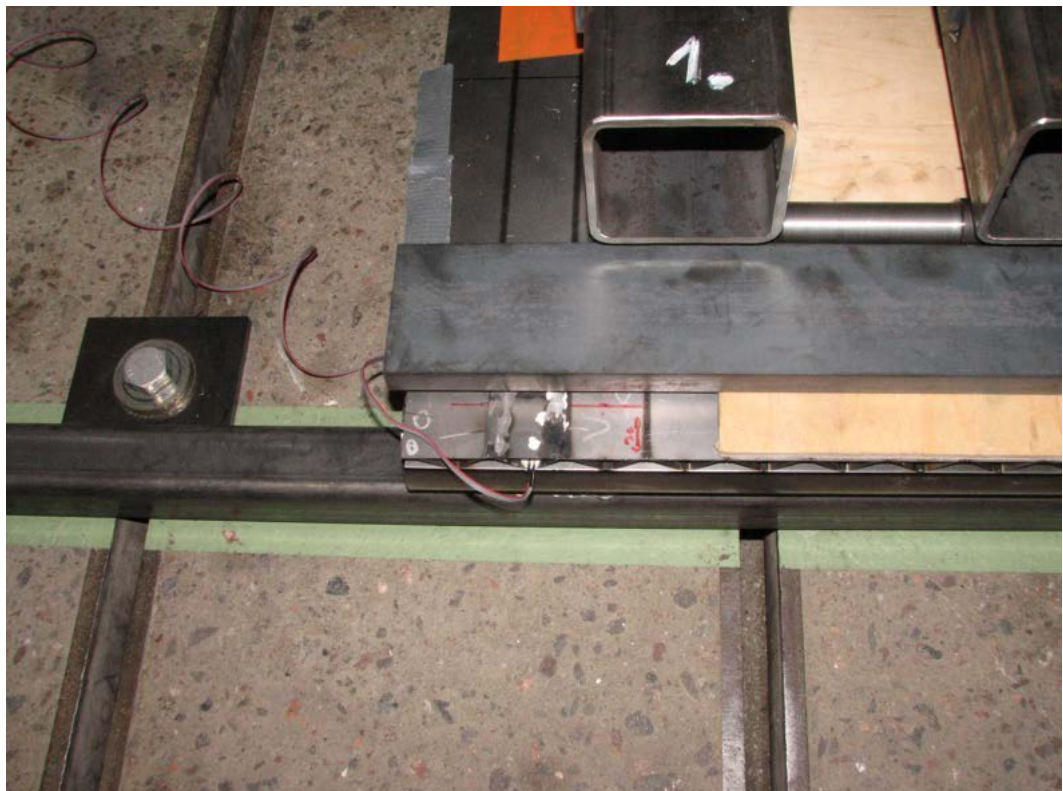
Figure D.3. Placement of SG4 strain gauge in KV-1.
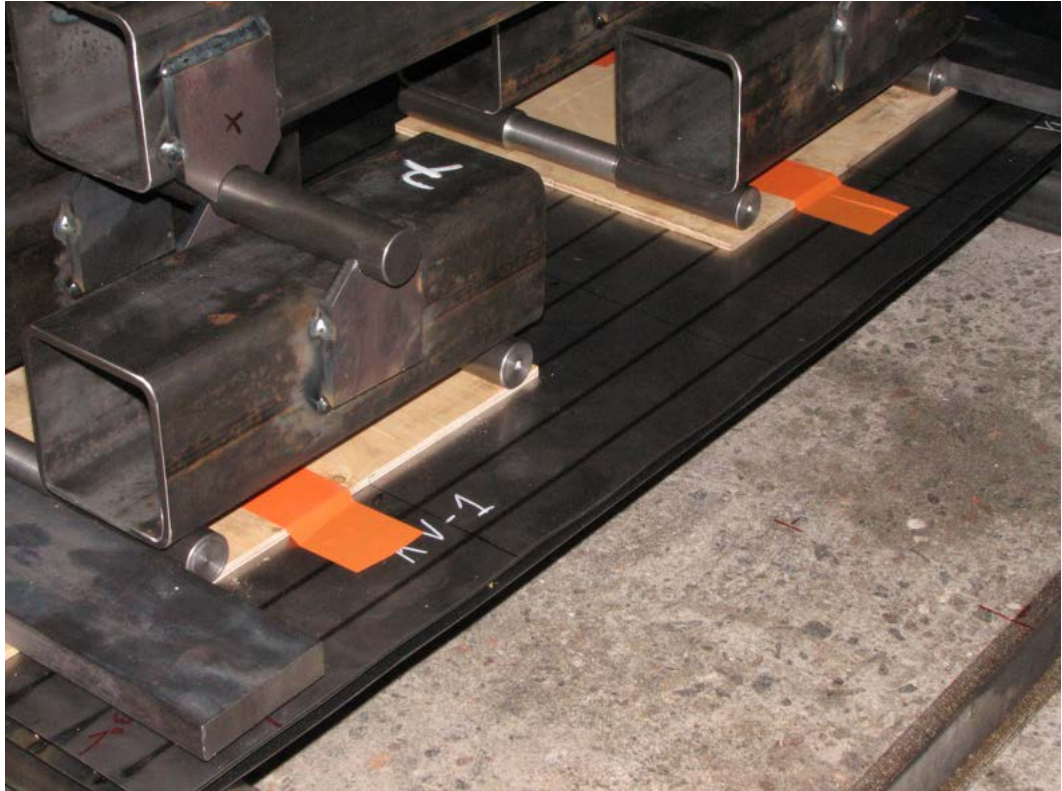
Figure D.4. Buckling of the upper faceplate starts to form at the edge in KV-1.
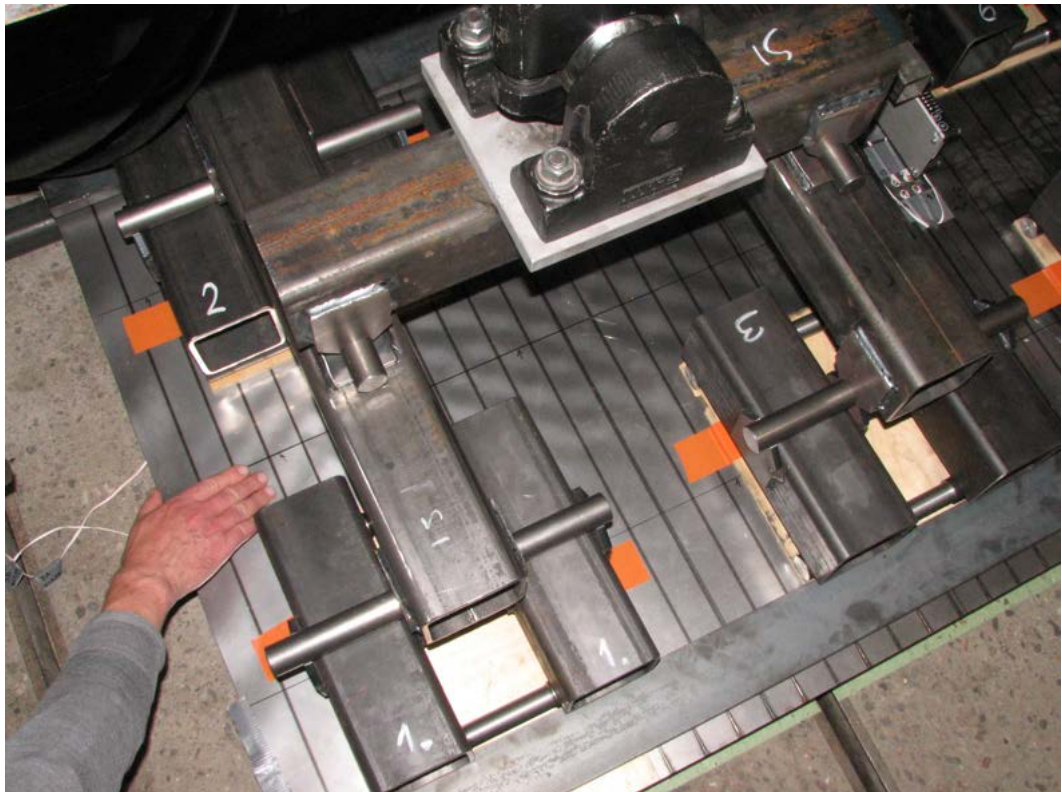
Figure D.5. As the test was continuing, the buckling of the upper plate came clearly visible.
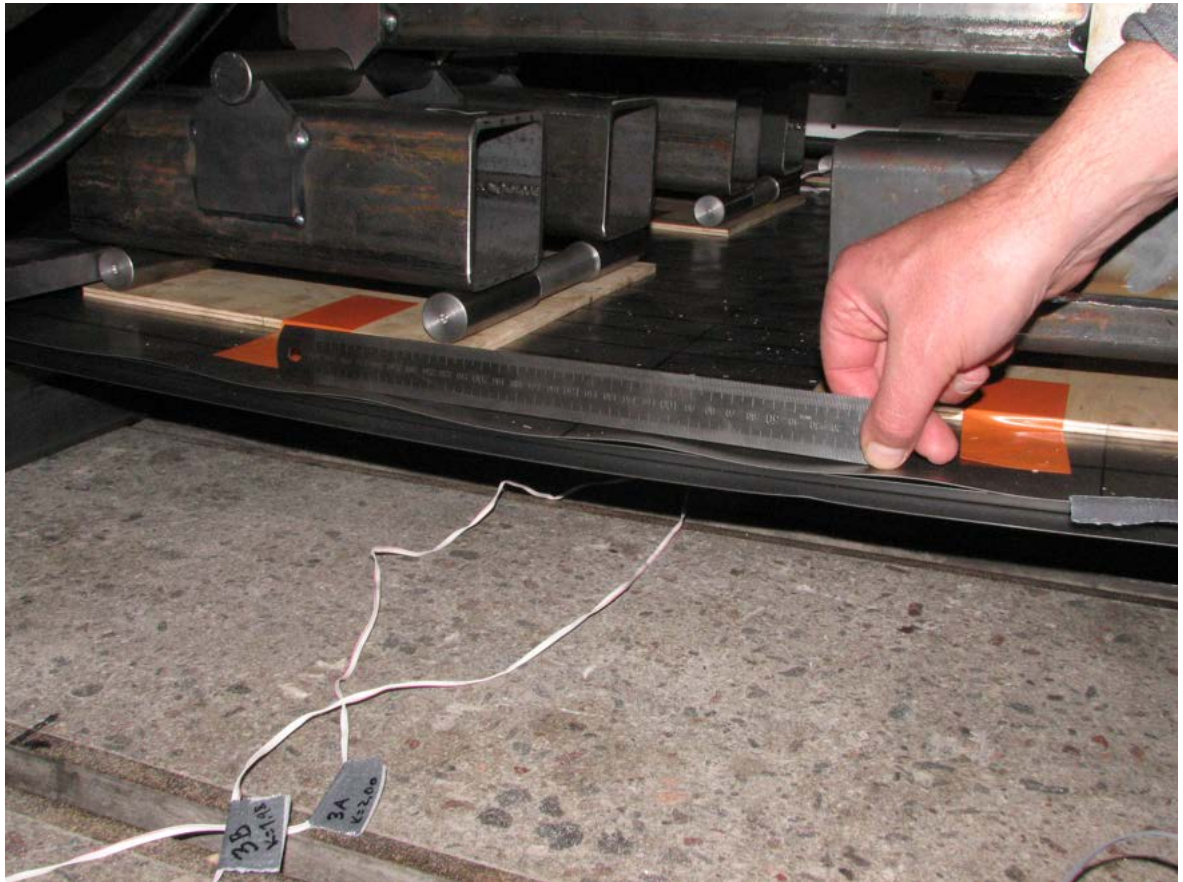
Figure D.6. Unwelded left upper edge buckled. The bottom of the wave near midline would create plastic hinge, as the loading capacity of the panel was exceeded.
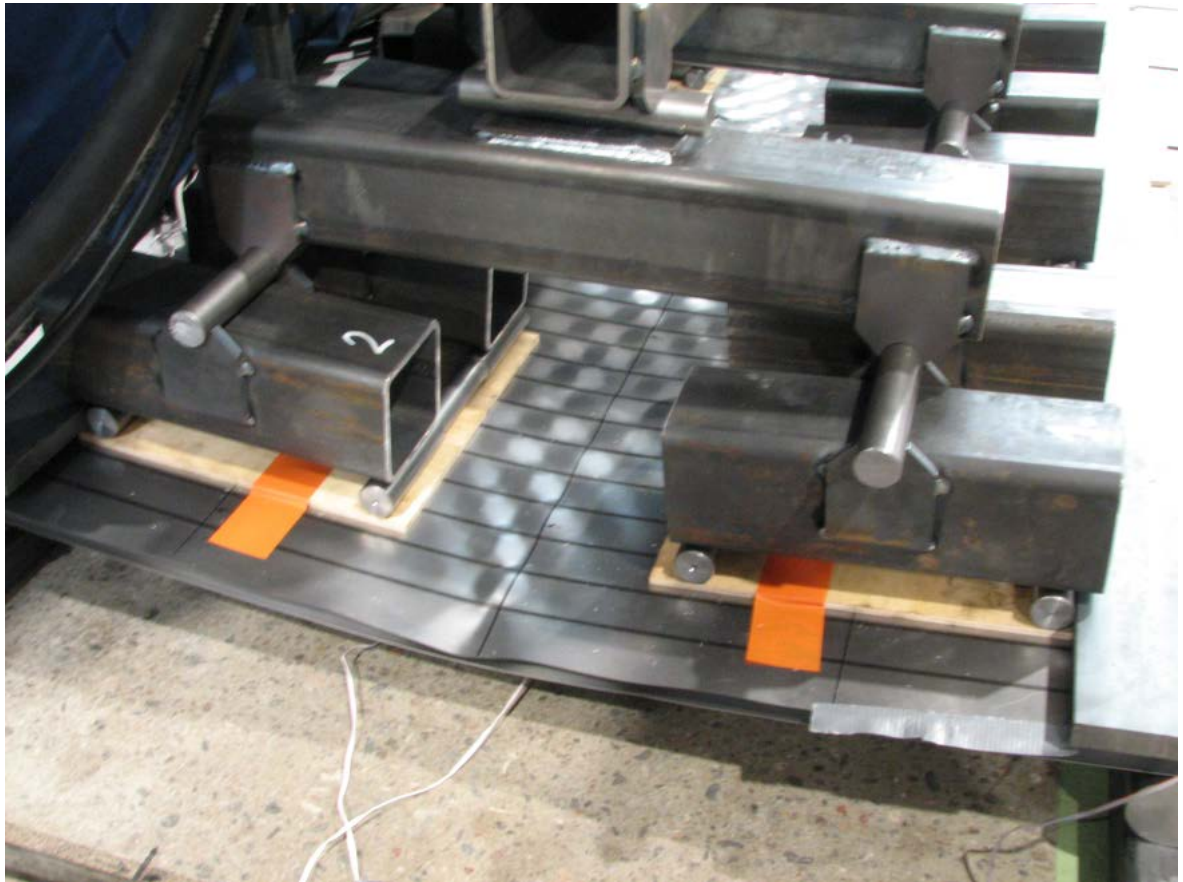
Figure D.7. Loading capacity was exceeded, and the force required to increase the deflection was coming down. The test was halted.
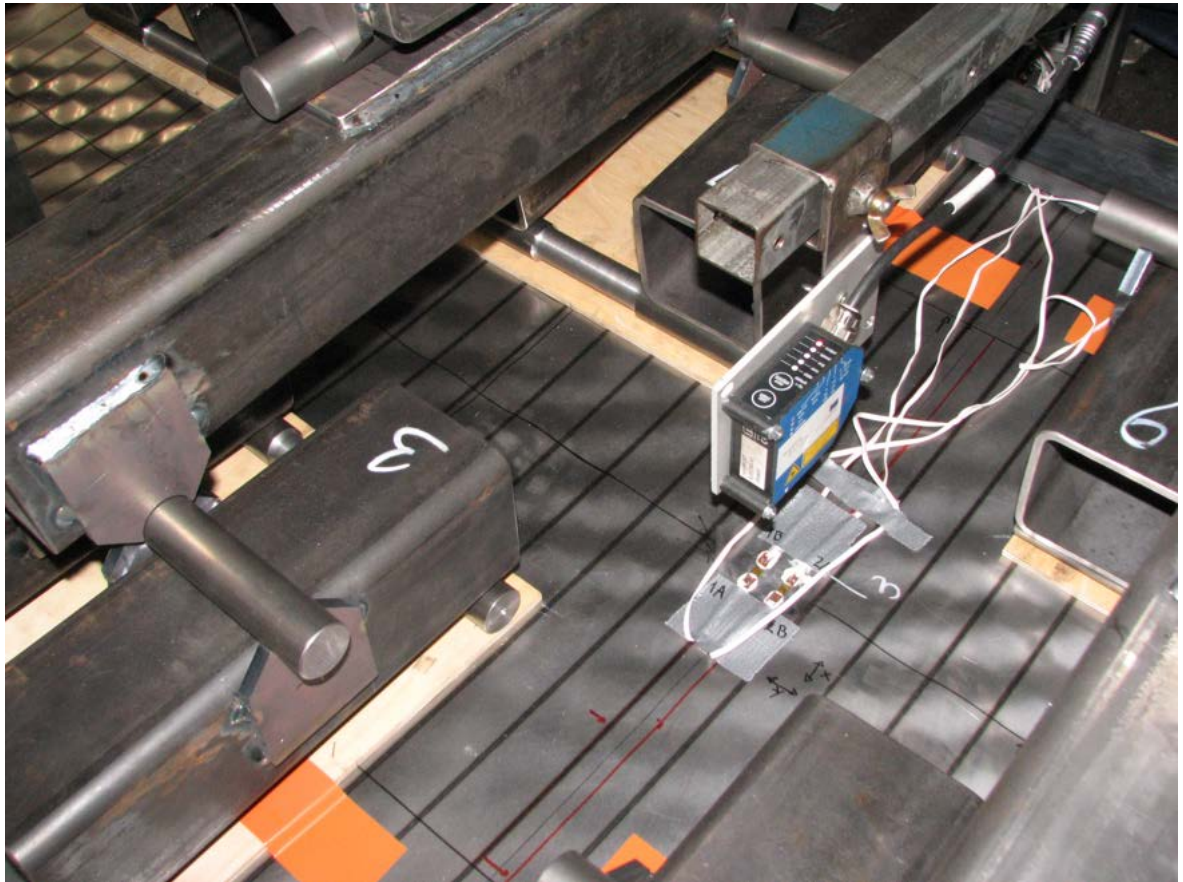
Figure D.8. Buckling of the upper plate gave very high readings from the strain gauges. These strains do not translate intoto equal stresses.

E   Photos of KV-2 test

Figure E.1. Test setup for the second test with KV-2.

Figure E.2. Support setup for the second test with KV-2.

Figure E.3. The upper plate of KV-2 has buckled, as happened with KV-1.
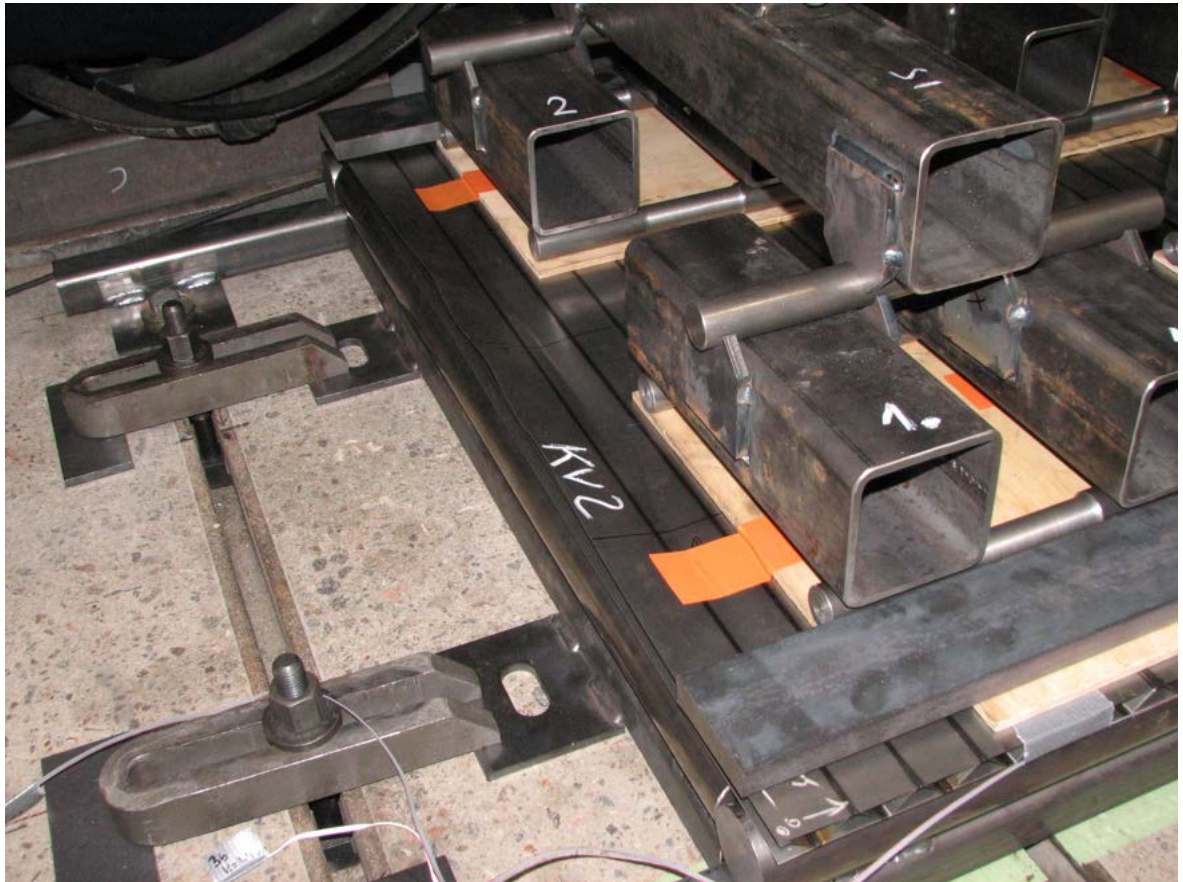
Figure E.4. Due to extra supports, there was formation of plastic hinges at the edges of the panel. The left edge formed the plastic hinge much earlier than the right, as the right edge was not as stiff.
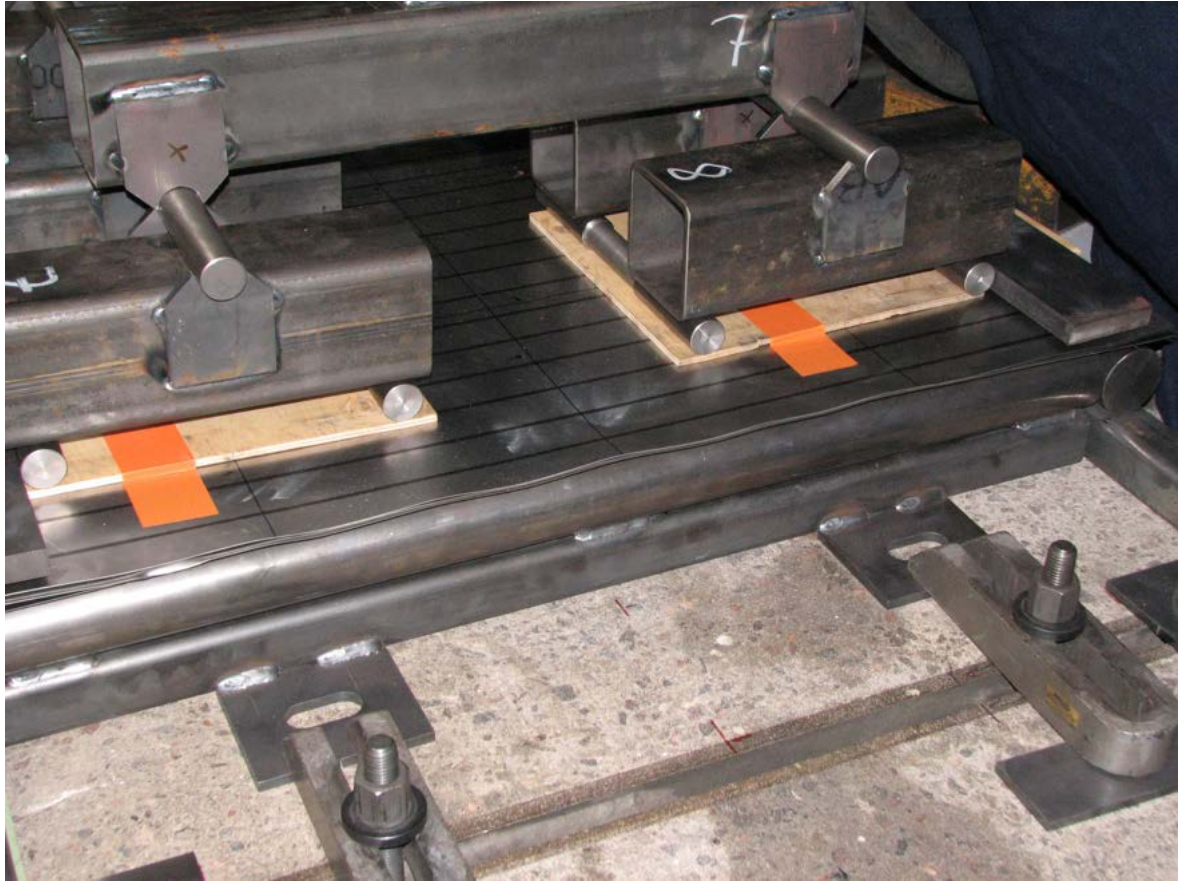
Figure E.5. As can be seen, the right edge was not initally as stiff as the left edge, and thus its formation of the plastic hinge came much later.
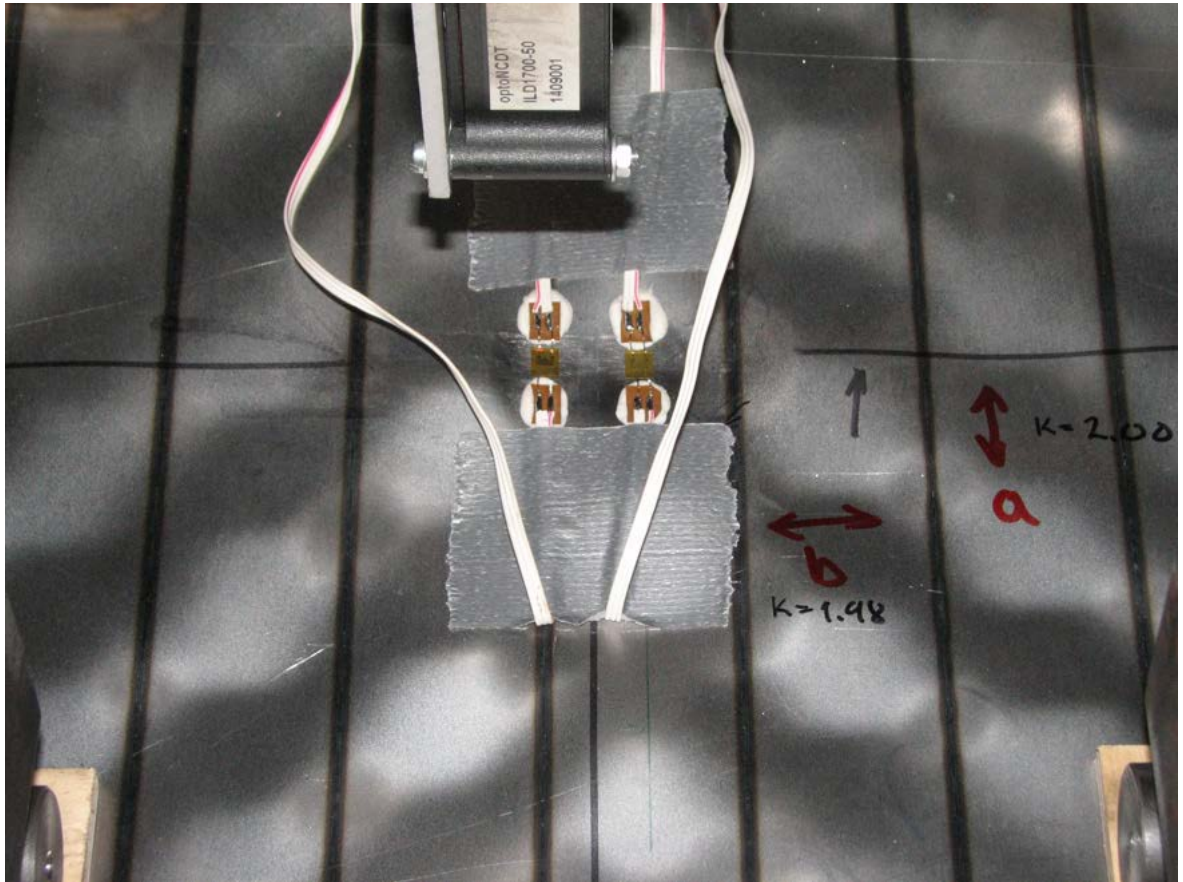
Figure E.6. As with the KV-1, the buckling of the upper plate introduced very high strains in KV-2 that do not necessarily translate into high stresses.

Figure E.7. Due to very pronounced plastic hinge, the left edge has lost its loading capacity, and the right edge carries more loading.
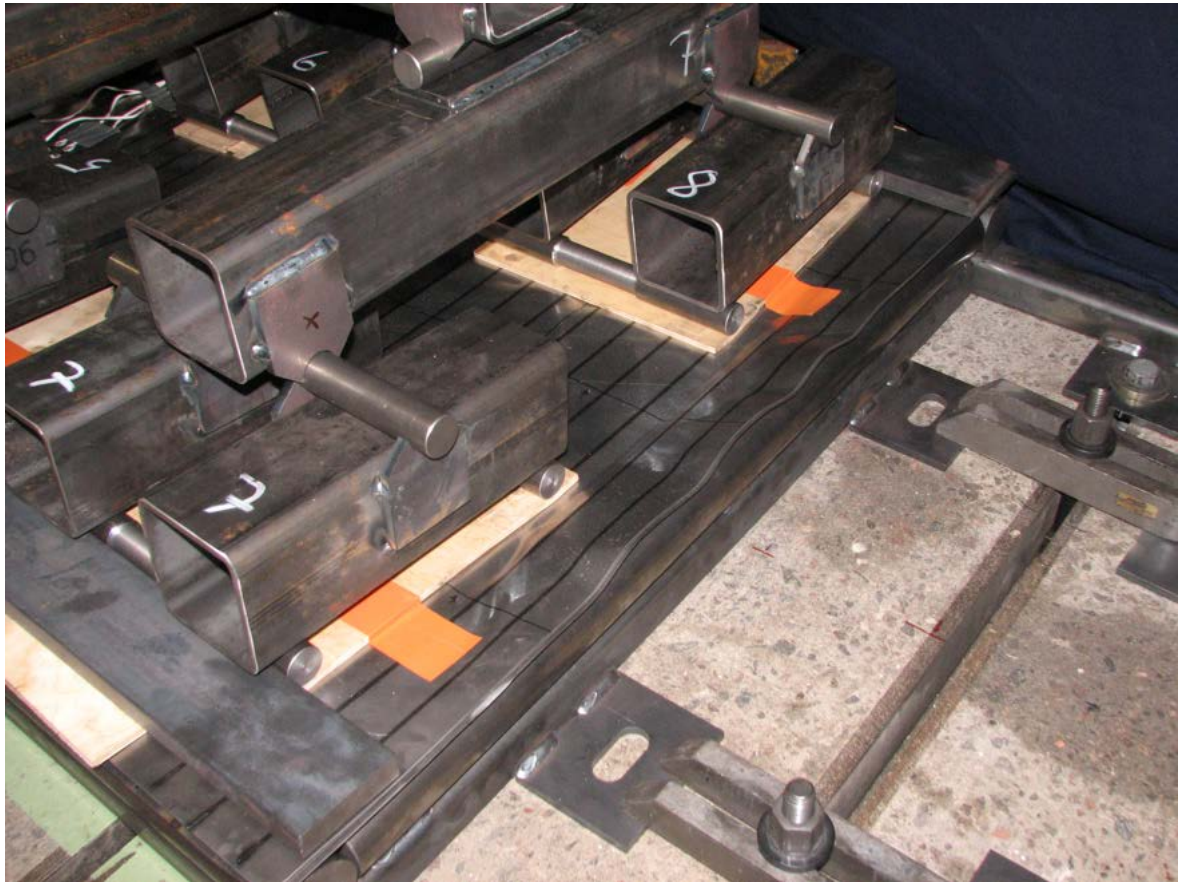
Figure E.8. Due to its lack of initial stiffness, the formation of plastic hinge in the right edge was delayed, and led to the situation where the right edge carried load after the left edge was overwhelmed.
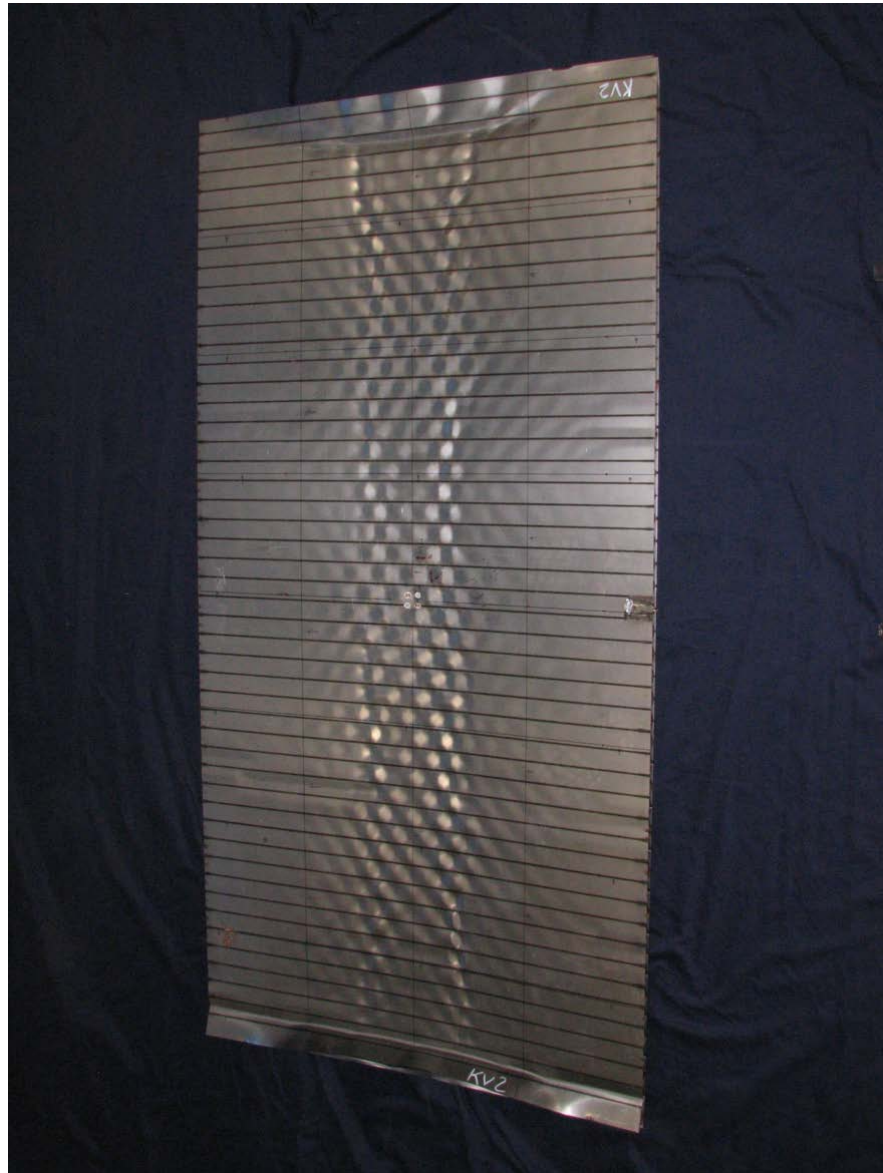
Figure E.9. The upper side of the KV-2 after the test. Plastic hinges and the bukcling of the upper plate are clearly visible.

Figure E.10. The lower side of the KV-2 shows little plastic deformation except the edges.

F Analytical results of the single-weld panel

Elastic constants:
Ex: 445926.230932578
Ey: 323549.624794409
Gxy: 148277.154859126
vx: 0.3
vy: 0.217670279757546
Dx: 21183904.3497473
Dy: 18540332.3014747
Dxy: 13604906.25
v_x: 0.3
v_y: 0.262562537982229

Eurocode 3

Effective area in x−dir of the profile is: 1.87470621721255
Critical axial load in x−dir is: 412.43536778676
Effective bending area of the profile is: 79.9632891949727
Centerline in x−dir due to effective widths: 7.78295919243591
Effective second moment of area in x−dir of the profile is:
    90.5292915015632
Effective section modulus in x−dir of the profile is:
    11.6317314871118
Critical moment in x−dir is: 2558.9809271646
Effective area in y−dir of the profile is: 1.37562398733823
Critical axial load in y−dir is: 302.637277214411
Effective bending area in y−dir is: 55.0249594935292
Centerline in y−dir due to effective widths is:
    8.10995599283409
Effective second moment of area in y−dir is: 75.5370045793512
Effective section modulus in y−dir is: 9.31410782575088
Critical moment in y−dir is: 2049.10372166519
Critical shear is: 79.5532717476048

Mindlin−Reissner theory
Deflection at the center is: 11.819612110314088 mm and max

deflections is: 11.819612110314088 mm at x: 500 y: 1000

Strain in x−dir at the center is 0.0008894935797363282 and max strain is: 0.0008894935797363282 at x: 500 y: 1000

Strain in y−dir at the center is 0.00022237339493408204 and max strain is: 0.00022237339493408204 at x: 500 y: 1000

Strain in xy−dir at the center is −8.497712274307855e−19 and max strain is: 0.0004447467898681641 at x: 1000 y: 0

Def. angle in x−dir at the center is 0.00011493468532704561 and max angle is 0.00011493468532704561 at x: 500 y: 1000

Def. angle in y−dir at the center is 2.578563915239019e−05 and max angle is 2.578563915239019e−05 at x: 500 y: 1000

Def. angle in xy−dir at the center is −2.0833850831180068e−19 and max angle is 0.00010903862096683032 at x: 1000 y: 0

Shear strain in x−dir at the center is: −2.393460641619533e −11 and max strain is: 0.0005475599690220115 at x: 0 y: 1000

Shear strain in y−dir at the center is: −9.400376909239771e −11 and max strain is: 0.002150555559474611 at x: 500 y: 0

Moment in x−dir at the center is: 2798.6324462003845 and max moment is: 2798.6324462003845

Moment in y−dir at the center is: 1212.8903676980835 and max moment is: 1212.8903676980835

Moment in xy−dir at the center is: −1.4172129108811335e−12 and max moment is: 741.7300943216969

Stress in x−dir at the center is: 266.5364234476557 and max stress is: 266.5364234476557

Stess in y−dir at the center is: 115.51336835219843 and max stress is: 115.51336835219843

Stress in xy−dir at the center is: −1.3497265817915556e−13 and max stress is: 70.64096136397113

Von Mises at the center is: 231.50914286773235

Shear in x−dir at the center is −4.35244434733383e−7 and max shear is: 9.95723201190197

Shear in y−dir at the center is: −1.85136054074924e−7 and max shear is: 4.23541921982592

Shear stress in x−dir is: 19.9144640238039

Shear stress y−dri is: 8.47083843965184

The critical uniform load in x−dir is: 0.0214

The critical uniforml load in y−dir is: 0.0394
Maximum shear is smaller than critical shear

  Classical laminate theory
Max shear stress in xy−dir of the face is: 0.0
Critical shear stress in xy−dir of the face is:
    528.640603552568
Critical shear stress in xy−dir of the core is:
    968.367778756805
Max compression stress of the face is: 0.0
Max compression stress of the core is: 0.0
Critical compression stress of the face is: 373.80535558257
Critical compression stress of the core is: 484.183889378403
Critical compression load is: 662.494641027739
Max bending stress in x−dir of the face is: 76.1314932080733
Max bending stress in y−dir of the face is: 33.6273858009149
Max bending stress in x−dir of the core is: 2.00339633297101

G Analytical results of the 1 mm faceplate panel

Elastic constants:

Ex: 549070.075631964

Ey: 429077.708896811

Gxy: 187726.951270073

vx: 0.3

vy: 0.234438769078585

Dx: 27962495.440938

Dy: 25450388.2860785

Dxy: 18739500.0

v_x: 0.3

v_y: 0.27304846600513

Eurocode 3

Effective area in x−dir of the profile is: 2.60213325164052

Critical axial load in x−dir is: 572.469315360914

Effective bending area of the profile is: 104.335053188235

Centerline in x−dir due to effective widths: 7.40065027527397

Effective second moment of area in x−dir of the profile is:
    126.631826663722

Effective section modulus in x−dir of the profile is:
    17.1109053871667

Critical moment in x−dir is: 3764.39918517667

Effective area in y−dir of the profile is: 1.99375692193463

Critical axial load in y−dir is: 438.626522825619

Effective bending area in y−dir is: 79.7502768773852

Centerline in y−dir due to effective widths is:
    7.52348485162616

Effective second moment of area in y−dir is: 112.313873635769

Effective section modulus in y−dir is: 14.928437532707

Critical moment in y−dir is: 3284.25625719555

Critical shear is: 78.4254364316123

Mindlin−Reissner theory

Deflection at the center is: 10.163457530750636 mm and max

deflections is: 10.163457530750636 mm at x: 500 y: 1000

Strain in x−dir at the center is 0.0007773971151123048 and max strain is: 0.0007773971151123048 at x: 500 y: 1000

Strain in y−dir at the center is 0.0001943492787780762 and max strain is: 0.0001943492787780762 at x: 500 y: 1000

Strain in xy−dir at the center is −7.426806845598128e−19 and max strain is: 0.00038869855755615233 at x: 1000 y: 0

Def. angle in x−dir at the center is 9.843812739706945e−05 and max angle is 9.843812739706945e−05 at x: 500 y: 1000

Def. angle in y−dir at the center is 2.1716246049427306e−05 and max angle is 2.1716246049427306e−05 at x: 500 y: 1000

Def. angle in xy−dir at the center is −1.7702798106009508e−19 and max angle is 9.265155579738933e−05 at x: 1000 y: 0

Shear strain in x−dir at the center is: −2.6035131685620033e−11 and max strain is: 0.0005956143857713883 at x: 0 y: 1000

Shear strain in y−dir at the center is: −9.353057498599176e−11 and max strain is: 0.002139730140174226 at x: 500 y: 0

Moment in x−dir at the center is: 3178.769237351674 and max moment is: 3178.769237351674

Moment in y−dir at the center is: 1420.644928064175 and max moment is: 1420.644928064175

Moment in xy−dir at the center is: −1.6587079255378258e−12 and max moment is: 868.1219149325887

Stress in x−dir at the center is: 227.05494552511956 and max stress is: 227.05494552511956

Stess in y−dir at the center is: 101.47463771886964 and max stress is: 101.47463771886964

Stress in xy−dir at the center is: −1.1847913753841614e−13 and max stress is: 62.00870820947062

Von Mises at the center is: 197.00439601225062

Shear in x−dir at the center is −4.96125472176204e−7 and max shear is: 11.3500277987448

Shear in y−dir at the center is: −2.16757280557275e−7 and max shear is: 4.95882855825559

Shear stress in x−dir is: 22.7000555974896

Shear stress y−dri is: 9.91765711651119

The critical uniform load in x−dir is: 0.0317

The critical uniforml load in y-dir is: 0.0618
Maximum shear is smaller than critical shear

  Classical laminate theory
Max shear stress in xy-dir of the face is: 0.0
Critical shear stress in xy-dir of the face is:
    939.805517426787
Critical shear stress in xy-dir of the core is:
    968.367778756805
Max compression stress of the face is: 0.0
Max compression stress of the core is: 0.0
Critical compression stress of the face is: 664.542854369013
Critical compression stress of the core is: 484.183889378403
Critical compression load is: 735.087973337936
Max bending stress in x-dir of the face is: 80.339842582167
Max bending stress in y-dir of the face is: 35.5069556428368
Max bending stress in x-dir of the core is: 2.11798967195765

H Analytical results of the 60°core panel

Elastic constants:
Ex: 476393.846830846
Ey: 324906.535176581
Gxy: 142372.714514277
vx: 0.3
vy: 0.204603735336623
Dx: 22199352.3498345
Dy: 18720315.7823027
Dxy: 13694265.0
v_x: 0.3
v_y: 0.252984620730735

Eurocode 3

Effective area in x−dir of the profile is: 2.26854212776593
Critical axial load in x−dir is: 499.079268108506
Effective bending area of the profile is: 63.927517160444
Centerline in x−dir due to effective widths: 7.34584673808724
Effective second moment of area in x−dir of the profile is:
    102.824677007499
Effective section modulus in x−dir of the profile is:
    13.9976616275381
Critical moment in x−dir is: 3079.48555805838
Effective area in y−dir of the profile is: 1.5
Critical axial load in y−dir is: 330.0
Effective bending area in y−dir is: 42.27
Centerline in y−dir due to effective widths is: 7.4625
Effective second moment of area in y−dir is: 83.603671875
Effective section modulus in y−dir is: 11.2031721105528
Critical moment in y−dir is: 2464.69786432161
Critical shear is: 98.0659755029333

Mindlin−Reissner theory
Deflection at the center is: 6.859950540611543 mm and max
    deflections is: 6.859950540611543 mm at x: 500 y: 1000

Strain in x−dir at the center is 0.0005179432350585938 and max strain is: 0.0005179432350585938 at x: 500 y: 1000

Strain in y−dir at the center is 0.00012948580876464844 and max strain is: 0.00012948580876464844 at x: 500 y: 1000

Strain in xy−dir at the center is −4.94813305707818e−19 and max strain is: 0.00025897161752929694 at x: 1000 y: 0

Def. angle in x−dir at the center is 6.707432821066591e−05 and max angle is 6.707432821066591e−05 at x: 500 y: 1000

Def. angle in y−dir at the center is 1.4364101685348828e−05 and max angle is 1.4364101685348828e−05 at x: 500 y: 1000

Def. angle in xy−dir at the center is −1.189695326687347e−19 and max angle is 6.22653674760306e−05 at x: 1000 y: 0

Shear strain in x−dir at the center is: −8.774993174168558e−12 and max strain is: 0.0002007484437832642 at x: 0 y: 1000

Shear strain in y−dir at the center is: −7.12982559075596e−11 and max strain is: 0.0016311139659957122 at x: 500 y: 0

Moment in x−dir at the center is: 1698.592150916527 and max moment is: 1698.592150916527

Moment in y−dir at the center is: 698.6181897998989 and max moment is: 698.6181897998989

Moment in xy−dir at the center is: −8.146001536459051e−13 and max moment is: 426.33922126957214

Stress in x−dir at the center is: 161.19498466586256 and max stress is: 161.19498466586256

Stess in y−dir at the center is: 66.29828610200701 and max stress is: 66.29828610200701

Stress in xy−dir at the center is: −7.730487816331247e−14 and max stress is: 40.45923808014919

Von Mises at the center is: 140.32937899778955

Shear in x−dir at the center is −2.62527374750279e−7 and max shear is: 6.00592625949455

Shear in y−dir at the center is: −1.06514586957843e−7 and max shear is: 2.43676970996961

Shear stress in x−dir is: 12.0118525189891

Shear stress y−dri is: 4.87353941993923

The critical uniform load in x−dir is: 0.0253

The critical uniforml load in y−dir is: 0.0492

Maximum shear is smaller than critical shear

  Classical laminate theory
Max shear stress in xy−dir of the face is: 0.0
 Critical shear stress in xy−dir of the face is:
    1261.53493695585
 Critical shear stress in xy−dir of the core is:
    2039.62351413177
Max compression stress of the face is: 0.0
Max compression stress of the core is: 0.0
 Critical compression stress of the face is: 892.039908625223
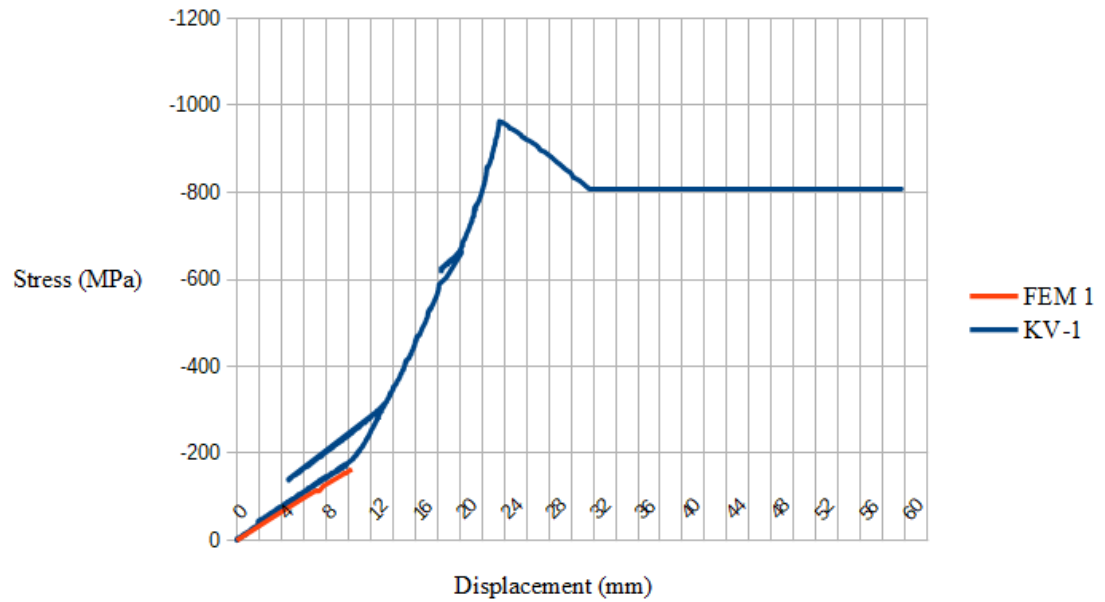 Critical compression stress of the core is: 721.115808955055
 Critical compression load is: 668.917265950255
Max bending stress in x−dir of the face is: 45.0575527905786
Max bending stress in y−dir of the face is: 19.8841535444553
Max bending stress in x−dir of the core is: 1.44879376127159

I Graphs of KV-1 test

Figure I.1. Stress-displacement of the weld of KV-1 in x-direction. FEM results are drawn as a reference.
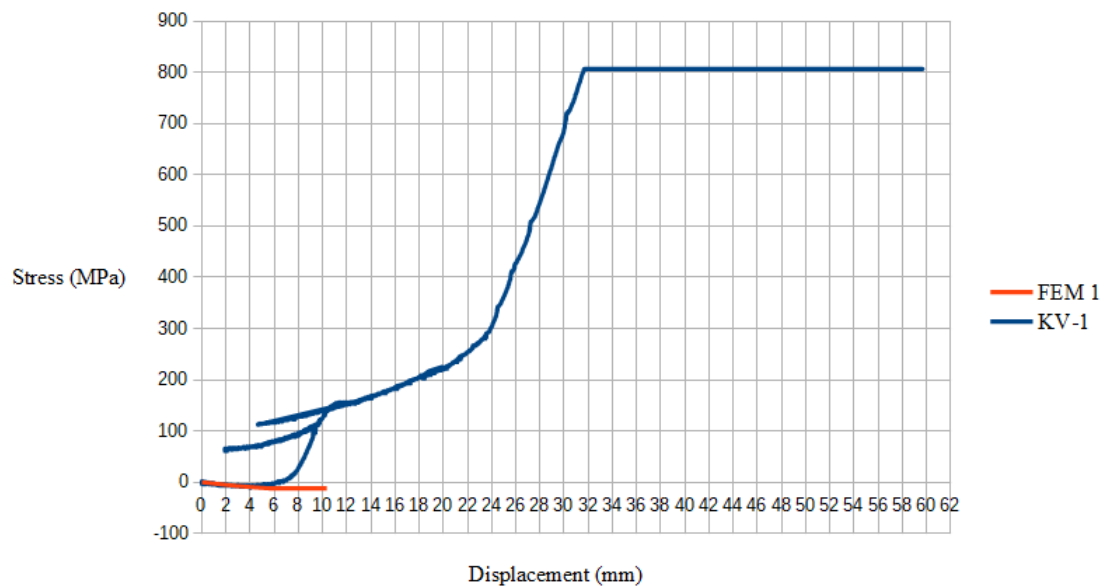
Figure I.2. Stress-displacement of the weld of KV-1 in y-direction. FEM results are drawn as a reference.
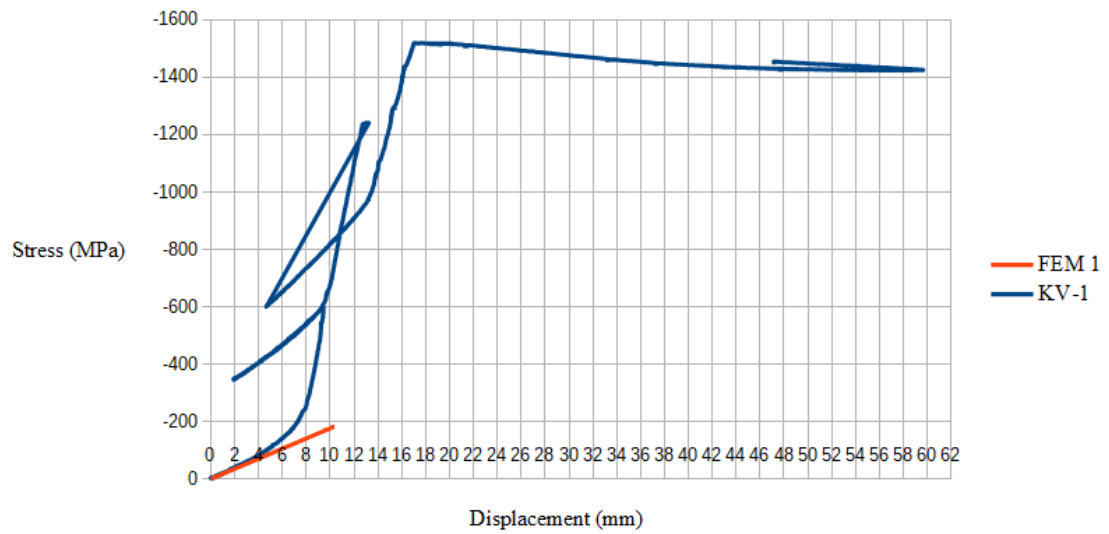
Figure I.3. Stress-displacement of the upper faceplate of KV-1 in x-direction. FEM results are drawn as a reference.
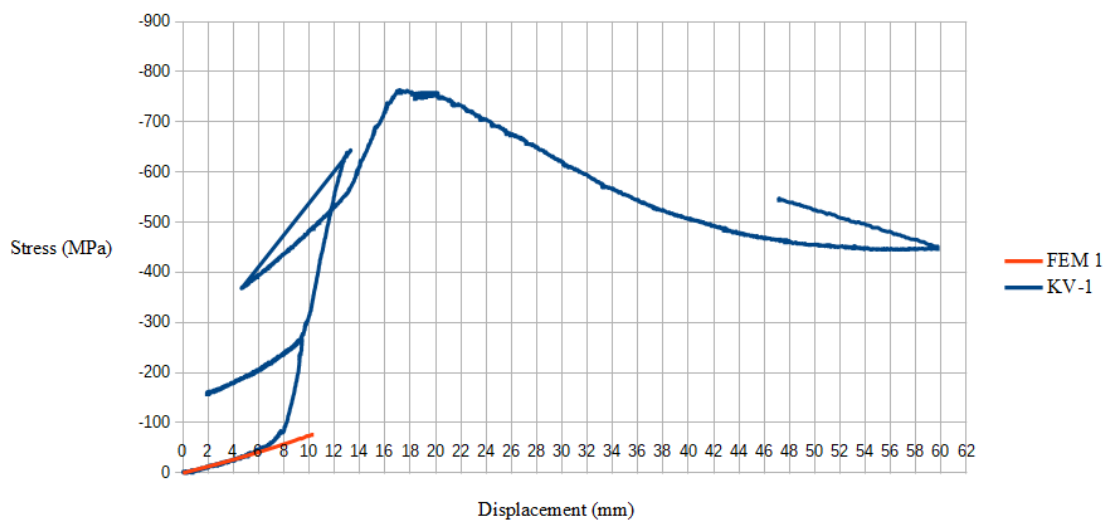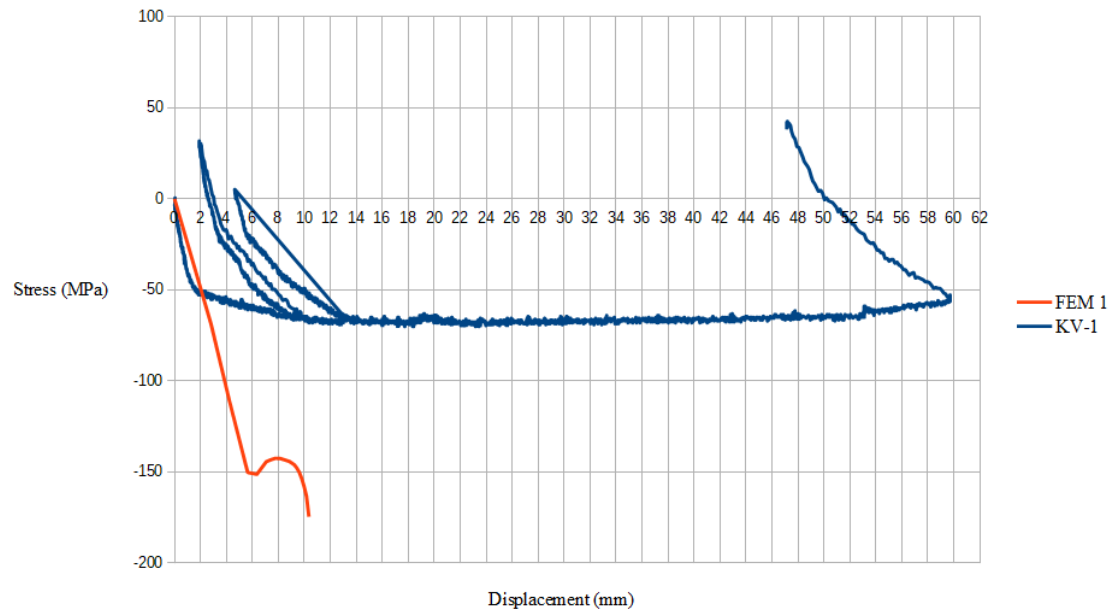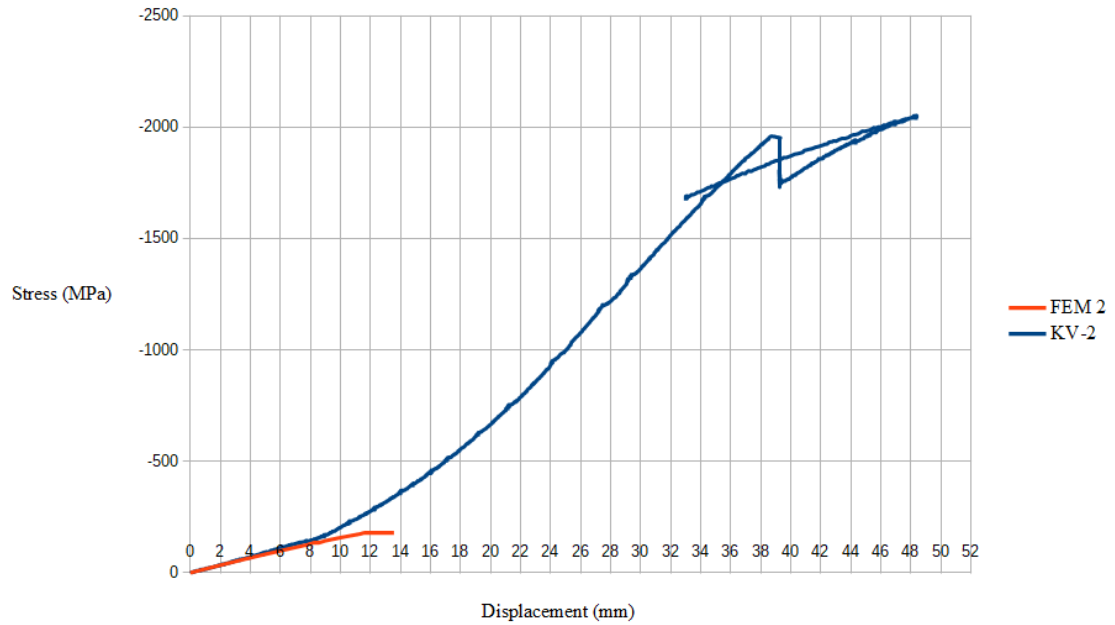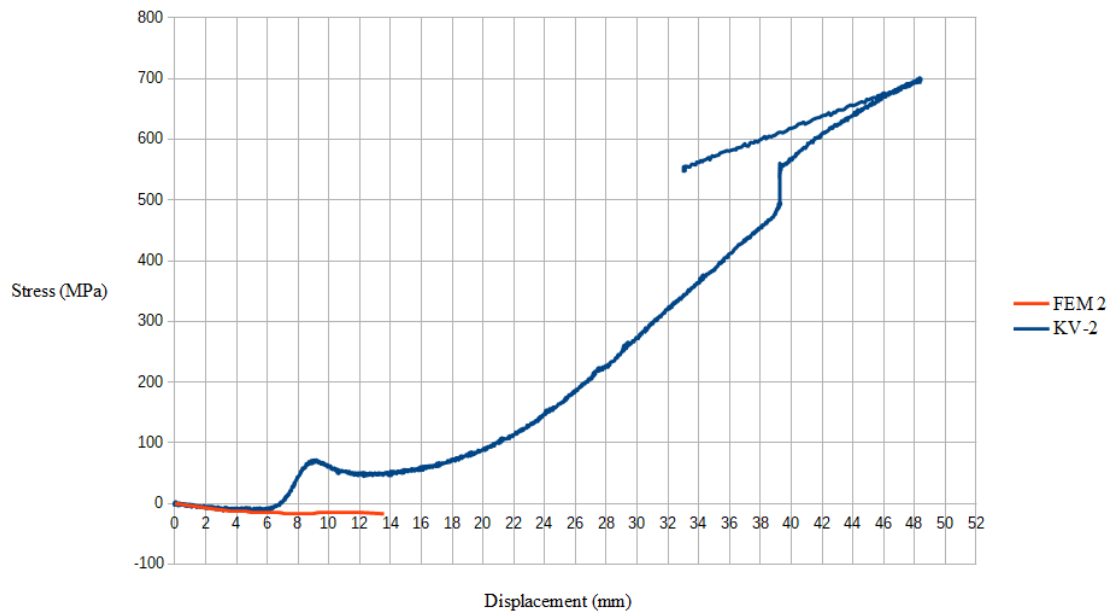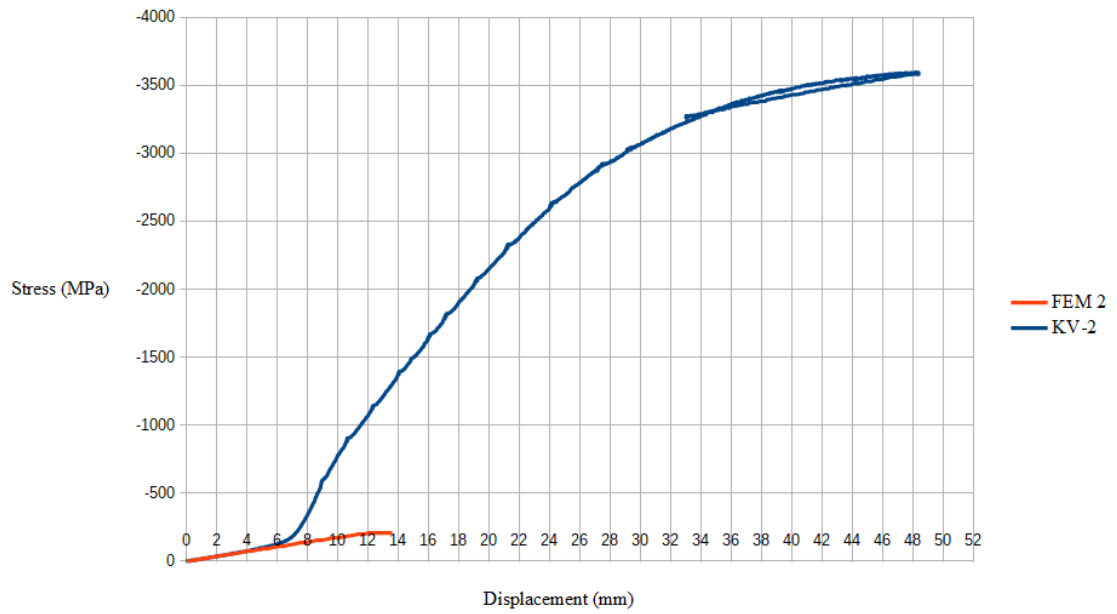

Figure I.4. Stress-displacement of the upper faceplate of KV-1 in y-direction. FEM results are drawn as a reference.
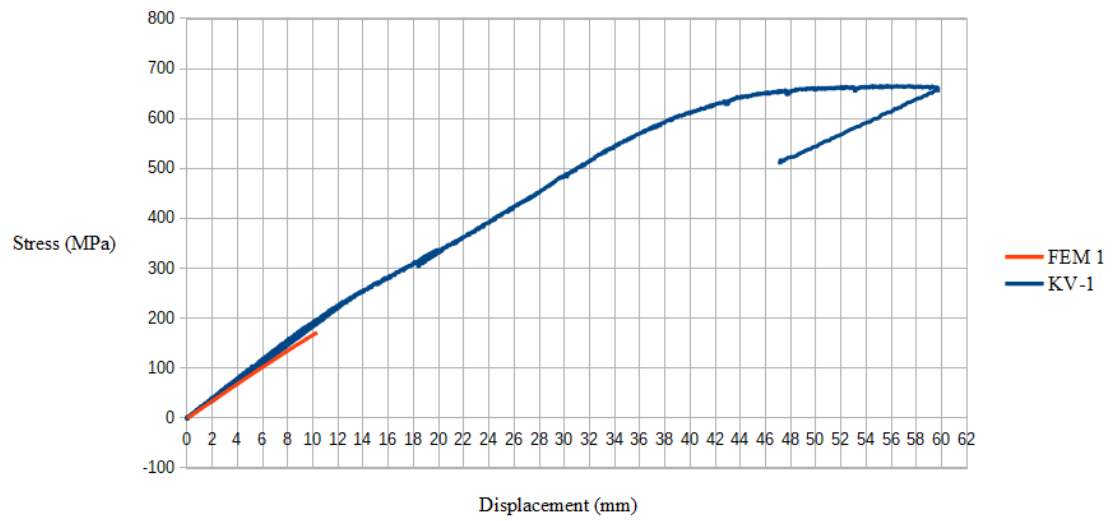
Figure I.5. Stress-displacement of the lower faceplate of KV-1 in x-direction. FEM results are drawn as a reference.
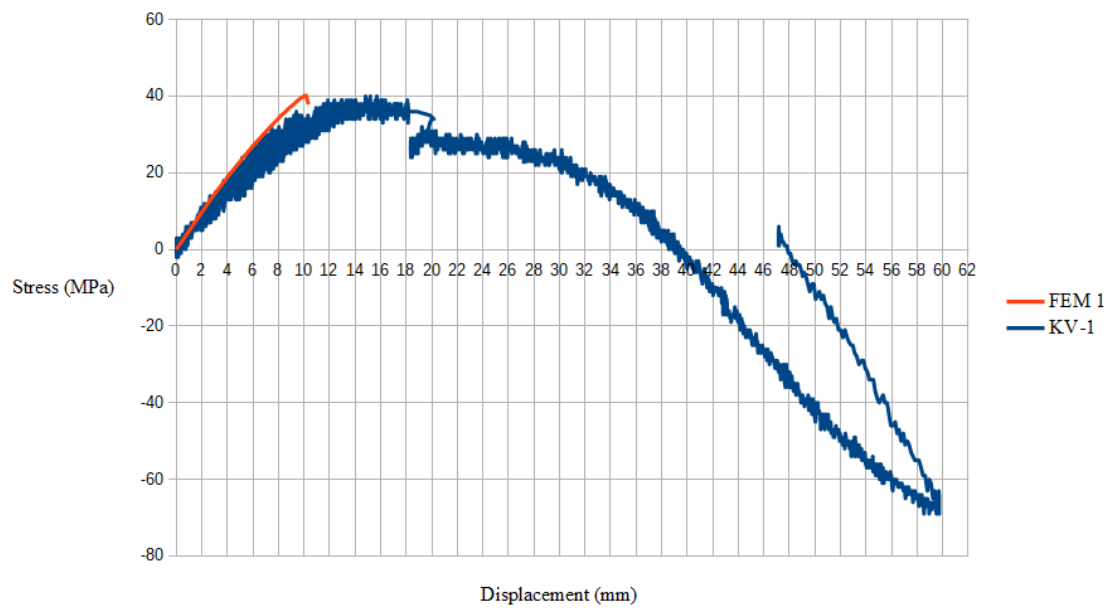
Figure I.6. Stress-displacement of the lower faceplate of KV-1 in y-direction. FEM results are drawn as a reference.

Figure I.7. Stress-displacement of the core diagonal of KV-1. FEM results are drawn as a reference.
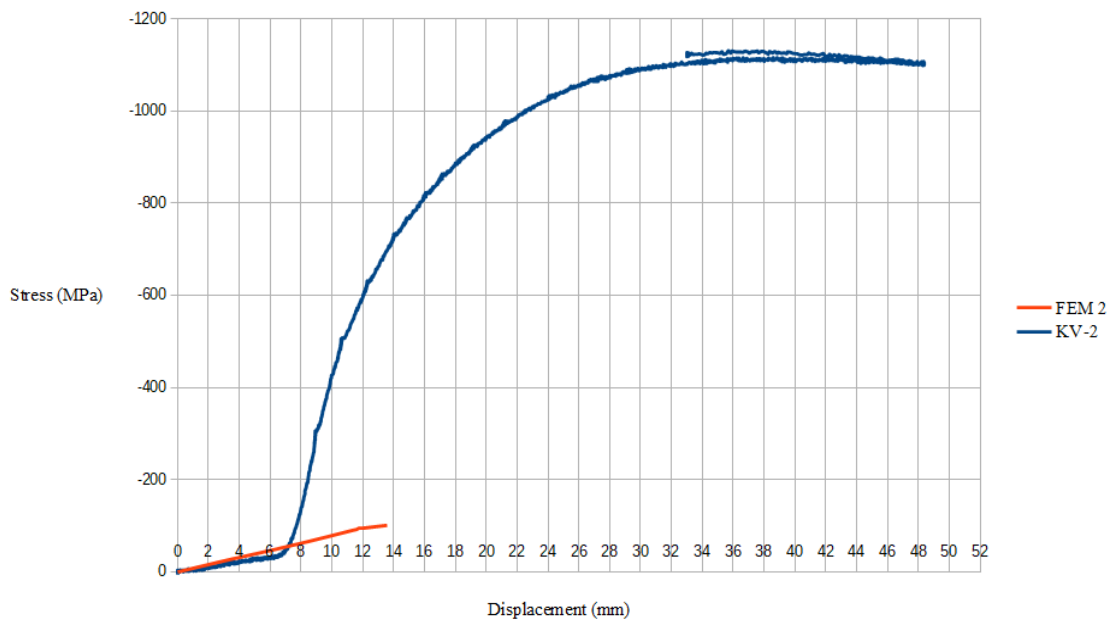
J Graphs of KV-2 test

Figure J.1. Stress-displacement of weld of KV-2 in x-direction. FEM results are drawn as a reference.
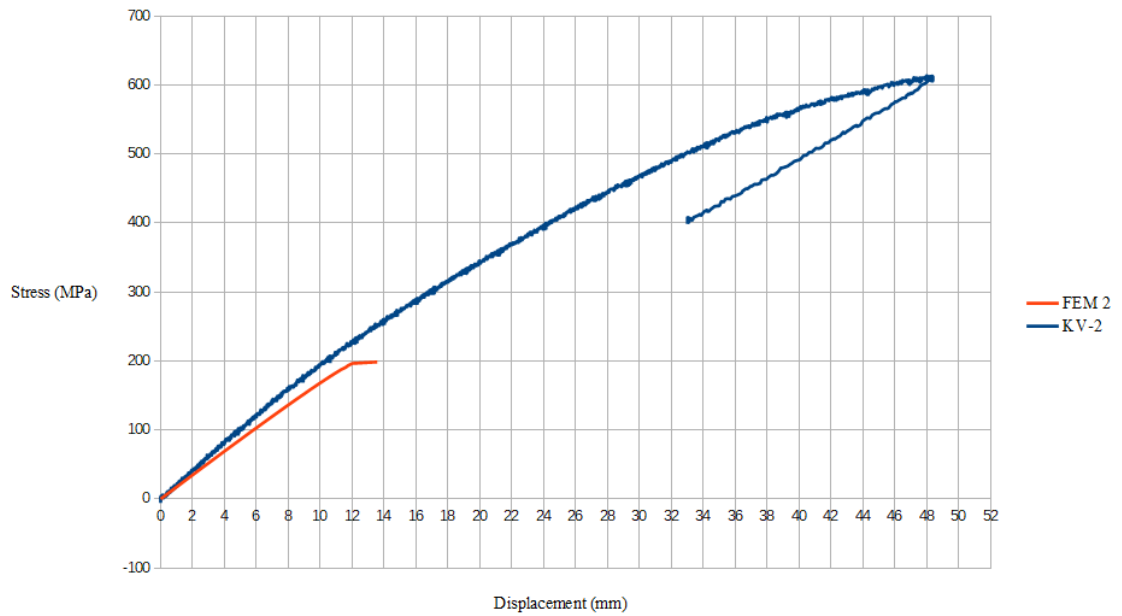

Figure J.2. Stress-displacement of weld of KV-2 in y-direction. FEM results are drawn as a reference.
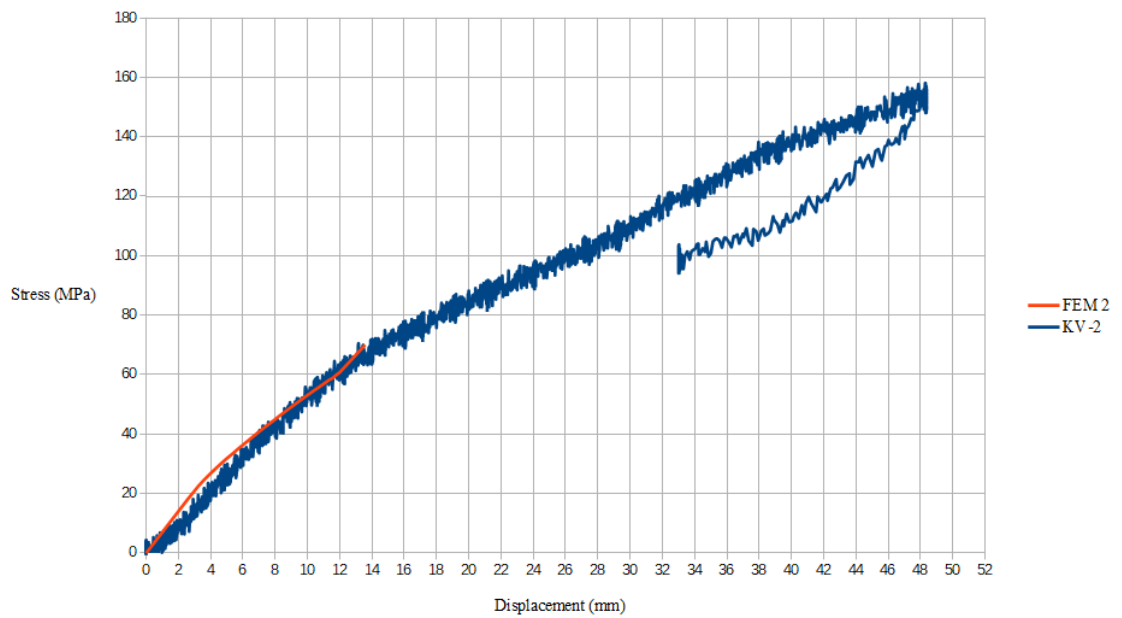
Figure J.3. Stress-displacement of the upper faceplate of KV-2 in x-direction. FEM results are drawn as a reference.
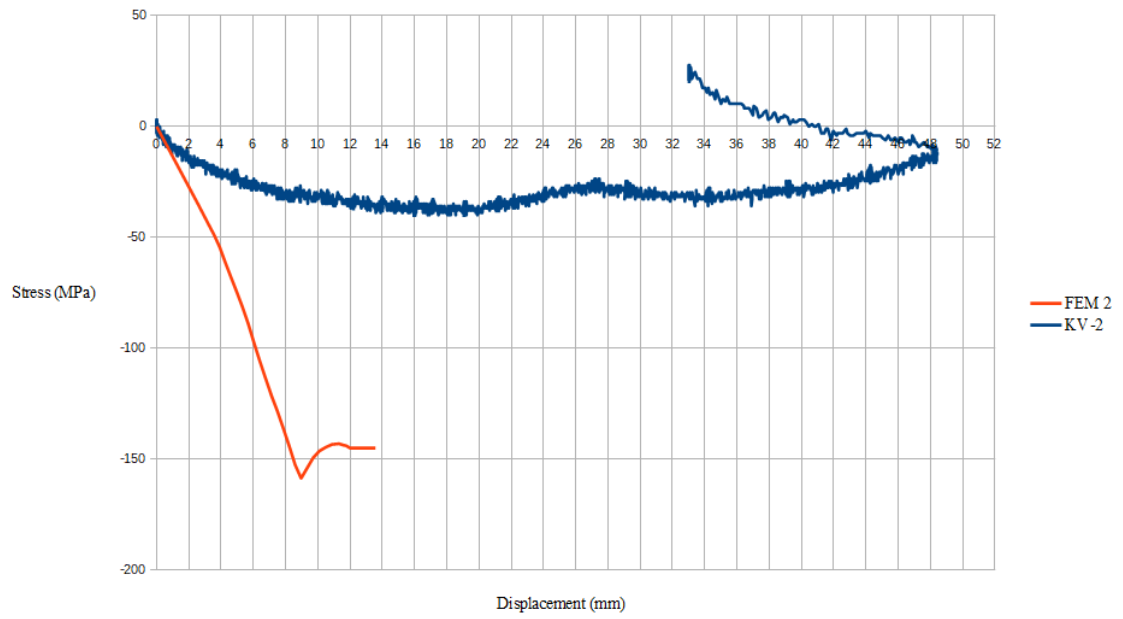

Figure J.4. Stress-displacement of the upper faceplate of KV-2 in y-direction. FEM results are drawn as a reference.

Figure J.5. Stress-displacement of the lower faceplate of KV-2 in x-direction. FEM results are drawn as a reference.

Figure J.6. Stress-displacement of the lower faceplate of KV-2 in y-direction. FEM results are drawn as a reference.

Figure J.7. Stress-displacement of the core diagonal of KV-2. FEM results are drawn as a reference.